MOLECULAR BONDING IN PRODUCT ENGINEERING

Except where references are made to the work of others, the work described in this dissertation is my own and was conducted with the consent of my advisor in collaboration with my advisory committee. This dissertation does not include proprietary or classified information.

Amol J. Thote

Certificate of Approval:

Ram B. Gupta, Chair
Alumni Professor
Chemical Engineering

Steve R. Duke
Associate Professor
Chemical Engineering

Christopher B. Roberts
Department Chair &
Professor
Chemical Engineering

William R. Ravis
Department Head &
Professor of Pharmaceutics
Pharmacal Sciences

Stephen L. McFarland
Dean
Graduate School

MOLECULAR BONDING IN PRODUCT ENGINEERING

Amol Janardan Thote

A

Dissertation

Submitted to the

Graduate Faculty of

Auburn University in

partial fulfillment of the

requirements for the

Degree of

Doctor of Philosophy

Auburn, Alabama

August 8, 2005

VITA

Amol Janardan Thote, son of Janardan G. Thote and Vijaya J. Thote, was born on December 21, 1978, in Bhopal, India. He completed his primary education at Bright High School, Mumbai and secondary and higher secondary school at St. Francis School and Deogiri College, Aurangabad. He, then, moved back to Mumbai to obtain his bachelor degree in Chemical Engineering at Mumbai University Department of Chemical Technology (UDCT, now renamed to UICT), Mumbai in 1996. He graduated with the degree of Bachelor of Chemical Engineering in the year 2000. He then moved to USA to obtain higher education and planned to accomplish a Doctor of Philosophy in Chemical Engineering at Auburn University.

DISSERTATION ABSTRACT

MOLECULAR BONDING IN PRODUCT ENGINEERING

Amol J. Thote

Doctor of Philosophy, August 08, 2005
(B.Ch.E., Mumbai University Institute of Chemical Technology, 2000)

187 typed pages

Directed by Prof. Ram B. Gupta

Molecular Bonding plays an important role in the performance of product and chemical processes. Various types of bonds are: ionic bond, covalent bond, co-ordinate bond, metallic bond, van der Waal's bond and hydrogen bond. This dissertation involves examination of hydrogen bonds, covalent bonds and van der Waal's bonds in order to improve performance of a wide variety of products in the present commercial world: liquid crystal display in computers and laptops, and sustained release formulations in Pharmaceutical Drug Delivery. Current challenges in the product performance are examined and then improvements in the product performance from a perspective of molecular

bonding are proposed. The most important factors that play a major role in molecular bonding are the intermolecular forces and intermolecular distances. By developing a fundamental understanding and means of enhancing the strength of these bonds, product improvement can be achieved for a better overall performance.

In liquid crystal displays (LCDs) the active element is a liquid crystal matrix with several dichroic dyes dissolved in them. The liquid crystal molecule responds to the change in the electric field (i.e., pixel switching), whereas the dye molecule exhibits optical absorption. For fast optical switching of the pixels, hydrogen bond between the liquid crystal molecule and dichroic dyes plays an important role. A strong hydrogen bond between the two enhances the contrast properties of the LCDs. This depends upon finding the right combination of liquid crystal and dichroic dye molecules that exhibits strong hydrogen bonding along the longitudinal length of the molecule. Strengths of h-bonding are examined using both Fourier transform infrared spectroscopy, and molecular modeling and simulation.

In controlled drug release applications, drug is encapsulated in polymer microspheres, and the drug release occurs by the biodegradation of the polymer. A current challenge is due to too much drug release (burst release) during the first day itself, causing the drug level to rise above the toxic limits. To address this challenge, surface covalent bonds are added to the drug/polymer micro-

spheres. This surface covalent bonding is carried out by polymerization of cross-linkable monomers by UV light. The surface layer imparts additional mass transfer barrier to the drug release, thereby reducing the initial burst release. Both hydrophilic and hydrophobic types of drugs are tested and reduction in initial burst release was obtained.

A further step into the development of sustained release formulations involves microencapsulation of active pharmaceutical ingredients (API) nanoparticles in solid form into biodegradable polymer microparticles. These particles are built on the basis of van der Waal's forces of attraction between the polymer strands and the API nanoparticles and amongst themselves. This helps in creating a uniform distribution of the API in the polymer matrix and therefore provides a sustained release of the API for a long period of time with almost no burst release. An extension of this process is towards utilizing the above process for sustained release formulations of proteins and peptides.

ACKNOWLEDGEMENTS

As somebody has righteously said, words are no substitute for feelings, and expressing my gratitude in words cannot fathom the depth of my feelings. But this is just an attempt to express my heartfelt gratitude to Prof. Ram B. Gupta who has been instrumental in providing me with suggestions for my research problems, adequate guidance in directing them, his patience, time and availability for consultation, and continuous support to accomplish this Doctor of Philosophy. I would also like to extend my gratitude to Prof. Christopher B. Roberts, Prof. Steve R. Duke, Prof. William R. Ravis, and Prof. Vishnu Suppiramaniam for enthusiastically agreeing to serve on my dissertation committee and giving their valuable inputs to my research.

I would also like to thank my parents, brother and sister for their continuous support and encouragement in my academic endeavors all throughout my life. Without their support, it would not have been possible for me to reach this far in my academic career.

I would like to thank Philip Bell for his research contributions, his advices, and his humorous attitude towards life. That made my life and research at Auburn highly enjoyable. I would also thank all my fellow colleagues: Ranjit Thakur, Kayoko Ono, Jayant Gadhe, Mukund Karanjikar, Gracie Bell, Raghu

Viswanathan, John Chappell, Deepak Sree, Sheena Lewis, Haley Brooks, Chandler McLeod, Chris Kitchens, Dan Obrzut, Nimir Elbashir, Madhu Anand, Debbie Boroughs, Parag Garhyan, P. Pradeep, Arindan Basu Sarkar, Umesh and others who have helped me in my day-today activities and have come up with valuable suggestions in my research. I want to express my gratitude to my superiors; Poongunran Muthukumaran, Pratibhash Chattopadhyay, and Rajesh Kumar for all their help and contribution towards my research.

I would want to thank Mr. Joe Alderholt and Mr. Wendel Sandlin for their fabulous ideas and their expertise in fabricating anything and everything that was possibly required in my laboratory experiments. I cannot miss this wonderful opportunity to thank Sue Ellen Abner and Kellie Wilson who directly or indirectly helped me in completing my PhD at Auburn. And I want to thank Mike Hornsby and Henry Cobb, who I know for sure, directly helped me in accomplishing my PhD at Auburn.

Last but not the least; I cannot end my acknowledgement without extending my heartiest gratitude to my beloved wife Shweta for her lifelong encouragement and support, patience during my research activities, delicious food, and her heartiest companionship. My academic as well as my personal life would have been incomplete without the deepest love of my wife in my life.

TABLE OF CONTENTS

CHAPTER 1

INTRODUCTION TO HYDROGEN BONDING

Molecular Bonding has played a vital role in determining the chemistry of various reactions yielding a multitude of reaction products, some of them being favorable, some of them not. However, the study of molecular bonding has been the most fundamental principle behind deciding the structure of a compound and feasibility of a reaction[1]. The most important factors that play a major role in molecular bonding are the intermolecular forces and intermolecular distances. These two parameters decide whether a bonding can occur and if it does, what kind of bond would it form. Obviously, that means there are various kinds of bonds, namely, ionic bond, covalent bond, co-ordinate bond, metallic bond, van der Waal's bond and hydrogen bond. An ionic bond is formed by donation of one or more electrons by an electropositive atom to an electronegative atom. A covalent bond is formed by sharing of equal number of electrons by two electronegative atoms. A coordinate bond is formed by sharing of a lone pair of electron, initially present on one molecule, between two molecules. Metallic

bond is formed by the strong forces of attraction between the positive nuclei and the delocalized electrons in a metal lattice. van der Waal's forces are the weak attractions between neighboring molecules due to their dipole and dispersion forces. And last but not the least, the most interesting type of bond is a hydrogen bond. It is defined as an attractive force between a lone pair of an electronegative atom and a slightly positively charged H atom, initially bonded to another electronegative atom. These forces are slightly weaker than covalent bond, but stronger than van der Waal's forces of attraction.

In organic chemistry, the two most important forces that play a major role are covalent bonds and hydrogen bonds. By modifying these forces, a substantial improvement can be brought about in the performance of various devices used in various fields. Hence, the concept of this dissertation is to demonstrate how molecular bonding can be brought about in a desired manner to achieve favorable results in a wide variety of fields.

The theory of hydrogen bond is one of the most fundamental yet inquisitive knowledge of chemical bonding. H bonding compounds are the type of compounds that involve weak bonds and exhibit unusual physical and chemical properties. A few examples can illustrate these facts about H bonding. H bond is prevalent in a number of organic compounds and inorganic crystalline hydrates. It is present in protein structure and is the key element in binding the appropriate base pair sequences in the DNA molecule. Moreover, the factor

responsible for a small molecule such as water retaining its liquid state at room temperature is the presence of strong intermolecular H bonding between its O and H atoms. Had H bond not been present in this world, life could not have survived in the absence of water as the most primitive forms of life have evolved from water. The most debatable question for the existence of life on Mars has been based on the existence of water on the planet. Therefore, H bond revolves around mankind such that it has become one of the most important factors in the existence of life.

H bond is defined as a bond that exists between a functional group A––H and an atom or a group of atoms B in the same or a different molecule when

(a) there is evidence of bond formation (association),

(b) there is evidence that this new bond linking A––H and B specifically involves the hydrogen atom already bonded to A.[2]

This bond is slightly weaker than covalent bond but stronger than van der Waal's interactions. There are two types of H bonds, intramolecular and intermolecular H bonds. In order for H bond to exist, two distinct groups are required to exist, a hydrogen bond donor and a hydrogen bond acceptor. Now if the donor and the acceptor, both are present on the same molecule, it is termed as intramolecular hydrogen bond and if they are present on two different molecules, it is termed as intermolecular hydrogen bond. Compounds exhibiting strong intermolecular hydrogen bond exist as polymeric compounds in the form

of chains and rings. Ortho substituted benzenes exhibit intramolecular hydrogen bond whereas water, alcohols and acids exhibit intermolecular hydrogen bond. Intramolecular hydrogen bond does not significantly vary the physical properties of the compound whereas intermolecular hydrogen bond increases a number of physical properties such as molecular weight, viscosity, conductivity, solubility, dipole moment, surface tension and last but not the least melting and boiling points.

Detection of H bond

There are various non-spectroscopic techniques for the detection of the presence and strength of H bond such as monitoring the changes in the above mentioned properties. However, the focus of the discussion here is the detection of H bond strength and extent using spectroscopic techniques, mainly Infrared (IR) Spectroscopy. Every bond present in a molecule vibrates at a certain known frequency. The frequency is represented in terms of wavenumber as follows:

$$E = h\nu = hc/\lambda = hc\upsilon$$

E = Energy of IR light (J)

h = Planck's constant (6.63×10^{-34} Js)

ν = frequency of IR light (s^{-1})

c = speed of light (3×10^{10} cm/s)

λ = wavelength corresponding to frequency (cm)

υ = wavenumber (cm^{-1})

When IR light is incident on this molecule, bonds vibrate and absorb IR energy at a certain wavenumber depending on the bond length and atoms that forms the bond. The remaining transmitted light is detected by the IR detector and develops an absorption spectrum of energy of light absorbed to the wavenumber of light absorbed. This forms the IR signature of the molecule. Now, when this molecule forms H bond with another molecule or itself, the frequency of stretching mode of the bond and its harmonics representing the species involved in H bond formation is shifted to lower frequencies whereas the bending mode of the same species shift higher. The integrated absorption coefficient of the fundamental frequencies increases by a great extent when H bond is formed, whereas the corresponding coefficients of the harmonics decrease slightly. The free and the bonded vibrations represent different peaks in the IR spectrum and the area under these peaks can be calibrated to give a quantitative measurement of the extent of H bonding.

Thermodynamics of H bonding

H bonding is associated with an equilibrium between the associated and unassociated species, which is a function of the temperature of the system, represented by an equilibrium constant as follows:

$$A - H + B \Leftrightarrow A - H \text{ --- } B$$

$$K = \frac{[A - H \cdots B]}{[AH][B]}$$

$$\Delta G = - RT \ln K$$

$$\left(\frac{\partial \ln K}{\partial T} \right) = \frac{\Delta H}{RT^2}$$

$$\Delta G = \Delta H - T\Delta S$$

Experimental determination of K can be done by a quantitative determination of the concentration of each species involved in the H bond formation using the area under the IR spectral peaks of different species.

The dissertation talks about various ways of modifying these molecular bonds, mainly, covalent and hydrogen bonds, for the enhancement in product properties. This dissertation consists of a collection of research papers that have been published in various journals or have been sent for publication. Chapter 1 gives a brief introduction about hydrogen bonding concepts and how these concepts can be used in the performance of LCDs. Chapter 2 deals with developing a thermodynamic understanding of hydrogen bonding of –OH group in 1-hexanol with a group of molecules of increasing molecular length containing –CN group as their functional group. The experimentally developed thermodynamic relations with variation to temperature were verified using thermodynamic equation of state (LFHB theory of hydrogen bonding) and extended to conditions beyond experimental feasibility. These thermodynamic trend in the results were also matched with those obtained from ab initio calculations using Guassian98. Chapter 3 extends this understanding to study

the interactions between a liquid crystal and a dichroic dye present in the liquid crystal matrix and quantifies the extent of hydrogen bonding in terms of enthalpy and entropy of hydrogen bonding using experimental conditions and LFHB theory of hydrogen bonding. Chapter 4 extends the concept of hydrogen bonding by illustrating a computational study of hydrogen bonding between carboxylic acids and their interactions with carbon dioxide in supercritical carbon dioxide medium.

References

[1] Vinogradov S. N., Linnell R. H., "Hydrogen Bonding", Van Nostrand Reinhold Company, 1971.

[2] Pimentel G. C., McClellan A. L., "The Hydrogen Bond", W. H. Freeman and Company, 1960.

CHAPTER 2

HYDROGEN-BONDING EFFECTS IN LIQUID CRYSTALS FOR APPLICATION TO LCDS

Abstract

Hydrogen-bonding plays an important role in the performance of liquid crystal display (LCDs) by controlling the solubility and dissolution stability of dichroic dyes in the liquid crystal medium, in the case of guest-host type of liquid crystal displays. Hydrogen-bonding behavior of 4-pentyl-4'-cyanobiphenyl (5CB) (liquid crystal), benzonitrile, and acetonitrile, with 1-hexanol in CCl_4 are studied using FTIR spectroscopy, and ab initio and equation of state calculations. In all three mixtures, the –OH group acts as a hydrogen-bond donor and the –CN group acts as a hydrogen-bond acceptor. Based on FTIR analysis, the enthalpy of hydrogen-bond formation for 1-hexanol/acetonitrile is –14.7 kJ/mol, for 1-hexanol/benzonitrile is –5.4 kJ/mol, and for 1-hexanol/5CB is –4.6 kJ/mol. The entropy of hydrogen-bond formation is more favorable for 1-hexanol/5CB than for 1-hexanol/acetonitrile or 1-hexanol/benzonitrile. Trends in the spectroscopic results agree with ab initio calculations. Lattice fluid hydrogen bonding parameters are obtained from the spectroscopic data.

Introduction

The most important molecular interaction in polar fluids is hydrogen bonding (H-bonding)[1] which is defined as attraction between a donor hydrogen atom and an electronegative acceptor atom usually, a lone pair of electrons.[2] It is responsible for maintaining small molecules like water and alcohols in the liquid state at room temperature.[3] H-bonds (25-40 kJ/mol) are weaker than ionic bonds (200-400 kJ/mol) but stronger than van der Waals interaction (5-10 kJ/mol).[4,5]

Fourier transform infrared (FTIR) spectroscopy is an important tool for determining the extent of H-bonding.[6] Free and H-bonded species have molecular vibrations at different infrared frequencies. For example, the fundamental vibrational stretching frequency for non-H-bonded –OH species is observed at 3,600-3,640 cm^{-1}, while the vibrational band for H-bonded –OH species is in the range 3,000-3,400 cm^{-1},[7] though these values may vary depending upon the solvent used. The corresponding overtone bands are found at approximately 7,100 cm^{-1} and 6,900 cm^{-1} for free and H-bonded species, respectively. [8,9,10,11,12,13]

The application of H-bonding has been widely extended to various thermodynamic processes of industrial importance[14,15] and fundamental research.[16,17,18] A recent application is in enhancing the performance of LCDs by H-bonding between the liquid crystal and the dichroic dye dissolved in it.[19,20,21]

Liquid crystals are substances that exist as a metaphase between solid and liquid phases. Other than liquid crystal thermometers used in optical imaging and medical applications,[22] the major application of liquid crystals is in liquid crystal displays (LCDs) which consists of two panels with polarization perpendicular to each other. The liquid crystal is the active ingredient between the two panels and has a dichroic dye dissolved in it.

Dichroic dyes are long rod-like chiral compounds that possess the property of absorbing plane polarized light more along one molecular axis as compared to the other. When dissolved in a liquid crystal, these molecules re-orient themselves so that their long molecular axes align along the LC-director.[23] Dichroic dyes H-bond with the liquid crystal molecules.[24,25] The liquid crystal molecule responds to change in the electric field by orienting themselves in the direction of the electric field and the H-bonded dichroic dyes, depending upon their molecular orientation, absorb light in a specific wavelength range and exhibit optical properties necessary to visualize the LCD pixels. For example, Iwanaga et al.[26] have devised a new kind of LCD element where a donor H-bonds with an acceptor and at least one of them exhibits absorption in the visible light range representing a dye with emphasis in changing the molecular properties of the dye by changing the functional groups of the molecule in order to increase the solubility of the dye in the liquid crystal medium. Naito et al.[27] devised another kind of LCD display device that comprises a three-ply guest-

host liquid crystal layer superimposed on a substrate. Each guest-host liquid crystal layer exhibits different absorption wavelengths from each other containing a host liquid crystal and a guest dichroic dye. At least one layer out of the three guest-host liquid crystal layer contains a fluorine-based liquid crystal and an anthraquinone-based magenta or cyan dichroic dye having at least two arylthio groups. Takashi Kato et al.[28] devised a self assembly of liquid crystalline complexes having angular structures through intermolecular H-bonding of 1:2 mole ratio of phthalic acid, isophthalic acid or terephthalic acid which acts as a bifunctional H-bond donor with trans-4-heptyl/octyl/decyl-4′-stilbazoles as H-bond acceptors. Another self-assembly of supramolecular liquid crystalline materials was synthesized by Takashi Kato and Jean J. M. Frechet.[29] Linear mesogenic structures were obtained by 1:1 association of 4-butoxybenzoic acid used as a H-bond donor and trans-[(4-ethoxybenzoyl)oxy]-4-stilbazole used as a H-bond acceptor.

There is a need for the rationale design of liquid crystal/dichroic dye pairs. An objective of this work is to study the H-bonding behavior of liquid crystals. This is achieved by studying the H-bonding interaction between –CN and –OH functional groups; –CN being a functional group present in the liquid crystal and the –OH being a functional group present in the dichroic dyes. Apparently, the performance of the LCDs is governed by the properties of the dichroic dye and the strength of H-bonding between the dye and the liquid

crystal. Hence, the ultimate design goal is to look for dyes that exhibit strong and stable H-bonding with the liquid crystal.

Choice of H-bonding Mixtures

We have chosen to study the H-bonding interactions of 1-hexanol donor with three nitrile acceptors: acetonitrile, benzonitrile and 4-pentyl-4'-cyanobiphenyl (5CB) liquid crystal. These results are used to develop an understanding of the H-bonding involved so that it can be extrapolated to H-bonding between commercial liquid crystals[30] having a similar –CN H-bond acceptor and a dichroic dyes having a similar –OH H-bond donors (e.g, 4-[N-Ethyl-N-(2-hydroxyethyl) amino]-4'-nitroazobenzene as shown in Figure 1). The H-bonding behavior is studied using FTIR spectroscopy, LFHB equation of state and ab initio calculations.

A suitable solvent for FTIR is one which does not interact with the alcohol and the cyanides, and is transparent in infrared region of –OH vibration. However, it should be active enough in order to dissolve the alcohol and the cyanides. CCl_4 is not a polar solvent but has a quadrapole moment which helps in solubilizing polar compounds like alcohol and cyanides to some extent. CCl_4 has also been used before as a solvent for studying the H-bonding behavior of various H-bond donors and acceptors.[31] Hence, CCl_4 was selected for spectroscopic studies in this work.

The choice of nitriles was made in order to develop a fundamental understanding of the trend in interaction between the –CN group present in the liquid crystals and –OH functional group. The trend studied in the H-bonding behavior was from acetonitrile having just a $–CH_3$ end group to benzonitrile with a benzene ring followed by the liquid crystal having a biphenyl structure with alkyl bi-substituted amine at the other end of the ring chain. Bertie and Lan[32] studied the H-bonding behavior between liquid water and acetonitrile using absolute integrated infrared absorption intensities. They observed the –C≡N stretching vibration[33] shift from 2275 to 2210 cm^{-1}, and concluded that the interaction is a result of H-bonding between lone pair electrons on the –C≡N group and the proton of the –OH group. Kryachko and Nyugen[34] have recently studied H-bonding between benzonitrile and water by ab initio calculations using hybrid B3LYP density functional theory in conjugation with 6-31+G(d,p) and aug-cc-pVDZ basis sets.

The purpose of this work is to understand the H-bonding effects between a dye and the liquid crystal. The liquid crystal has a –CN functional end group and the dye has an –OH functional end group. The dye is an azo benzene. In this work, the dye was not used due to it's non-availability. 1-Hexanol has a linear chain of six carbons with a similar –OH functional end group. In addition,

there has been past FTIR studies on 1-hexanol.[35,36] Hence, 1-hexanol was used as H-bond donor instead of the dichroic dye.

The structures of free and H-bonded molecules in this study are shown in Figure 2. The concentration of 1-hexanol is kept low enough so that no self H-bonding occurs, and only -OH cross H-bonds with –CN.

Experimental Work

Materials

Carbon tetrachloride (99.9%, HPLC grade), 1-hexanol (98%) and benzonitrile (99.9% HPLC grade) from Aldrich and acetonitrile (Certified ACS 99.9%) from Fisher Scientific were dried using Molecular Sieves (Fisher Scientific, 3 ^{o}A) before using. The liquid crystal: 4-pentyl-4-cyanobiphenyl (98%) was used as supplied from Aldrich. N_2 gas (grade 5.0, BOC gases) is used to purge the sample compartment of the FTIR spectrometer to remove the background moisture.

Apparatus and Procedure

A schematic of the apparatus is as shown in Figure 3. It consists of a mixing chamber (*C*) where the solution to be analyzed by infrared is taken. A reciprocating pump (*P*) [Fluid Metering, Inc., model QG 400] is used to pump the solution from the mixing chamber to the FTIR cell. A six-port injection valve (*V*)

(Rheodyne Model 7012 loop filler port) is installed inline for addition of external solutions using a micro-liter loop of 5, 20 or 200 μL volume, as needed. Two temperature sensors (T_s) and a temperature controller (T_c) device (Cole Parmer Digi-Sense model 2186-20) are installed for temperature control. Heat is supplied using a heater through a 1/16th inch stainless steel heating coil. The IR cell and all the tubings are insulated with foam for better temperature control. A liquid sampling cell (not shown in the figure) is used to carry out the IR-analysis using a Perkin-Elmer Spectrum 2000 FTIR. The IR cell (made in-house) contains a pair of sapphire windows separated by teflon spacers with a spacing of about 1.5 mm. For experiments below room temperature, a cooling coil (made in-house from 1/16th inch stainless steel tubings) is connected in series to the flow circuit. A chiller (Cole Parmer Model C1283-60) with ice and glycol/water mixture is used for cooling the coil.

The FTIR is initially purged with nitrogen for at least half an hour to remove ambient moisture. Then, 50 ml CCl_4 solvent is taken in the mixing chamber and pumped through the cell. The temperature is maintained at 30±0.1^{o}C. After achieving a steady flow of CCl_4 through the liquid sampling cell, the FTIR-background of pure CCl_4 is recorded. Pure 1-hexanol is added to the system using the 20 μL micro-liter loop in the six-port injection. After equilibration, FTIR spectra are recorded at different 1-hexanol concentrations. The alcohol concentration is always kept below the self-association limit. Then

acetonitrile is added at constant 1-hexanol concentration to study the cross association of the alcohol with acetonitrile. An average of 50 IR scans over 5 minutes is taken with 0.1 cm^{-1} resolution in order to reduce the noise/signal ratio. Similar experiments are performed for benzonitrile and 5CB. Experiments are then repeated at 15 and 45°C.

Results and Discussion

Figure 4 shows the FTIR spectra of 1-hexanol with acetonitrile in CCl_4 solvent at 30 °C. Spectra were obtained for increasing concentration of 1-hexanol from 0-8 mM to the extent where there is no self-association between the 1-hexanol molecules. Then at the constant –OH concentration, acetonitrile was added from 0-140 mM and spectra were recorded for free (3638 cm^{-1}) and bonded (3555 cm^{-1}) OH peaks. Similar spectra were recorded for benzonitrile from 0 to 70 mM (Figure 5) and for 5CB from 0 to 89 mM (Figure 6). The experiments were then repeated at 15 and 45°C. Figure 7 shows FTIR spectra for 5CB with 1-hexanol at constant concentrations but varying temperature.

The free -OH concentration was determined from the area under the peak at 3638 cm^{-1}. Extinction coefficients needed were determined experimentally from spectra of dilute 1-hexanol in CCl_4. Bonded –OH was determined by difference of total and free –OH concentrations. Percentage H-bonding increases with increasing cyanide concentration as shown in Table 1. Assuming 1:1 H-

bonding, bonded –CN concentration was assumed to be equal to the bonded –OH concentration. Again, free –CN concentration was determined by difference of total and bonded –CN.

The equilibrium constant (K) for H-bond formation was obtained from free and bonded –OH, and –CN concentrations as,

$$K = \frac{[Bonded\ -OH]}{[Free\ -OH][Free\ -CN]}$$

K values were found to vary from 2.8 to 1.6 L/mol for association of 1-hexanol/acetonitrile, 3.0 to 2.4 L/mol for 1-hexanol/benzonitrile and from 5.1 to 4.8 L/mol for 1-hexanol/5CB H-bonding in the temperature range of 15-45 ^{o}C as shown in Table 2. These are similar to K values for other similar H-bonding:[37,38] 4.89 L/mol for phenol/acetonitrile and 3.45 L/mol for phenol/benzonitrile, 1.02 L/mol for methanol/acetonitrile, 0.87 L/mol for methanol/ propionitrile and 0.87 L/mol for methanol/benzonitrile. Lopes and Thompson[39] observed a decrease in K from 5.62 to 1.52 L/mol for H-bonding between phenol and acetonitrile in tetrachloroethylene with an increase in temperature from 23 to 78 ^{o}C due to the increase in thermal energy. This is consistent with the trend we have observed in the experimental results.

Enthalpy (ΔH) and entropy (ΔS) of H-bonding were obtained from lnK versus $1/T$ plot, as slope and y-intercept, respectively. These values are shown in Table 3. The trend we observed from acetonitrile to benzonitrile to 5CB agrees

with the trend observed by Lopes and Thompson[39] for phenol/acetonitrile (ΔH = –21.8 kJ/mol and ΔS = –58.6 J/mol/K) and for phenol/benzonitrile (ΔH = –19.3 kJ/mol and ΔS = –51.9 J/mol/K).

The alcohol and cyanides in this study are dissolved in CCl_4; and the liquid crystal does not remain in the liquid crystalline state when dissolved in CCl_4. As a result, the exact conditions inside the LCD are not reproduced here. Nonetheless, some understanding of h-bonding bonding equilibria specially the energies can be easily extended to LCDs. Liquid crystal matrix has specific orientation and order, which can impose additional entropic restrictions. For example, restricted mobility within the liquid crystal matrix may actually strengthen H-bonds of the liquid crystal molecules with the dichroic dyes present in the matrix.

Equation of State Modeling

Recent equations of state for H-bonding mixtures are based on chemical equilibria approach,[40] perturbed-hard-chain theory,[41,42] statistical association fluid theory,[43,44] mobile and static molecular disorder,[45] and lattice-fluid-hydrogen-bonding (LFHB).[2,46,47,48,49] Here, we have used LFHB theory because its general form is valid for mixtures containing multiple H-bondings and is applicable over a wide range of conditions. In this theory, H-bonding contribution of the partition function is derived from the number of ways of distributing the H-bonds among the donor and acceptor groups in the mixture.

The donor and acceptor must be in close spatial proximity as described by a mean field probability.[1] The LFHB equations are well established by Panayiotou and Sanchez[2] and applied to various thermodynamic problems[46] including a ternary mixture of an H-bond donor, an H-bond acceptor, and an 'inert' solvent. For a system of N_1 molecules of type 1 (1-hexanol), N_2 molecules of type 2 (nitriles) that form N_{12} number of H-bonded species by cross-association in N_3 molecules of inert solvent of type 3 (CCl_4) at temperature T and pressure P, LFHB equilibria can be written as:

$$\ln\left[\frac{r}{\tilde{\rho}}\frac{N_{12}/N}{\left(N_1/N - N_{12}/N\right)\left(N_2/N - N_{12}/N\right)}\right] = -\frac{E_{12}^0 + PV_{12}^0}{RT} + \frac{S_{12}^0}{R} = -\frac{G_{12}^0}{RT}$$

where, $N = N_1 + N_2 + N_3$, r is average segment length, $\tilde{\rho}$ is the reduced density, and E^0_{12}, V^0_{12}, S^0_{12} are standard energy, volume, and entropy of H-bonding, respectively.

Using spectroscopic values of N_1/N, N_2/N, N_3/N and N_{12}/N from the previous section, $\tilde{\rho}$ and r for pure CCl_4 (since the alcohol and nitrile are very dilute),[50] ΔG^0_{12} for 1-hexanol with all the nitriles are calculated. $\Delta G^0_{12}/T$ is then plotted versus $1/T$ to obtain ($E^0_{12} + PV^0_{12}$) as the slope and S^0_{12} as the intercept. Using P = 1 atm and V^0_{12} = –5.6 cm^3/mol as reported by Gupta et al.[46], E^0_{12} and S^0_{12} were evaluated as shown in Table 4.

Now with the availability of LFHB parameters, H-bonding calculations can be made for the conditions where experimental data are not available. We have performed LFHB calculation at 0, 30 and 60 ^{o}C over a wide range of nitrile concentrations (0-1000 mM) as shown in Figure 9 for 1-hexanol/acetonitrile, Figure 10 for 1-hexanol/benzonitrile and Figure 11 for 1-hexanol/5CB.

Ab initio Calculations

Recently, computational work[51,52] has been used to study the molecular properties of 5CB liquid crystal using ab initio calculations using RHF/6-31G(d), B3LYP/6-31G(d) as well as MP2/6-31G(d)] and semi-empirical methods like MOPAC with AM1. Bukowski et al.[53] have utilized symmetry adapted perturbation theory to compute interaction energies for pair configurations for acetonitrile-acetonitrile and methanol-methanol. Sum et al.[54,55,56] have conducted Gibbs Ensemble Monte Carlo (GEMC) simulations of acetonitrile and methanol using ab initio based pair potentials.

The objective of performing ab initio simulations here is to estimate the H-bond energies on a molecular level and compare with those observed experimentally and using LFHB theory. Methanol is used in the place of 1-hexanol and 4-biphenyl carbonitrile in the place of 5CB to reduce the computational time. It is a well established practice to model simplified geometry to simulate the behavior of bulky compounds using the calculated

properties of the simplified structure[57,58] in order to reduce the computational time with the advantage of simulating the behavior of the functional groups at relatively higher and more accurate basis sets. Taking proper care that the functional groups and the atoms affecting the group the most are retained, hexanol can be fairly easily substituted by methanol in order to compute the hydrogen-bonding energies. Moreover, 4-biphenyl carbonitrile has been well established to exhibit liquid crystal properties[59,60] and have been used as an intermediate in the synthesis of complex liquid crystal formulations.[61] 4-biphenyl carbonitrile has a similar active structure as the liquid crystal without the pentyl tail at the opposite end of the molecule. Aliphatic pentyl chain would possibly bring about a very weak electropositivity effect to the overall electron density distribution over the two benzene rings. This would eventually make the –CN group a little more electron rich enhancing the energy of H-bonding by a small factor. This interaction of the pentyl group should be relatively less important as compared to the interaction of the –CN functional group with the H-bond donor group (–OH). Hence, 4-biphenyl carbonitrile was used instead of 5CB for computational purposes. Moreover, it also follows the trend of increasing molecular complexity in going from acetonitrile to benzonitrile to 4-biphenyl carbonitrile and finally leading to 5CB. The simplification may change the H-bonding energies by a small extent. However, the trend obtained would still remain the same and can be easily compared to the experimental results.

Ab initio calculations are done using Gaussian98W.[62,63] H-bonding energies are calculated by evaluating the energy of the H-bonded complexes and subtracting the energies of the individual molecules. These energies were corrected for basis set superposition error (BSSE) using counterpoise correction method by Boys and Bernardi.[64] The procedure used for carrying out these calculations is also outlined by Wolbach and Sandler.[65]

Effect of CCl_4 solvent was incorporated by using SCRF keyword[66] with "Dipole and Sphere" reaction model of solvation,[63,67] following the methodology by Foresman and Frisch.[63] The dielectric constant of the medium was set to 2.228 by choosing Solvent=CCl_4 and the size of the molecular cavity (a_0) required for this simulation was obtained by optimizing the geometry initially in vacuum with "Volume" keyword.[66]

Figure 12 shows the optimized molecular structures. The orientation of the cyanides and methanol shows the presence of H-bond between –OH and –CN groups. The H-bonded energies calculated for different basis sets are listed in Table 5. A general trend can be observed that the H-bonding energies decrease from the association of methanol/acetonitrile to methanol/benzonitrile to methanol/4-cyanobiphenyl. The trend agrees with the spectroscopic data for all the basis sets studied.

Conclusion

There is significant H-bonding between the –OH group of 1-hexanol and –CN groups of acetonitrile, benzonitrile and 5CB liquid crystal molecules. The extent of H-bonding decreases from acetonitrile to 5CB. The enthalpy of H-bond formation becomes less negative from acetonitrile to 5CB, but the entropy of H-bonding becomes less negative from acetonitrile to 5CB to a greater extent. Hence, the H-bonding in the liquid crystal appears to be controlled more by entropic interactions. Ab initio calculations agree well with the spectroscopic data. Parameters for LFHB equation of state, estimated from the experimental data, are used to extrapolate the extent of percentage hydrogen-bonding at higher cyanide concentrations.

Table 1. Percentage H-bonding for varying temperature and cyanide concentrations at 8.37 mM/L 1-hexanol.

H-bond Acceptor	Concentration (mM/L)	Temperature (°C)	%H-bonding
Acetonitrile	60.8	15	14.3
	67.6	15	15.9
	74.3	15	17.0
	63.0	30	11.5
	70.0	30	12.4
	77.0	30	13.4
	63.0	45	9.2
	70.0	45	10.1
	77.0	45	10.8
Benzonitrile	58.7	15	14.7
	62.2	15	15.4
	65.6	15	16.3
	60.8	30	13.4
	64.4	30	14.0
	68.0	30	14.9
	60.8	45	12.7
	64.4	45	13.4
	68.0	45	14.0
5CB	89.1	15	32.7
	44.6	30	17.9
	66.8	30	24.4
	89.1	30	31.0
	89.1	45	29.0

Table 2. Equilibrium constant (*K*) for hydrogen-bond at varying temperatures in CCl_4. The errors in *K* values are about ±0.2 $(mol/L)^{-1}$.

H-bonding		T (K)	*K* $(mol/L)^{-1}$
1-hexanol ---	acetonitrile	289	2.8
		303	2.1
		318	1.6
1-hexanol ---	benzonitrile	288	3.0
		303	2.6
		318	2.4
1-hexanol ---	5CB	303	5.1
		310	4.9
		318	4.7

Table 3. Enthalpy, Entropy and Free Energy of hydrogen bonding for 1-hexanol with acetonitrile, benzonitrile and 5CB in CCl_4

H-bonding	ΔH (kJ/mol)	ΔS (J/mol.K)	ΔG (kJ/mol) at 298 K
1-hexanol ---acetonitrile	-14.7±2.1	-42.3±2.1	-2.1
1-hexanol ---benzonitrile	-5.4±1.6	-9.7±1.6	-2.5
1-hexanol ---5CB	-4.6±0.9	-1.0±0.9	-4.3

Table 4. Lattice-Fluid Hydrogen-Bonding Parameters

Components	S^0_{12} J/mol/K	E^0_{12} kJ/mol
1-Hexanol-Acetonitrile	-17.0	-17.7
1-Hexanol-Benzonitrile	-11.9	-11.8
1-Hexanol-5CB	-9.0	-8.0

Table 5. Hydrogen-bonding energies from ab initio calculations

			Methanol/Acetonitrile			Methanol/Benzonitrile			Methanol/4-cyanobiphenyl		
Theory	**Basis Set**	**Solvent Effect**	a_0 Å	H-bond Energy kJ/mol	BSSE kJ/mol	a_0 Å	H-bond Energy kJ/mol	BSSE kJ/mol	a_0 Å	H-bond Energy kJ/mol	BSSE kJ/mol
HF	6-31+G(d)	Dipole&Sphere	3.83	-24.3	4.3	4.30	-20.6	2.3	5.20	-18.8	2.2
HF	6-31+G(d)	Gas Phase Energy		-17.5	4.2		-14.4	2.4		-14.7	2.3
HF	cc-pVDZ	Dipole&Sphere	3.83	-19.9	4.3	4.30	-18.6	4.0	5.20	-17.0	3.8
HF	cc-pVDZ	Gas Phase Energy		-13.6	4.0		-13.1	4.1		-13.7	4.1
HF	cc-pVTZ	Dipole&Sphere	3.83	-19.9		4.30	-19.7		5.20	-18.2	
HF	cc-pVTZ	Gas Phase Energy		-13.9			-13.7			-14.4	

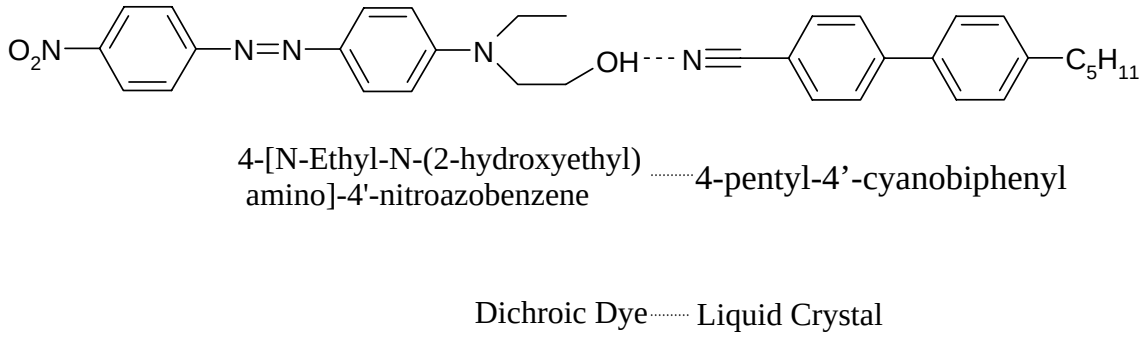

Figure 1. Hydrogen bonding between a dichroic dye and a liquid crystal.

(A) Individual Molecules

1. Hydrogen Bond Acceptors

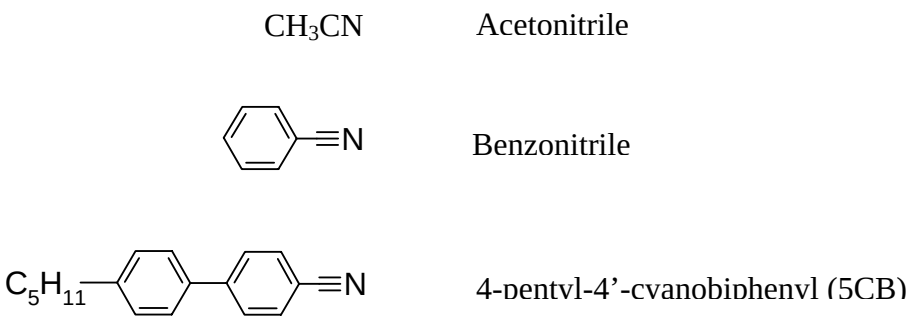

2. Hydrogen Bond Donor

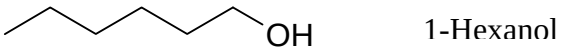

(B) Hydrogen Bonded Structures:

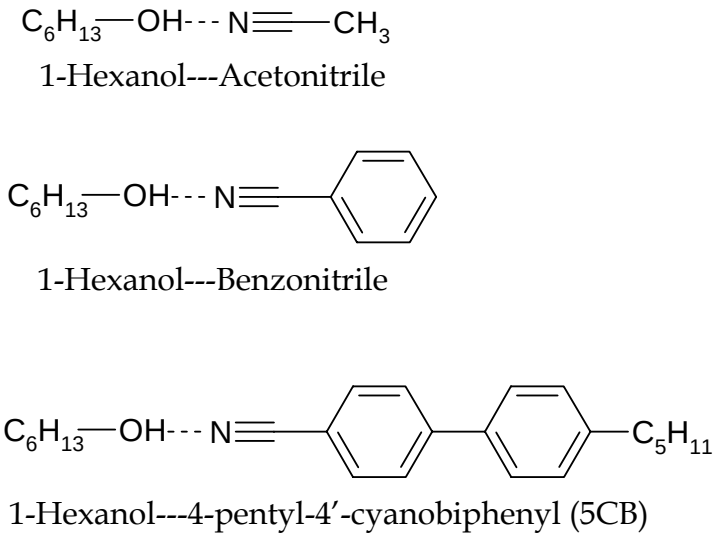

Figure 2. Structures of the free and H-bonded molecules used in the experiment.

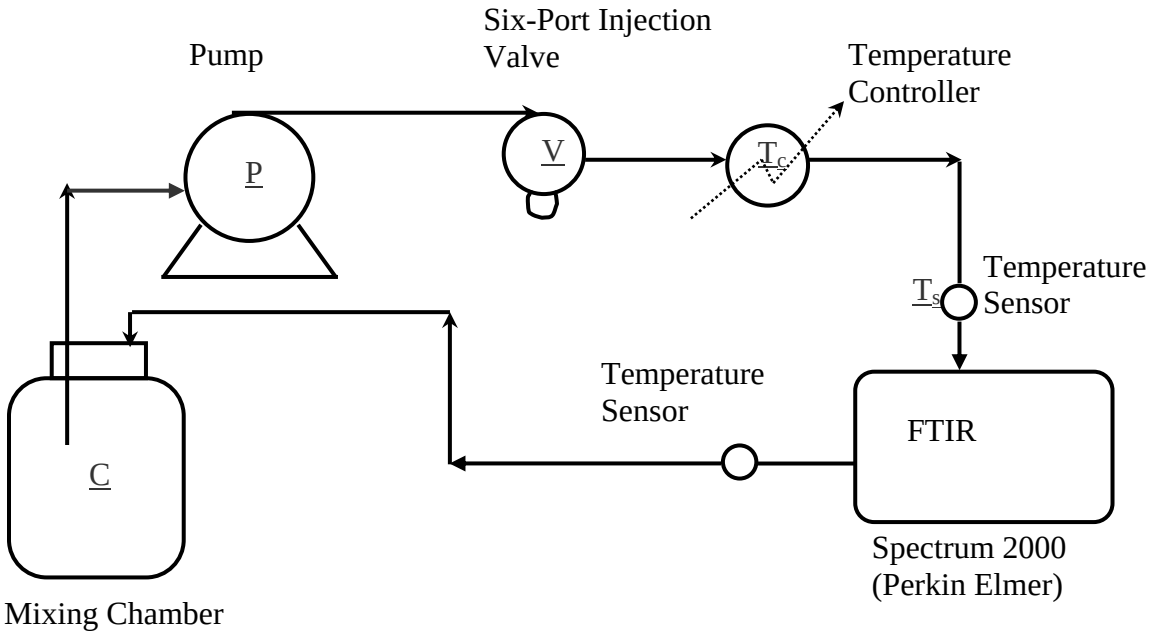

Figure 3. Schematic of the hydrogen-bonding FTIR apparatus.

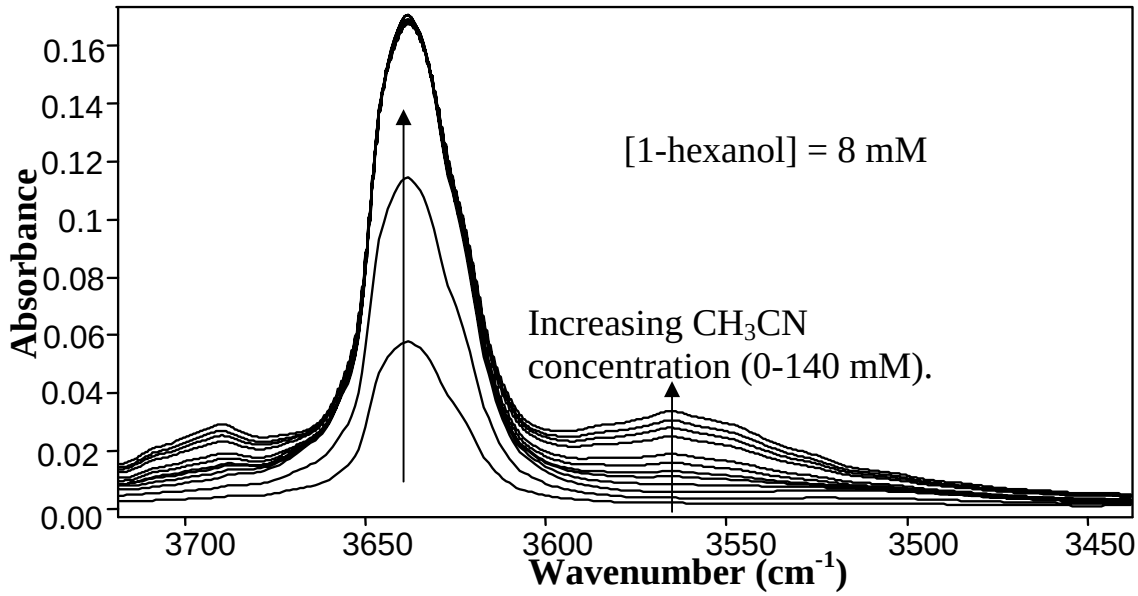

Figure 4. FTIR Spectra showing free and H-bonded –OH peaks for increasing concentration of acetonitrile.

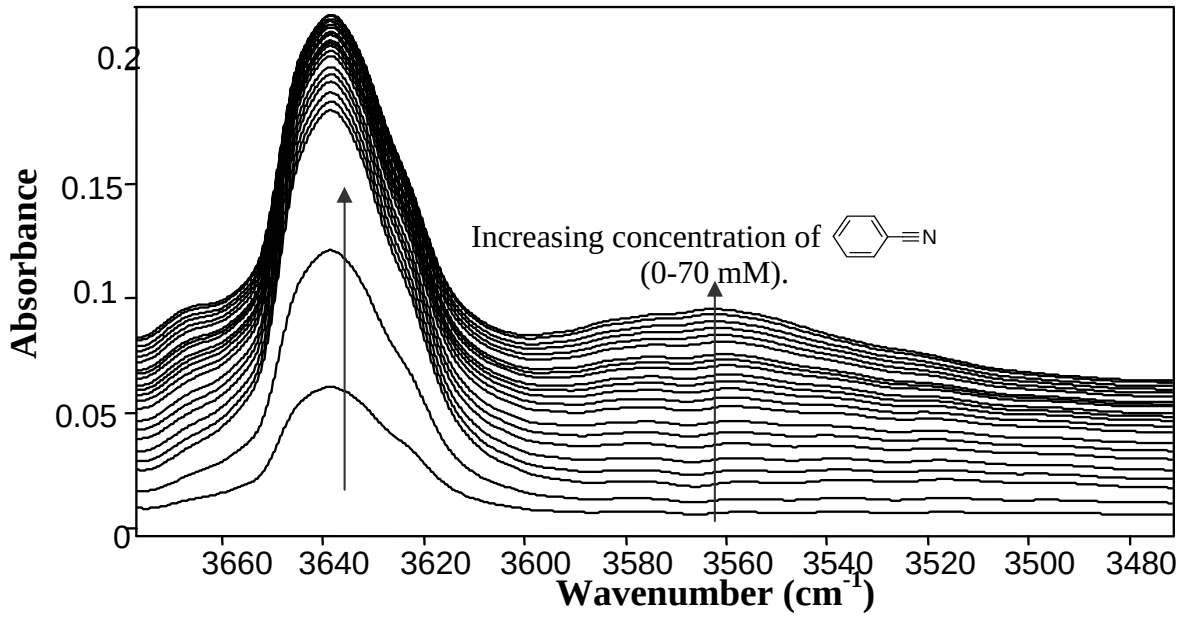

Figure 5. FTIR Spectra showing free and H-bonded –OH peaks for increasing concentration of benzonitrile.

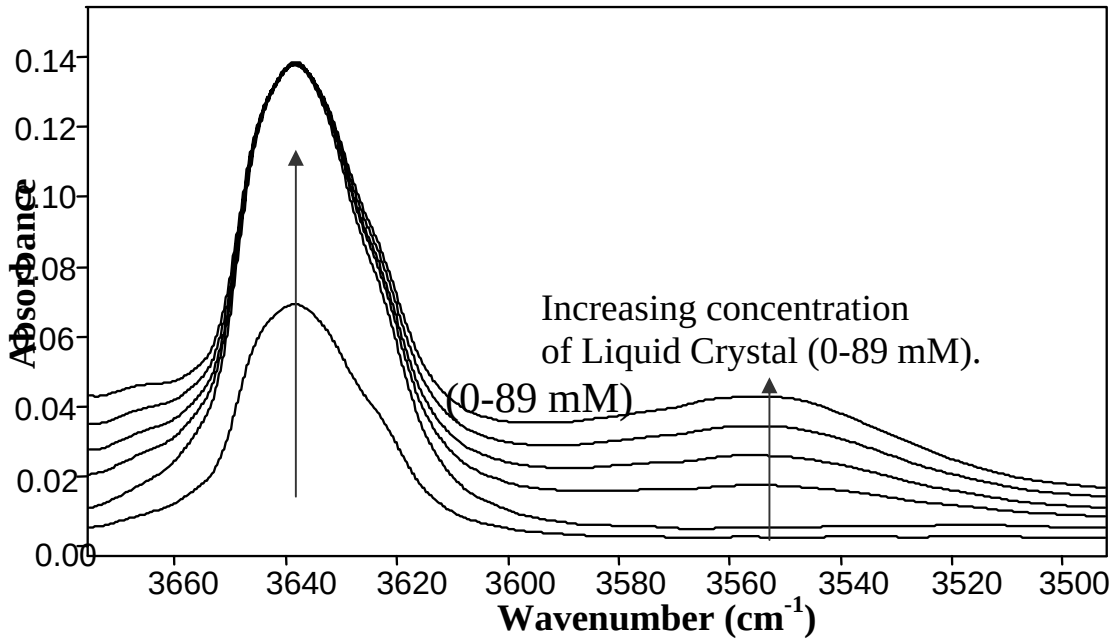

Figure 6. FTIR spectra showing free and H-bonded –OH peaks for increasing concentration of liquid crystal.

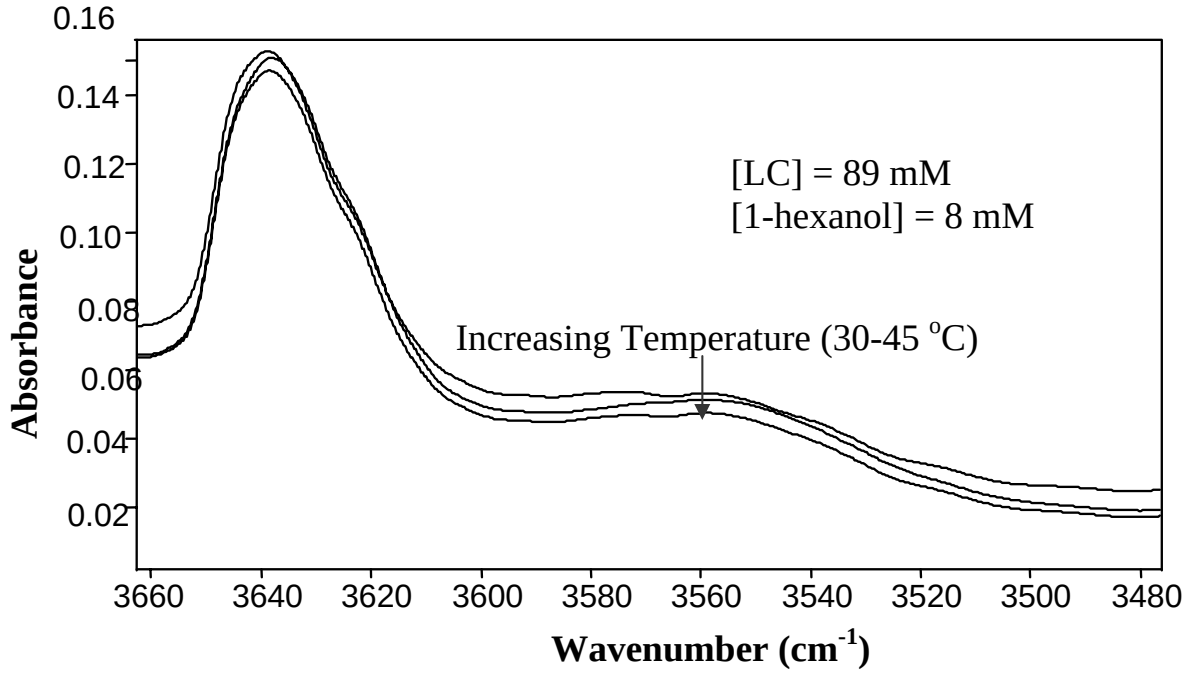

Figure 7. FTIR Spectra showing free and H-bonded –OH peaks for constant concentration of acetonitrile and 1-hexanol at different temperatures.

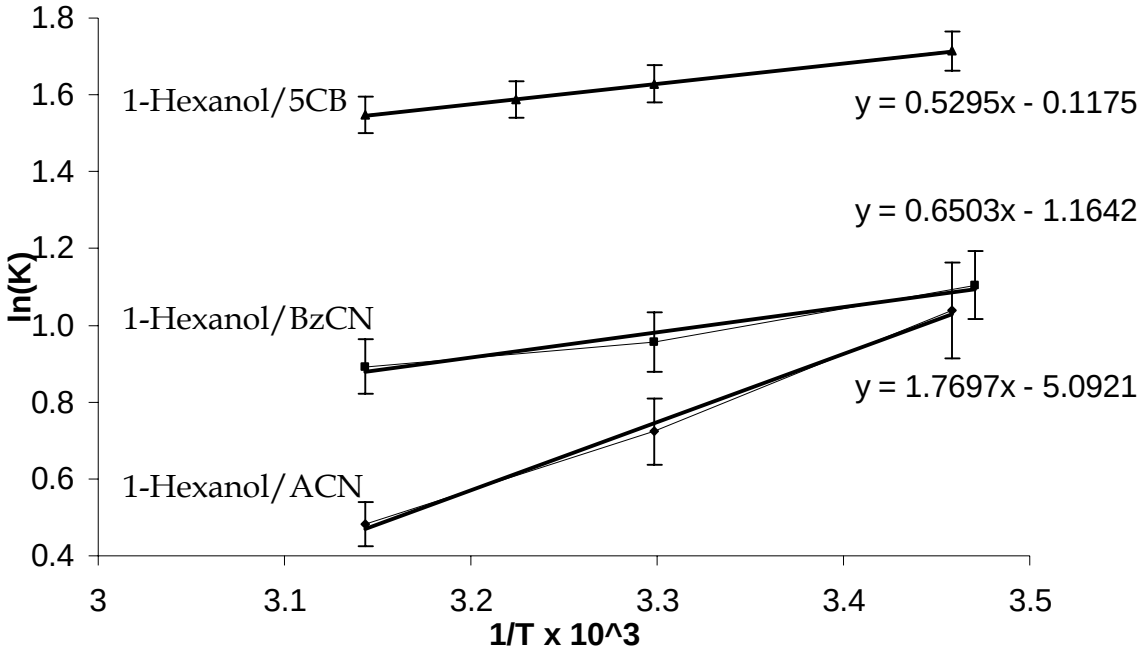

Figure 8. Temperature dependence of equilibrium constants.

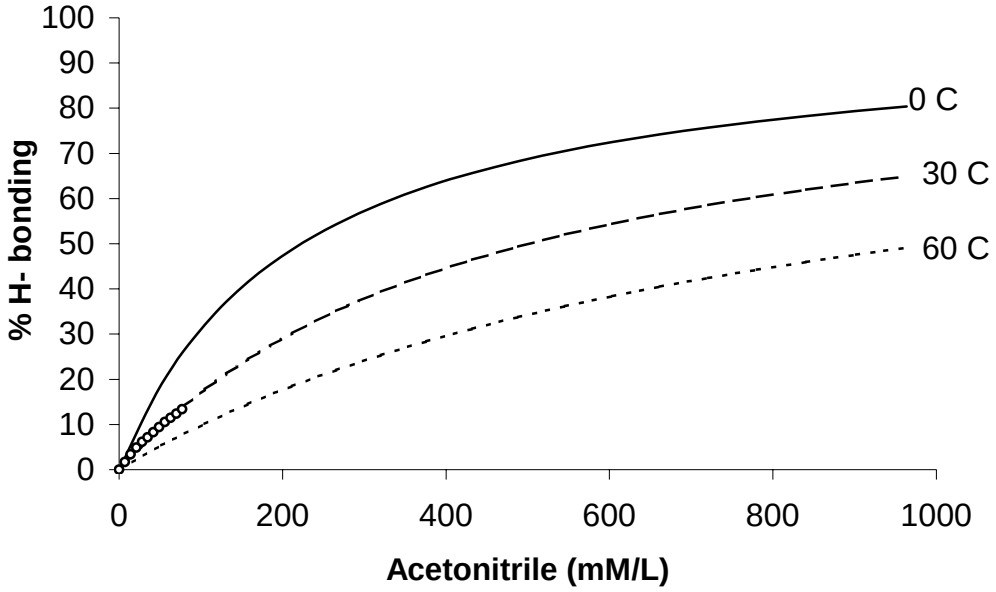

Figure 9. H-bonding between 1-hexanol (8.37 mM) and acetonitrile (points are experimental data and lines are LFHB calculations).

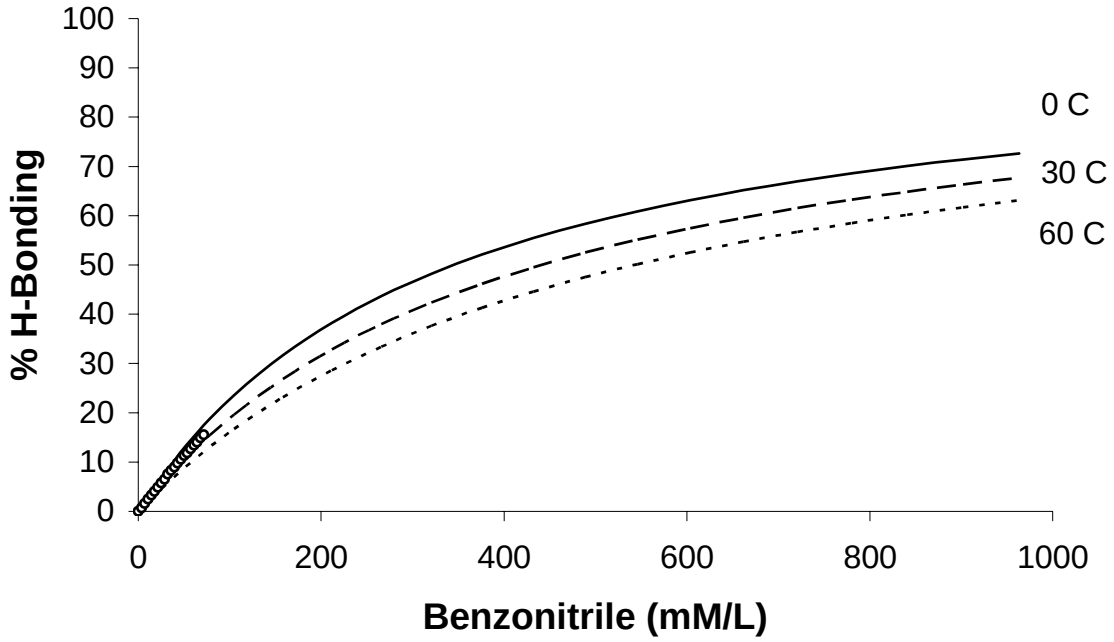

Figure 10. H-bonding between 1-hexanol (8.37 mM) and benzonitrile (points are experimental data and lines are LFHB calculations)

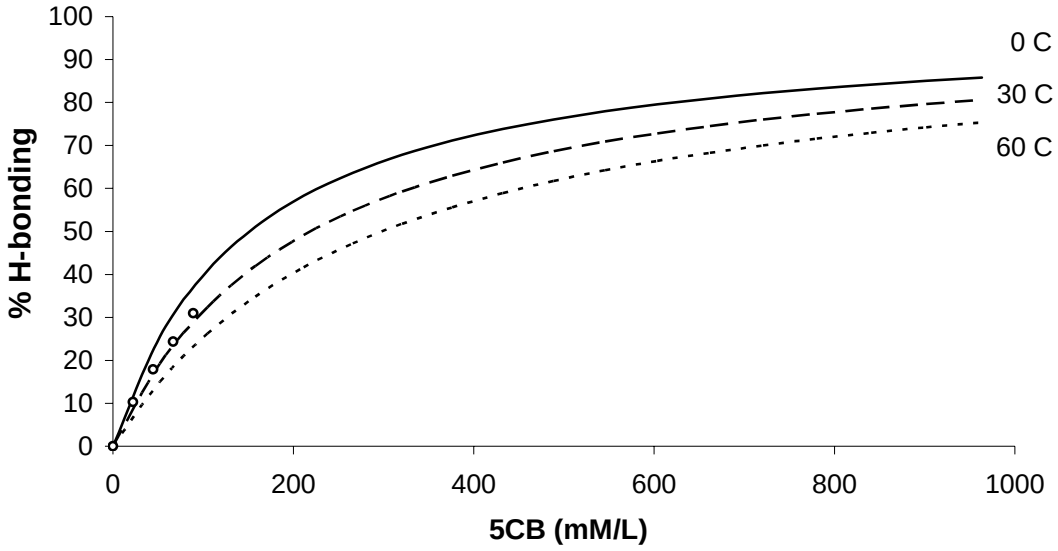

Figure 11. H-bonding between 1-hexanol (8.37 mM) and 5CB (points are experimental data and lines are LFHB calculations).

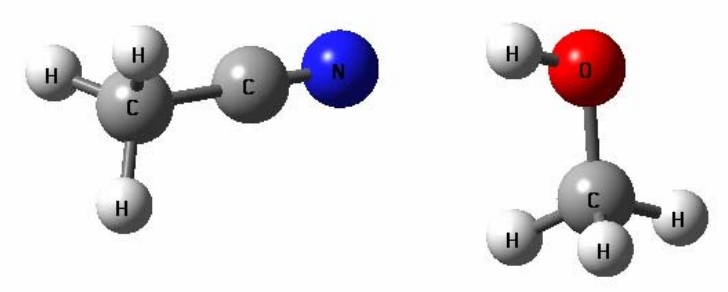

i. Acetonitrile and Methanol

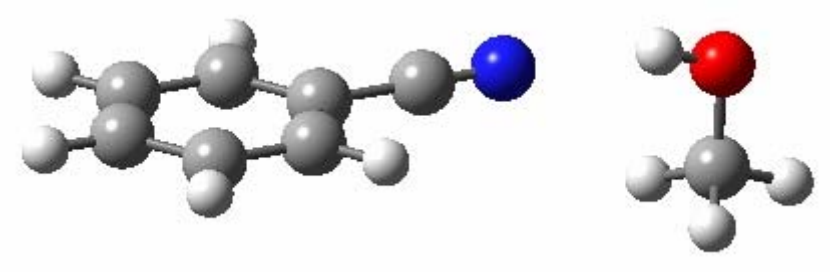

ii. Benzonitrile and Methanol

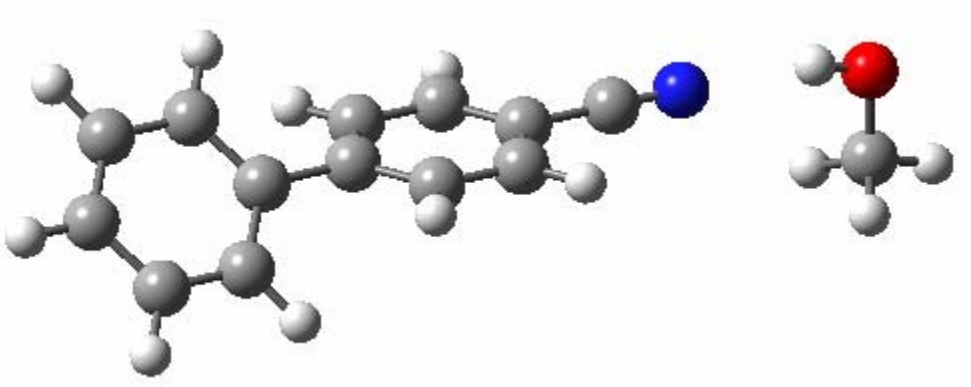

iii. 4-Cyanobiphenyl and Methanol

Figure 12. Ab Initio optimized molecular geometries.

References

[1] Veytsman, B. A., *J. Phys. Chem*. **1990**, *94*, 8499.

[2] Panayiotou, C., Sanchez, I. C., *J. Chem. Phy*. **1991**, *95*, 10090.

[3] Pimentel, G. C., McClellan, A. L., *The Hydrogen-bond*, Freeman and Co., San Francisco, CA, **1960**.

[4] Prausnitz, J. M., Lichlenthater, R. N., E. G. de Azevedo, Chapter 6 *Prentice-Hall, Englewood Cliffs*, NJ, **1986**.

[5] Huyskens, P. L., W. A. P. Luck, Th. Zeegers-Huyskens, Springer-Verlag, Berlin, **1991**.

[6] Brinkley, R. L., Gupta R. B., *AIChE Journal*, **2001**, *47* (4) 948-953.

[7] Martinez, S., *Spectrochimica. Acta,* **1986**, *42A*, 531.

[8] Coleman, M. M.; P. C. Painter, *Progress in PoIy. Sci.* **1995,** *20*, 1.

[9] Coleman, M. M., C. J. Serman, D. E. Bhagwagar, P. C. Painter, *Pober*, **1990**, *31*, 1187.

[10] Luck, W. A. P., Borgholte, H., Habermehl T., *J. Molecular Structures,* **1988**, *177*, 523.

[11] Luck, W. A. P., *Angewandte Chemie*, Int. Ed. Eng. **1980**, *19*, 28.

[12] Economou, I. G., M. D. Donohue, *AIChE J.* **1991**, *37,* 1875.

[13] Walsh, J. M., M. D. Donahue, *Fluid Phase Equiibria* **1989**, *52*, 397.

[14] Ikhlaq, M. *Chem. Eng*.-London, **1992**, *N521*, 21-22.

[15] Lammers, J. N. *Oil Gas J*, **1991** *89*, 50.

[16] Voutsas, E. C.; Boulougouris, G. C.; Economou, I. G.; Tassios, D. P. *Industrial & Engineering Chemistry Research,* **2000**, *39* (3), 797-804.

[17] Govil, G.; Khetrapal, C. L. *Current Science (India)* **1965**, *34* (4), 116-117.

[18] Crisp, G. T.; Jiang, Y. L., *Tetrahedron Letters*, **2002**, *43* (17), 3157-3160.

[19] Kobayashi, S.; Miyazaki, Y.; Motomura, T., *JP 100254*, **2001**.

[20] Kadowaki, M.; Sato, H., *JP 044955*, **2000**.

[21] Matsude, M., *JP 019564*, **2000**.

[22] Park Woo-Sang, *Journal of the Korean Physical Society,* **2000,** *37* (3), 331-334.

[23] Heilmeier, G. H., Zanoni, L. A., *Applied Physical Letters*, **1968**,.*13*, 91.

[24] Ghanadzadeh, A.; Ghanadzadeh, H.; Ghasmi, G., *Journal of Molecular Liquids*, **2000**, 88(2-3), 299-308.

[25] Griffiths, J.; Feng, K. C., *Journal of Materials Chemistry*, **1999**, *9* (10), 2333-2338.

[26] Iwanaga, H., Naito, K., *US Patent No. 6057906*, **2000**.

[27] Naito; K.; Iwanaga; H., *US Patent No. 5958291*, **1997**.

[28] Kato, Takashi; Adachi, Hajime; Fujishima, Akira; Frechet, Jean M. J., *Chemical Letters*, **1992**, 265-268.

[29] Takashi K., Fréchet J. M. J., *Macromolecular Symposium*, **1995**, *98*, 311-326.

[30] Demus, D.; Inukai, T. *Liquid Crystals*, **1999**, *26* (9), 1257-1266.

[31] Kolbe, A.; Kaps, P.; Plass, M., *Z. Phys. Chem.* (Munich), **1995**, *191* (2), 191-95.

[32] Bertie J.E., Lan Z., Liquid Water-Acetonitrile mixtures at 25 ^{o}C: *Journal of Physical Chemistry B*, **1997**, *101*, 4111-4119.

[33] Jamroz, D.; Stangret, J.; Lindgren, J., *Journal of the American Chemical Society*, **1993**, *115*, 6165.

[34] Kryachko E.S., Nguyen M.T., *Journal of Chemical Physics*, **2001**, *115* (2), 833-841.

[35] Gupta R. B., Brinkley R. L., *AIChE Journal*, **1998**, *44* (1), 207-213.

[36] Sum, A. K.; Sandler, S. I., *Journal Physical Chemistry A*, **2000**, *104* (6), 1121-1129.

[37] White, S. C.; Thompsom, H. W., *Proceedings of Royal Society*, **1966**, *A291*, 460.

[38] Thomas R. K., Dissertation, *Oxford*, **1964**.

[39] Lopes, Mario C. Sousa; Thompson, H. W. *Spectrochi. Acta*, **1968**, *24A*, 1367-1383.

[40] Heidemann, R. A.; Prausnitz, J. M. *Proc. Natl. Acad. Sci.* U.S.A. **1976**, *73*, 1773-1776.

[41] Walsh, J. M.; Donohue, M. D. *Fluid Phase Equilb.* **1989**, *62*, 397-404.

[42] Economou; I. G., Donohue, M. D. *AIChE J.* **1991**, *37*, 1876-1894.

[43] Huang, S. H.; Radosz, M. *Ind. Eng. Chem. Res.* **1990**, *29*, 2284-2294.

[44] Economou, I. G.; Donohue, M. D., *Fluid Phase Equilib.*, **1996**, *116* (1-2), 518-29.

[45] Huyskens, P. L., *J. Mol. Struct*. **1992**, *274*, 223-246.

[46] Gupta, R. B.; Panayiotou, C. G.; Sanchez, I. C.; Johnston, K. P. *AIChE J.* **1992**, *38*, 1243-1253.

[47] Gupta, R. B.; Johnston, K. P., *Fluid Phase Equilib.* **1994**, *99*, 136-161.

[48] Gupta, R. B.; Prausnitz, J. M., *Ind. Eng. Chem. Res.* **1996**, *36*, 1226-1230.

[49] Gupta, R. B.; Brinkley, R. L., *AIChE J*. **1998**, *44*, 207-213.

[50] Sanchez, I. C., Lacombe R. H., *J. Phys. Chem.* **1976**, *80* (21), 2352-2362.

[51] Demus D., Inukai T., *Liquid Crystals*, **1999**, *26*(9), 1257-1266.

[52] Maier W., Meier G., *Z. Naturforsch*, **1961**.

[53] Bukowski, R.; Szalewicz, K.; Chabalowski, C. F.; *Journal of Physical Chemistry A*, **1999**, *103*(36), 7322-7340.

[54] Hloucha, M.; Sum, A. K.; Sandler, S. I., *Journal of Chemical Physics*, **2000**, *113*(13), 5401-5406.

[55] Sum, A. K.; Sandler, S. I.; Bukowski, R.; Szalewicz, K., *Journal of Chemical Physics*, **2002**, *116*(17), 7627-7636.

[56] Sum, A. K.; Sandler, S. I.; Bukowski, R.; Szalewicz, K., *Journal of Chemical Physics*, **2002**, *116*(17), 7637-7644.

[57] Fernandez-Ramos, A.; Rodriguez-Otero, J.; Rios, M. A.; Soto, J., *THEOCHEM* **1999**, *489(2-3)*, 255-262.

[58] Osguthorpe D. J., *Proteins* **1999**, *3*, 186-93.

[59] Richardson, Patricia R.; Bates, Simon P.; Crain, Jason; Jones, Anita C., *Liquid Crystals* 2000, *27(6)*, 845-850.

[60] Goodby, John W., *Handbook of Liquid Crystals*, **1998**, *2A*, 411-440.

[61] Clark, S. J.; Adam, C. J.; Ackland, G. J.; Crain, J. Molecular Crystals and Liquid Crystals Science and Technology, Section A: *Molecular Crystals and Liquid Crystals* **1997**, *299*, 39-44.

[62] Gaussian 98 (Version 5.4, Revision A.11.2), M. J. Frisch, G. W. Trucks, H. B. Schlegel, G. E. Scuseria, M. A. Robb, J. R. Cheeseman, V. G. Zakrzewski, J. A.

Montgomery, Jr., R. E. Stratmann, J. C. Burant, S. Dapprich, J. M. Millam, A. D. Daniels, K. N. Kudin, M. C. Strain, O. Farkas, J. Tomasi, V. Barone, M. Cossi, R. Cammi, B. Mennucci, C. Pomelli, C. Adamo, S. Clifford, J. Ochterski, G. A. Petersson, P. Y. Ayala, Q. Cui, K. Morokuma, P. Salvador, J. J. Dannenberg, D. K. Malick, A. D. Rabuck, K. Raghavachari, J. B. Foresman, J. Cioslowski, J. V. Ortiz, A. G. Baboul, B. B. Stefanov, G. Liu, A. Liashenko, P. Piskorz, I. Komaromi, R. Gomperts, R. L. Martin, D. J. Fox, T. Keith, M. A. Al-Laham, C. Y. Peng, A. Nanayakkara, M. Challacombe, P. M. W. Gill, B. Johnson, W. Chen, M. W. Wong, J. L. Andres, C. Gonzalez, M. Head-Gordon, E. S. Replogle,, J. A. Pople, Gaussian, Inc., Pittsburgh PA, **2001**.

[63] Foresman, J. B., Frisch, Æ., *Exploring Chemistry with Electronic Structure Methods: 2nd Edition,* Gaussian, Inc., PA, **1996**.

[64] Boys S.F., Bernardi F., *Molecular Physics,* **1970**, 19(4), 553-566.

[65] Wolbach J. P., Sandler S. I., *AIChE Journal*, **1997**, *43*(6), 1589-1596.

[66] Frisch, Æ., Frisch, M. J., "Gaussian98 User's Reference, Second Edition, Gaussian Inc., PA, **1999**.

[67] Wong, M.W.; Frisch, M.J.; Wiberg, K.B.; Solvent Effects. 1. The Mediation of Electrostatic Effects by Solvents, J. Am. Chem. Soc., **1991**, *113*, 4776.

CHAPTER 3

HYDROGEN-BONDING BETWEEN A DICHROIC DYE AND LIQUID-CRYSTAL FORMING MOLECULE, FOR APPLICATION TO LCDs

Abstract

The performance of guest-host type liquid crystal displays (LCDs) is governed by the solubility and dissolution stability of dichroic dyes in the liquid crystal medium in guest-host kind of LCDs. The solubility and stability is influenced by hydrogen-bonding between the dye and the liquid crystal host. An earlier work was carried out to study the hydrogen-bonding behavior of 4-pentyl-4'-cyanobiphenyl (5CB) (liquid crystal), benzonitrile, and acetonitrile, with 1-hexanol in CCl_4 using FTIR spectroscopy, ab initio and equation of state calculations [1]. To gain further thermodynamic understanding, hydrogen-bonding behavior of (5CB) (liquid crystal), benzonitrile, and acetonitrile, with a dichroic dye Disperse Red1 (DR1) {2-[ethyl[4-[(4-nitrophenyl)azo] phenyl]amino] ethanol} in CCl_4 were studied in this work. In all three mixtures, –OH acts as a hydrogen-bond donor and –CN acts as hydrogen-bond acceptor. Based on FTIR analysis for DR1/acetonitrile, DR1/benzonitrile, and DR1/5CB, the enthalpy of hydrogen-bond formation are –24.2, –23.7, and –3.7 kJ/mol, respectively; and the entropies of hydrogen-bond formation is –58.9, –58.1, and

–0.4 J/mol/K, respectively. Though, for DR1/5CB, enthalpy of h-bonding is not too negative, the entropy of h-bonding is more favorable; hence the h-bonding appears to be entropically driven. Lattice fluid hydrogen bonding (LFHB) parameters obtained from the spectroscopic data were observed to match well with the experimental trends. LFHB equation of state was then used to predict hydrogen bonding for a wider range of conditions.

Keywords: hydrogen-bonding, liquid crystal, dichroic dye, FTIR, LFHB

Introduction

Hydrogen-bonding plays an important role in the properties and use of liquid crystals in various applications [2,3,4]. Hydrogen-bonding is defined as the attraction between a donor hydrogen atom and an electronegative hydrogen acceptor atom usually, a lone pair of electrons [5]. Hydrogen-bonds are responsible for maintaining small polar molecules like water and alcohols in liquid state at room temperature. H-bonds (–10 to –40 kJ/mol) are weaker than ionic bonds (–200 to –400 kJ/mol) but stronger than van der Waals interaction (–0.5 to –1 kJ/mol) [6,7].

Fourier transform infrared (FTIR) spectroscopy is an important tool for determining the extent of H-bonding interactions [8]. Free and H-bonded species have molecular vibrations at different infrared frequencies. For example, the fundamental vibrational stretching frequency for non-H-bonded –OH species is observed at 3,600-3,640 cm^{-1}, while the vibrational band for H-bonded –OH

species is in the range 3,000-3,400 cm^{-1} though these values may vary depending upon the solvent used [9]. The corresponding overtone bands are found at approximately 7,100 cm^{-1} and 6,900 cm^{-1} for free and H-bonded species, respectively [10,11,12,13,14,15].

The application of H-bonding has been widely extended to various thermodynamic processes of industrial importance [16,17] and fundamental research [18,19,20]. A recent application is in enhancing the performance of liquid crystal displays (LCDs) by the formation of a hydrogen-bond between the liquid crystal and dichroic dye dissolved in it [21,22,23].

Liquid crystals are substances that exist as a metaphase between solid and liquid phases within a certain range of temperature. Some compounds exists as liquid crystals within a certain range of temperature (e.g. cyanobiphenyls). Some can be formed by the association of H-bonding donors (e.g. carboxylic acids) and the acceptors (e.g Nitrogen containing compounds like azoles or pyridines). Various temperature dependent and time dependent FTIR studies have been conducted on such liquid crystals for various applications from thermotropic liquid crystalline polymer to biodegradable polymer. For example, using temperature variable FTIR, two dynamic equilibria of hydrogen bonding molten liquid crystalline complex of 4-hexyloxybenzoic acid and 4,4'-bipyridine was observed [24]. Investigations into the changes in molecular structure during the phase transition by temperature dependent FTIR and FT-Raman spectroscopy,

for H-bonded complex of *trans*-butene diacid (proton donor) and 4-(2,3,4-tridecyloxybenzoyloxy)-4-stilbazoles (proton acceptor) concluded that the intermolecular hydrogen bonding is stable in the liquid crystalline phase but weakens with temperature to form an isotropic phase [25]. A study has also been carried out using theory of polymer association combined with McMillan's molecular theory of liquid crystallization that shows the formation of liquid crystalline materials through intermolecular hydrogen-bonding between carboxylic acids with alkyl or alkoxy terminal groups [26]. Also, a self assembling liquid crystal having an angular structure through intermolecular H-bonding of 1:2 mole ratio of a bifunctional donor (phthalic acid, isophthalic acid or terephthalic acid) with trans-4-heptyl/octyl/decyl-4'-stilbazoles acceptors was devised [27]. Another self-assembling supramolecular liquid crystal was synthesized [28] where linear mesogenic structures were obtained by 1:1 association of 4-butoxybenzoic acid (H-bond donor) and trans-[(4-ethoxybenzoyl)oxy]-4-stilbazole (H-bond acceptor).

Other than liquid crystal thermometers, in optical imaging and medical applications [29] the major application of liquid crystals is in LCDs. It consists of two panels with polarization perpendicular to each other. The liquid crystal is filled as an active ingredient between the two panels with dichroic dye dissolved in it.

Dichroic dyes are long rod-like optically active compounds that possess a property of absorbing plane polarized light more along one molecular axis as compared to the other. When dissolved in a liquid crystal, these molecules reorient themselves so that their long molecular axes align with the LC-director [30]. The liquid crystal molecule responds to the change in the electric field by orienting themselves in the direction of the electric field and H-bonded dichroic dyes [31,32] depending upon their molecular orientation, absorb light in a specific wavelength range and exhibit optical properties for the visibility of the LCD pixels. The dichroic dyes appear to control the performance of the LCDs, as even a 0.1% dye can enhance the optical torque acting on the liquid crystal molecules by almost two orders of magnitude [33].

A new kind of LCD element has been devised [34] where a hydrogen bond donor H-bonds with an acceptor and at least one of them exhibits absorption in the visible light range representing a dye. Their emphasis was on changing the molecular properties of the dye by changing the functional groups of the molecule in order to increase the solubility of the dye in the liquid crystal medium.

Due to the need for rationale design of liquid crystal/dichroic dye pairs, the objective of this work was to study the H-bonding behavior of liquid crystalline compounds. This was achieved by studying the H-bonding interaction between –CN and –OH functional groups; –CN being a functional

group present in the liquid crystal and –OH being a functional group present in the dichroic dyes. Apparently, the performance of the LCDs is governed by the dichroic dye properties and the strength of H-bonding between the dye and liquid crystal. Hence, the ultimate design goal is to look for dyes that exhibit strong and stable H-bonding with the liquid crystal.

We have recently conducted a study of H-bonding interactions of 1-hexanol as a H-bond donor with three nitriles acceptors: acetonitrile, benzonitrile and 4-pentyl-4'-cyanobiphenyl (5CB) liquid crystal [1]. In this work, H-bonding of dichroic dye, (2-[ethyl[4-[(4-nitrophenyl)azo]phenyl]amino] ethanol), with the same three nitriles is studied using FTIR spectroscopy and LFHB equation of state. A representation of the H-bond between the dye and the liquid crystal is shown in Figure 1.

Choice of H-bonding Mixtures and Solvent

A suitable solvent for FTIR is one which does not interact with the alcohol and the cyanides, and is transparent in infrared region of –OH vibration. However, it should be polar enough in order to dissolve polar compounds like alcohol and the cyanides. CCl_4 is not a polar solvent but has a quadrapole moment which helps is solubilizing the polar compounds like alcohol and cyanides to some extent. CCl_4 has also been used before as a solvent for studying the H-bonding behavior of various H-bond donors and acceptors [35]. Hence, CCl_4 is selected for spectroscopic studies in this work.

The choice of nitriles was made in order to develop a fundamental understanding and follow a trend in the interaction between –CN and –OH functional groups because the liquid crystal has a –CN functional group towards one end of the aromatic ring chain. Hence, in order to obtain a trend in the hydrogen bonding behavior, an increment is made from acetonitrile having just a $–CH_3$ end group to benzonitrile with a benzene ring followed by the liquid crystal having a biphenyl structure with pentyl chain at the other end of the ring chain. H-bonding studies were conducted [36] between liquid water and acetonitrile using infrared absolute integrated absorption intensities observed due to –C≡N stretching vibration [37] between 2275 and 2210 cm^{-1}, and concluded that the interaction is a result of H-bonding between lone pair electrons on the –C≡N group and the proton of the –OH group. A recent study on H-bonding between benzonitrile and water by ab initio calculations using hybrid B3LYP density functional in conjugation with 6-31+G(d,p) and aug-cc-pVDZ basis sets showed similar results [38].

The purpose of this work is to understand the H-bonding effects between a dye and the liquid crystal. The liquid crystal has a –CN functional end group and the dye has an –OH functional end group. The dye is basically an alcohol, namely (2-[ethyl[4-[(4-nitrophenyl)azo]phenyl]amino] ethanol), with the second carbon of ethanol being N-substituted to an azobenzene and hence is linear in structure.

The structures of free and H-bonded molecules in this study are shown in Figure 2. The dye is very sparingly soluble in CCl_4, with the solubility of only 1mM/L. In the experiments, the concentration of the dye is taken low enough such that no self H-bonding occurs, and only cross H-bonding of –OH with –CN is possible.

Experimental Work

Materials

Disperse red 1 dye {2-[ethyl[4-[(4-nitrophenyl)azo]phenyl]amino] ethanol} (95%) is obtained from Aldrich. Carbon tetrachloride (99.9% HPLC grade, Aldrich), acetonitrile (Certified ACS 99.9 %, Fisher), benzonitrile (99.9% HPLC grade, Aldrich cat. no. 27,031-8), were dried using molecular sieves (Fisher Scientific, pore size 3^{o}A) before using in the experiments. The liquid crystal: 4-pentyl-4-cyanobiphenyl (5CB) (98%) was used as supplied from Aldrich. N_2 gas (grade 5.0, BOC gases) is used to purge the compartments of the FTIR spectrometer to remove the background moisture.

Apparatus and Procedure

A schematic of the apparatus is as shown in Figure 3. It consists of a mixing chamber (*C*) where the solution to be analyzed by infrared is taken. A reciprocating pump (*P*) [Fluid Metering, Inc., model QG 400] was used to pump

the solution from the mixing chamber to the FTIR cell. A six-port injection valve (V) (Rheodyne Model 7010) was installed inline for addition of external sample to the solution using a micro-liter loop of 5, 20 or 200 μL volume, as needed. Two temperature sensors (T_s) and a temperature controller (T_c) device (Cole Parmer Digi-Sense model 2186-20) were installed for temperature control. Heat was supplied using a heater through a 1/16th inch stainless steel heating coil. The IR cell and all the tubings were insulated with foam for a better temperature control. A liquid sampling cell (not shown in the figure) was used to carry out the IR-analysis using a Perkin-Elmer Spectrum 2000 FTIR. The IR cell (made in-house) contains sapphire windows separated by teflon spacers with a spacing of about 1-1.5 mm. For experiments below room temperature, a cooling coil (made in-house from 1/16th inch stainless steel tubings) was connected in series to the flow circuit.

The dichroic dye is sparingly soluble in CCl_4. Hence, a known quantity of solid dye is mixed in CCl_4 and left for shaking over-night. The undissolved dye is then filtered out using a Cole Parmer 0.2 μm PTFE NP 25 mm filter unit leaving behind a clear red solution. Using a predetermined UV-visible spectroscopy calibration at 487nm, the concentration of the saturated solution of dye in CCl_4 is determined.

The FTIR spectrometer was initially purged with nitrogen to remove ambient moisture for atleast half an hour before starting the experiment. To

proceed with the experiment, 40 ml CCl_4 solvent was taken in the mixing chamber and pumped through the cell. The temperature was maintained at 30 ± 0.1°C. After achieving a steady flow of CCl_4 through the liquid sampling cell, FTIR-background of pure CCl_4 was recorded. This liquid was then replaced by a 40 ml solution of dichroic dye in CCl_4 and a sample FTIR spectrum was recorded. Then acetonitrile was added at constant dye concentration using the 20 μL injection loop to study the cross association of acetonitrile with the dye. An average of 50 IR scans over 5 minutes was taken with 0.1 cm^{-1} resolution in order to reduce the noise/signal ratio. Acetonitrile quantity was then increased from 0 to 400 μL with 20 μL increments to obtain a series of –OH and –CN peaks. Similar experiments are performed for benzonitrile and 5CB. All the experiments are then repeated at 45 and 55°C.

Results and Discussion

Figure 4 shows the FTIR spectra of the dye DR1 with acetonitrile in CCl_4 solvent at 30°C. The concentration of the dye in CCl_4 is low enough (~1 mM/L) to avoid any self-association. Hence, spectra of cross association of dye dissolved in CCl_4 with increasing concentration of acetonitrile from 0-192 mM were taken with CCl_4 as the background solvent. Free and bonded –OH peaks were observed at 3638 cm^{-1} and 3555 cm^{-1}. Similar spectra were recorded for benzonitrile from 0 to 98 mM (Figure 5) and for 5CB from 0 to 40 mM (Figure 6).

The experiments were then repeated for 45 and 55°C. Figure 7 shows FTIR spectra for 5CB with the dye at constant concentrations but varying temperature. Free –OH concentration was determined from the area under the peak at 3638 cm^{-1}. Extinction coefficients needed were determined experimentally from spectra of the dye DR1 in CCl_4. Bonded –OH was determined by difference of total and free –OH concentrations. Percentage H-bonding increases with increasing cyanide concentration as shown in Table 1. Assuming 1:1 H-bonding, bonded –CN concentration was equal to the bonded –OH concentration. Free –CN concentration was then determined by difference of total and bonded –CN.

The equilibrium constant (*K*) for H-bond formation was obtained from free and bonded –OH, and –CN concentrations:

$$K = \frac{[Bonded\ -OH]}{[Free\ -OH][Free\ -CN]}$$

K values were found to vary from 12.28 to 5.9 L/mol for an association of DR1/acetonitrile, 11.28 to 5.5 L/mol for DR1/benzonitrile and from 4.07 to 3.55 L/mol for DR1/5CB H-bonding in the temperature range of 30-55 °C as shown in Table 2. These are similar to *K* values for other similar H-bonding; [39,40] 4.89 L/mol for phenol/acetonitrile and 3.45 L/mol for phenol/benzonitrile, 1.02 L/mol for methanol/acetonitrile, 0.87 L/mol for methanol/ propionitrile and 0.87 L/mol for methanol/benzonitrile. Lopes and Thompson41, for H-bonding between phenol and acetonitrile in tetrachloroethylene, observed a decrease in *K*

from 5.62 to 1.52 L/mol with increase in temperature from 23 to 78°C, which is consistent with the trend we have observed, due to increase in the thermal energy.

Enthalpy (ΔH) and entropy (ΔS) of H-bonding were obtained from a plot of lnK versus $1/T$ as shown in Figure 8, as slope and y-intercept, respectively. These values are shown in Table 3. The trend we observed from acetonitrile to benzonitrile to 5CB agrees with the trend observed by Lopes and Thompson[41] for phenol/acetonitrile (ΔH = –21.8 kJ/mol and ΔS = –58.6 J/mol/K) and for phenol/benzonitrile (ΔH = –19.3 kJ/mol and ΔS = –51.9 J/mol/K).

However, a somewhat different result was obtained here as compared to the results obtained for the hydrogen bonding of cyanides with 1-hexanol [1]. There are minor variations in the equilibrium constants (K), enthaly (ΔH) and entropy (ΔS) between DR1/acetonitrile and DR1/benzonitrile at temperatures observed. But, the values for DR1/5CB are very different. This observation could be attributed to the fact that both acetonitrile and benzonitrile are smaller molecules as compared to the dye molecule and therefore have more mobility (less steric effect) thereby exhibiting better hydrogen-bonding with the dye. On the other hand, the molecular size of 5CB is comparable to that of dye and therefore has a restrained mobility as compared to the other cyanides in the H-bonded state. Even though, the enthalpy of H-bond formation is low in this case (–3.7 kJ/mol), the stability of H-bond formation is controlled by the entropy of

the system. Hence, the H-bond with the dye and 5CB is entropy controlled. All these experiments were conducted in CCl_4 as the solvent medium. In actual case of an LCD, there is no solvent present. Hence, in the pure liquid crystal medium, the liquid crystalline order, compactness and reduced mobility of the dye and high viscosity of the liquid crystal medium may enhance hydrogen-bonding making the association stronger. This increased hydrogen bonding association would lead to increase in the order parameter of the liquid crystals [42,32] and is believed to enhance the optical response of the liquid crystal medium to the change in electric field [43]. No experimental studies were carried out to determine if hydrogen bonding increased the solubility of the dyes in the liquid crystal medium because the objective of this study was to determine the presence and thermodynamic stability of hydrogen bonding between the dyes and the liquid crystal molecules. However, given that there exists a hydrogen bonding between the two molecules, one could fairly presume that the hydrogen bonding interactions could lead to increase in the solubility of the dyes in the liquid crystal medium.

Such difference was not observed in the hydrogen-bonding study of cyanides with 1-hexanol [1], because the molecular size of 1-hexanol lies somewhere between benzonitrile and the liquid crystal thereby exhibiting a gradual change in hydrogen-bonding. The results clearly show a difference

between the hydrogen-bonding extent of the cyanides with 1-hexanol versus the actual dye.

A better dye could be one with –OH group present at the other end with para substitution on the polarizable aromatic ring as shown in Figure 9. This dye has a higher length to breadth ratio, therefore has a higher dicroic ratio and has –OH group attached to a polarizable atomic ring which delocalizes electron cloud better than the aliphatic groups, thereby favoring hydrogen-bonding.

Equation of State Modeling

Recent equations of state for H-bonding mixtures are based on chemical equilibria approach, [44] perturbed-hard-chain theory, [45,46] statistical association fluid theory, [47,48] mobile and static molecular disorder, [49] and lattice-fluid-hydrogen-bonding (LFHB) [50,51,52,53,54]. In order to model the liquid crystalline phases, statistical theories like Onsager theory with hydrogen bonding free energy term [55] and others [56,57] could be used that were developed specifically for liquid crystals. However, the mixture under consideration in this study was not a liquid crystalline phase. It was 5CB and the dye dissolved in CCl_4 in mM quantities thereby CCl_4 occupying the major bulk of the solution medium. Not being a liquid crystalline phase give rise to significant molecular randomness. In order to correctly utilize our spectroscopic data, we have used LFHB theory here because its general form is valid for regular liquid

mixtures containing multiple H-bondings and is applicable over a wide range of conditions. In this theory, H-bonding contribution of the partition function is derived from the number of ways of distributing the H-bonds among the donor and acceptor groups in the mixture. The donor and acceptor must be in close spatial proximity as described by a mean field probability [58]. The LFHB equations are well established by Panayiotou and Sanchez [50] and applied to various thermodynamic problems [51] including a ternary mixture of a H-bond donor, a H-bond acceptor, and an 'inert' solvent. For a system of N_1 molecules of type 1 (DR1), N_2 molecules of type 2 (nitriles) that form N_{12} number of H-bonded species by cross-association in N_3 molecules of inert solvent of type 3 (CCl_4) at temperature T and pressure P, LFHB equilibria can be written as:

$$\ln\left[\frac{r}{\tilde{\rho}}\frac{N_{12}/N}{\left(N_1/N - N_{12}/N\right)\left(N_2/N - N_{12}/N\right)}\right] = -\frac{E_{12}^0 + PV_{12}^0}{RT} + \frac{S_{12}^0}{R} = -\frac{G_{12}^0}{RT}$$

where, $N = N_1 + N_2 + N_3$, r is average segment length, $\tilde{\rho}$ is reduced density, and E^0_{12}, V^0_{12}, S^0_{12} are standard energy, volume, and entropy of H-bonding, respectively.

Using spectroscopic values of N_1/N, N_2/N, N_3/N and N_{12}/N from the previous section, $\tilde{\rho}$ and r for pure CCl_4 (since dye and nitriles are very dilute),59 ΔG^0_{12} for DR1 with all the nitriles are calculated. $\Delta G^0_{12}/T$ is then plotted versus $1/T$ to obtain ($E^0_{12} + PV^0_{12}$) as the slope and S^0_{12} as the intercept. Using P = 1atm

and V^0_{12} = –5.6 cm^3/mol as reported by Gupta et al.[51], E^0_{12} and S^0_{12} were evaluated (Table 4).

Now with the availability of LFHB parameters, H-bonding calculations can be made for the conditions where experimental data is not available. We have done LFHB calculation at 0, 30 and 60^{o}C for a wide range of nitrile concentrations (0-1000 mM) as shown in Figure 10 for DR1/acetonitrile, Figure 11 for DR1/benzonitrile and Figure 12 for DR1/5CB.

Conclusion

H-bonding was observed between the –OH group of the dichroic dye Disperse Red 1 and –CN groups of acetonitrile, benzonitrile and 5CB liquid crystal molecules. The extent of H-bonding decreases from acetonitrile to 5CB. The enthalpy of H-bond formation becomes less negative from acetonitrile to 5CB, but the entropy of H-bonding becomes less negative from acetonitrile to 5CB to a greater extent. The H-bonding in the liquid crystal with the dye appears to be controlled more by entropic interactions. Parameters for LFHB equation of state are estimated from the experimental data and the extent of hydrogen-bonding derived from these data are found to fit well with the experimental data. H-bonding is then predicted for a wide range of conditions.

Table 1. Percentage hydrogen bonding for increasing cyanide concentration at constant dye concentration of 1mM/L at different temperatures.

H-bond Acceptor	Temperature (^{o}C)	Concentration (mM/L)	%H-bonding
Acetonitrile	30	134.8	60
	30	144.4	64
	30	154.0	65
	45	173.3	56
	45	182.9	58
	45	192.5	62
	55	173.3	50
	55	182.9	55
	55	192.5	57
Benzonitrile	30	88.6	50
	30	93.5	53
	30	98.4	55
	45	88.6	44
	45	93.5	46
	45	98.4	48
	55	88.6	35
	55	93.5	37
	55	98.4	40
5CB	30	28.4	10.6
	30	30.5	10.9
	30	32.5	11.5
	45	28.4	7.2
	45	30.8	8.7
	45	32.5	9.9
	55	28.4	8.7
	55	30.5	9.2
	55	32.5	9.5

Table 2. Equilibrium constant for hydrogen-bond formation at different temperatures in CCl_4. The errors in *K* values are about ±0.3 $(mol/L)^{-1}$.

H-bonding	T (K)	K $(mol/L)^{-1}$
Disperse Red 1 ---Acetonitrile.	303	12.3
	318	7.9
	328	5.9
Disperse Red 1 ---Benzonitrile	303	11.3
	318	7.3
	328	5.5
Disperse Red 1 ---5CB	303	4.1
	318	3.9
	328	3.6

Table 3. Enthalpy, Entropy and Free Energy of hydrogen bonding for dye DR1 with acetonitrile, benzonitrile and liquid crystal in CCl_4

Associations	$\Delta(H)$ kJ/mol	$\Delta(S)$ J/mol/K	ΔG at 298 K (kJ/mol)
Dye DR1/ACN	-24.2±0.7	-58.9±0.7	-6.6±0.7
Dye DR1/BzCN	-23.7±0.8	-58.1±0.8	-6.4±0.8
Dye DR1/5CB	-3.7±0.1	-0.4±0.1	-3.6±0.1

Table 4. Lattice-Fluid Hydrogen-Bonding Parameters.

Components	S^0_{12} J/mol/K	E^0_{12} kJ/mol
Dye DR1/ACN	-22.19	-23.74
Dye DR1/BzCN	-22.33	-22.40
Dye DR1/5CB	-12.01	-18.55

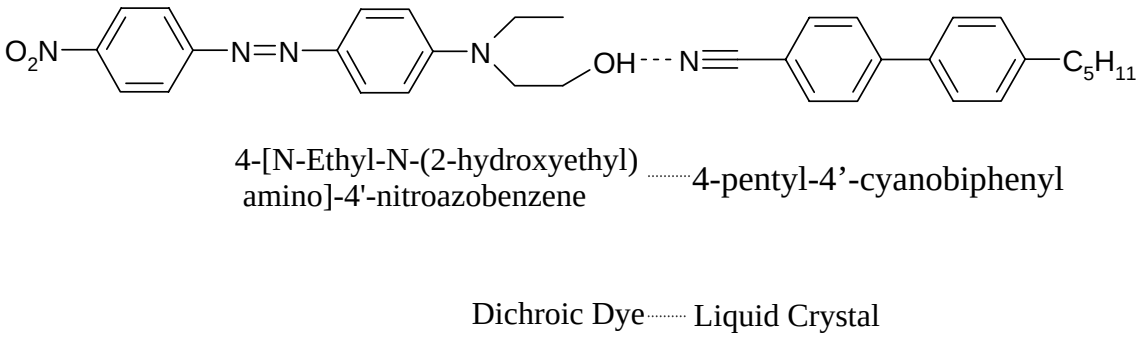

Figure 1. Hydrogen bonding between a dichroic dye and a liquid crystal.

(A) Individual Molecules

1. Hydrogen Bond Acceptors

CH_3CN Acetonitrile

Benzonitrile

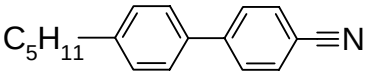

4-pentyl-4'-cyanobiphyl (5CB)

2. Hydrogen Bond Donor

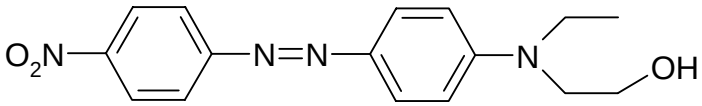

Dye DR1

(B) Hydrogen Bonded Structures:

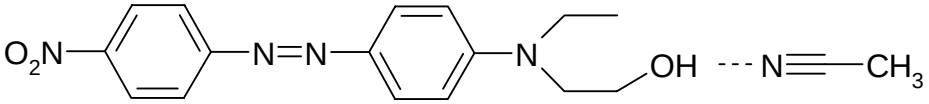

DR1---Acetonitrile

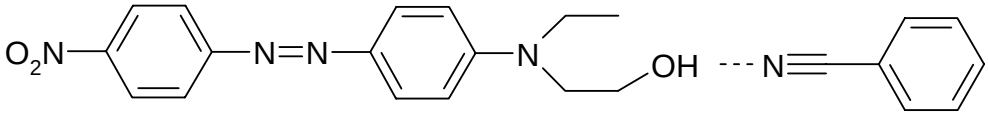

DR1---Benzonitrile

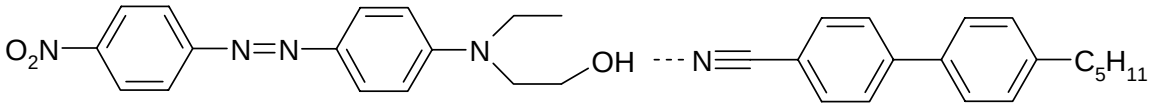

DR1---4-pentyl-4′-cyanobiphenyl (5CB)

Figure 2. Structures of the free and H-bonded molecules used in the experiment.

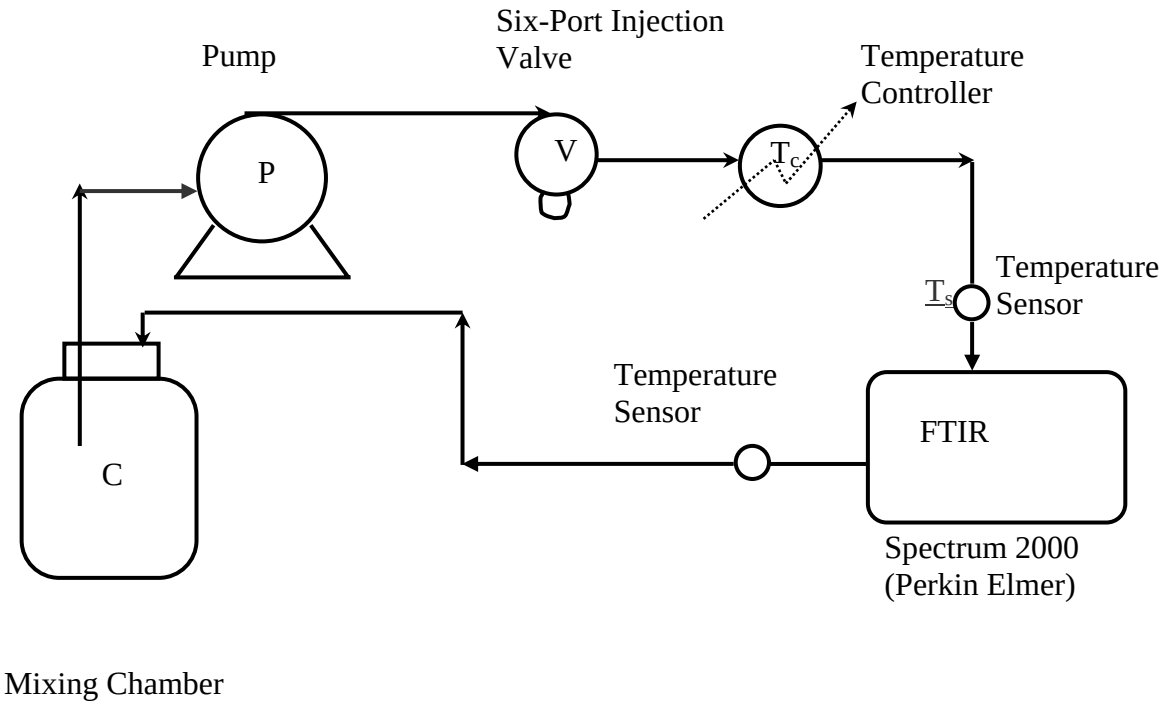

Figure 3. Schematic of the hydrogen-bonding FTIR apparatus.

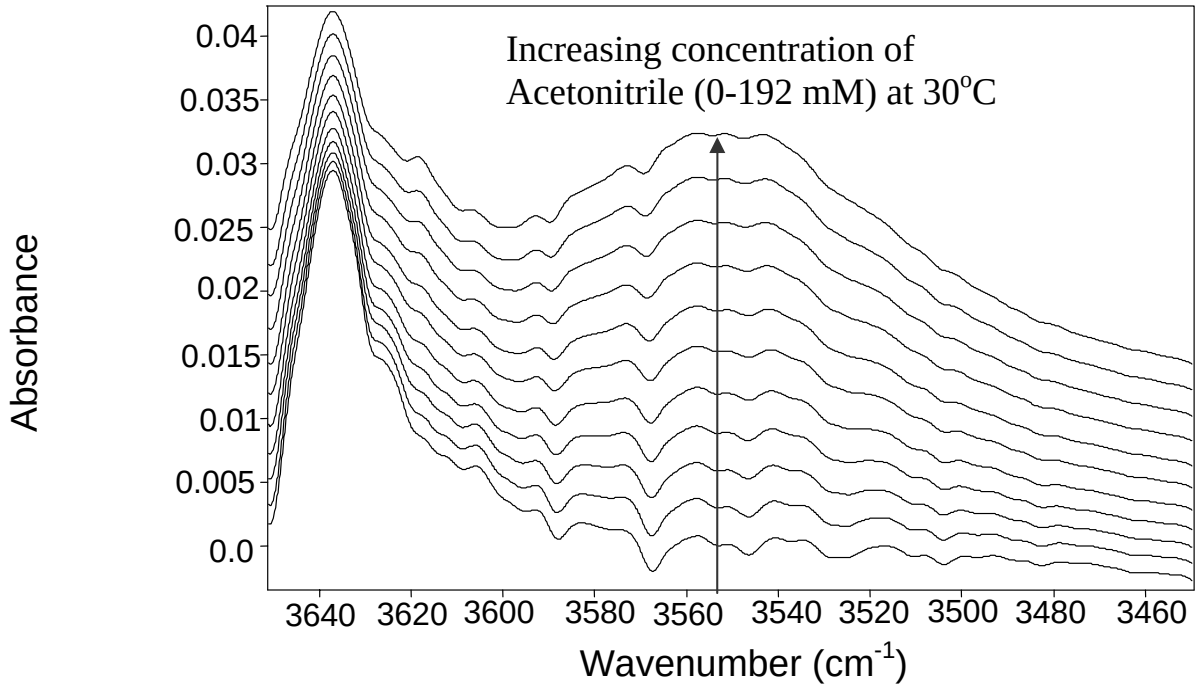

Figure 4. FTIR Spectra showing free and H-bonded –OH peaks for increasing concentration of acetonitrile.

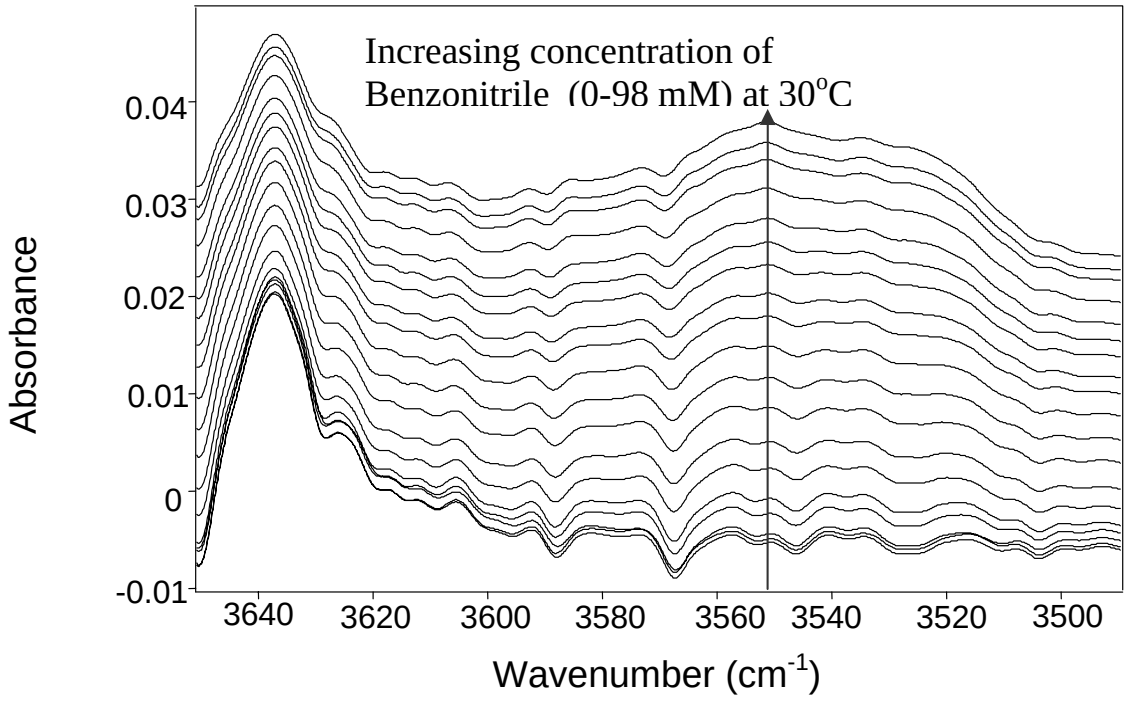

Figure 5. FTIR Spectra showing free and H-bonded –OH peaks for increasing concentration of benzonitrile.

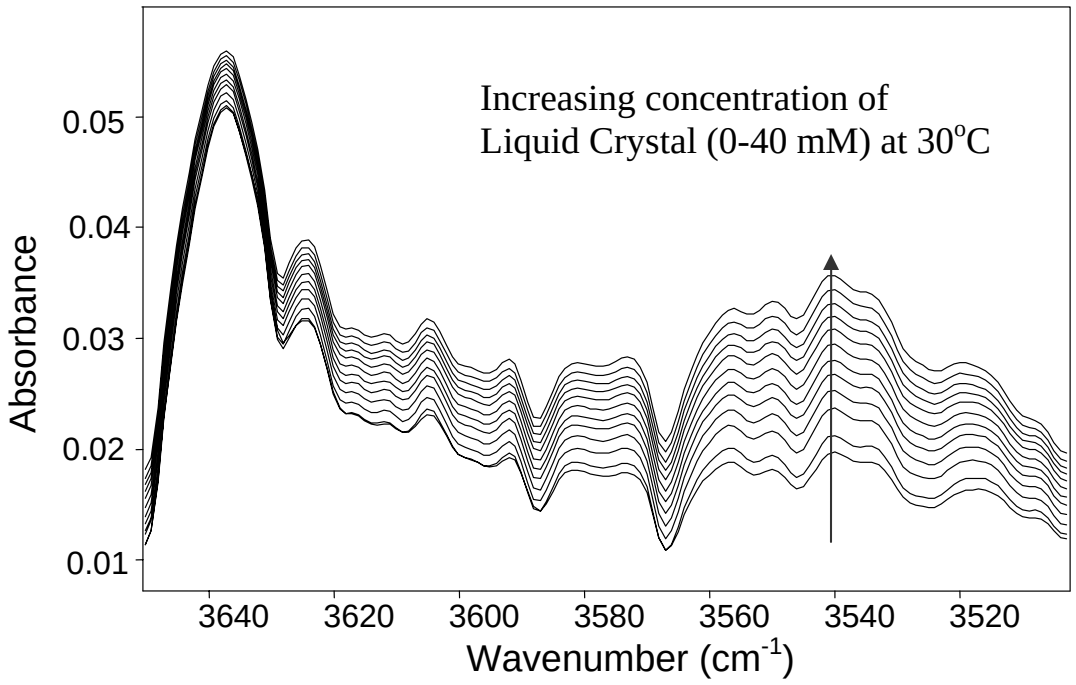

Figure 6. FTIR spectra showing free and H-bonded –OH peaks for increasing concentration of liquid crystal.

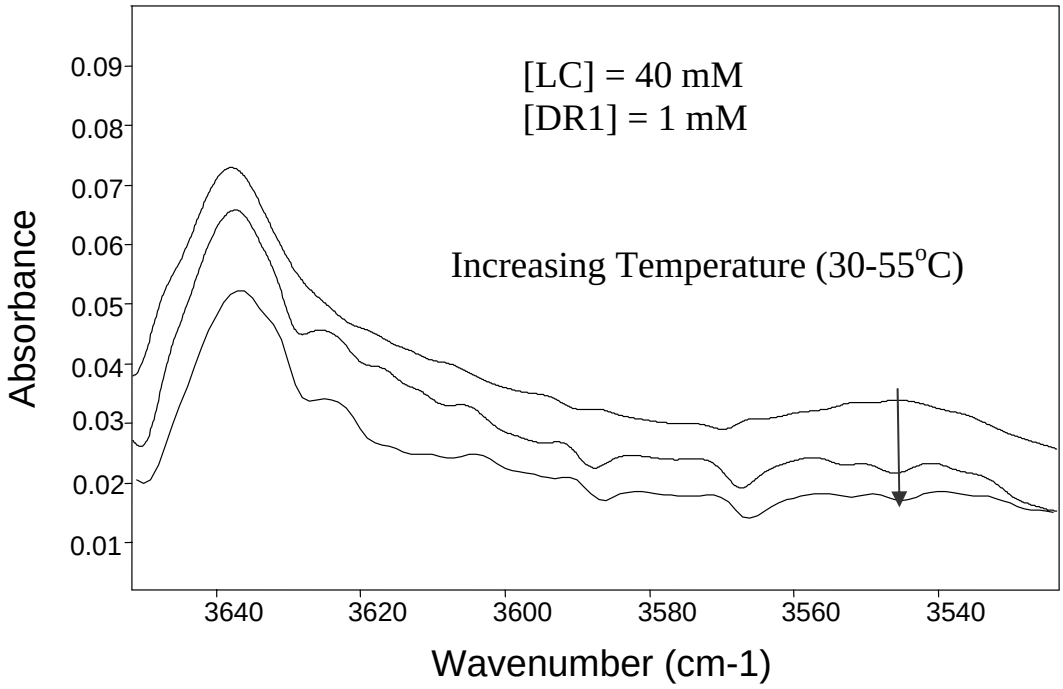

Figure 7. FTIR Spectra showing free and H-bonded –OH peaks for constant concentration of acetonitrile and dye DR1 at different temperatures.

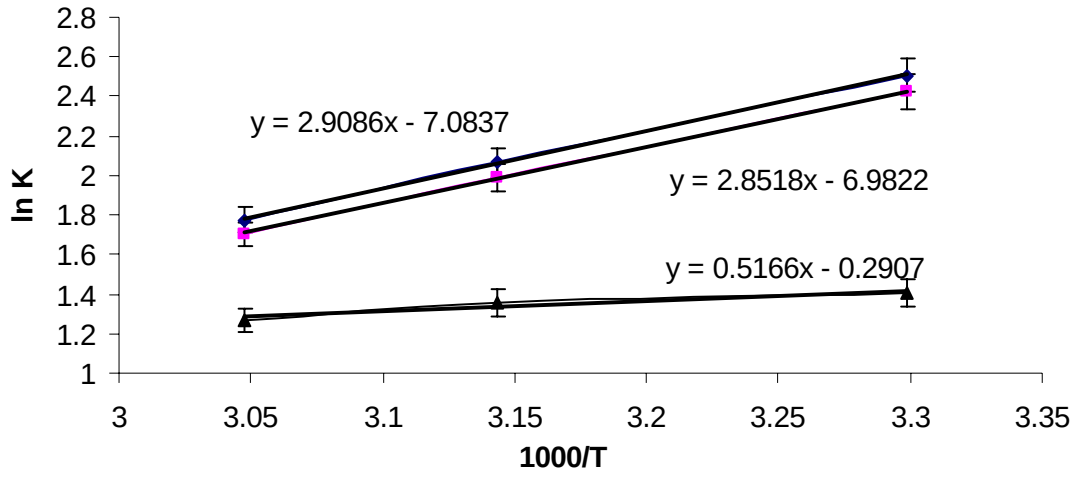

Figure 8. Temperature dependence of equilibrium constants, from Table 2.

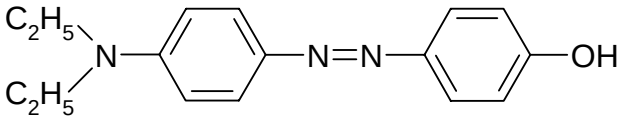

a) Dichroic Dye: 4-[[4-(diethylamino)phenyl]azo] phenol

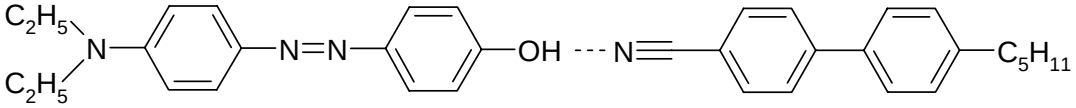

b) Hydrogen-bonding between 4-[[4-(diethylamino)phenyl]azo] phenol (dichroic dye) and 5CB (liquid crystal).

Figure 9. Proposed dye for hydrogen-bonding.

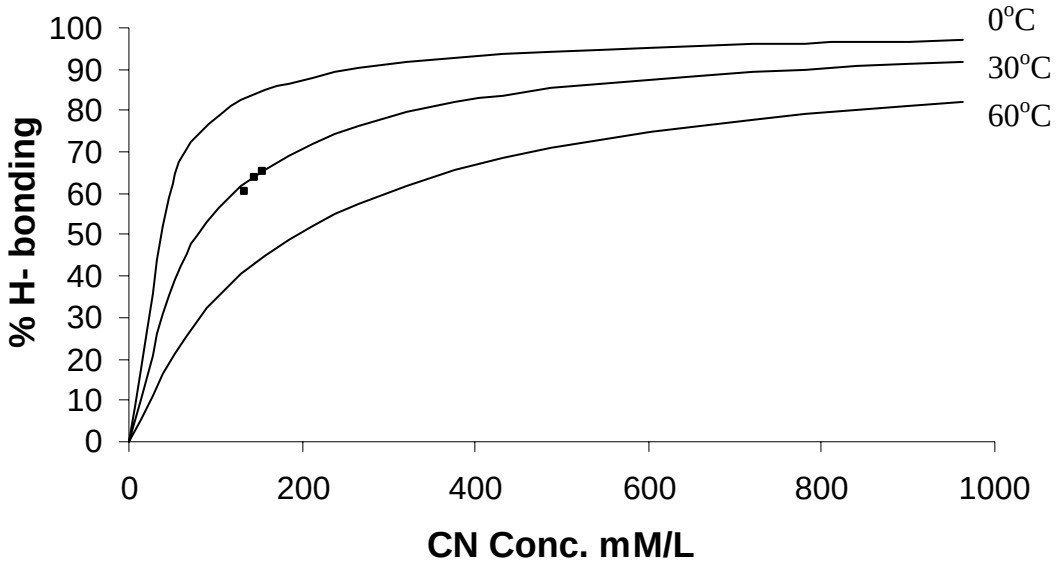

Figure 10. H-bonding between dye DR1 (1.0 mM) and increasing acetonitrile concentration. (Points are spectroscopic data and lines are result from LFHB model)

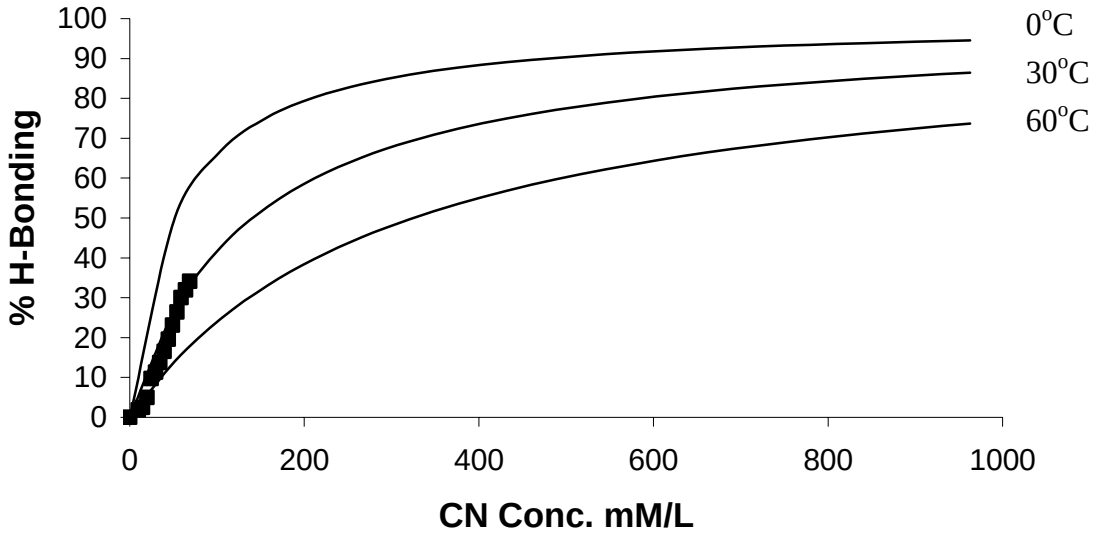

Figure 11. H-bonding between DR1 (1.0 mM) and increasing benzonitrile concentration. (Points are spectroscopic data and lines are result from LFHB model)

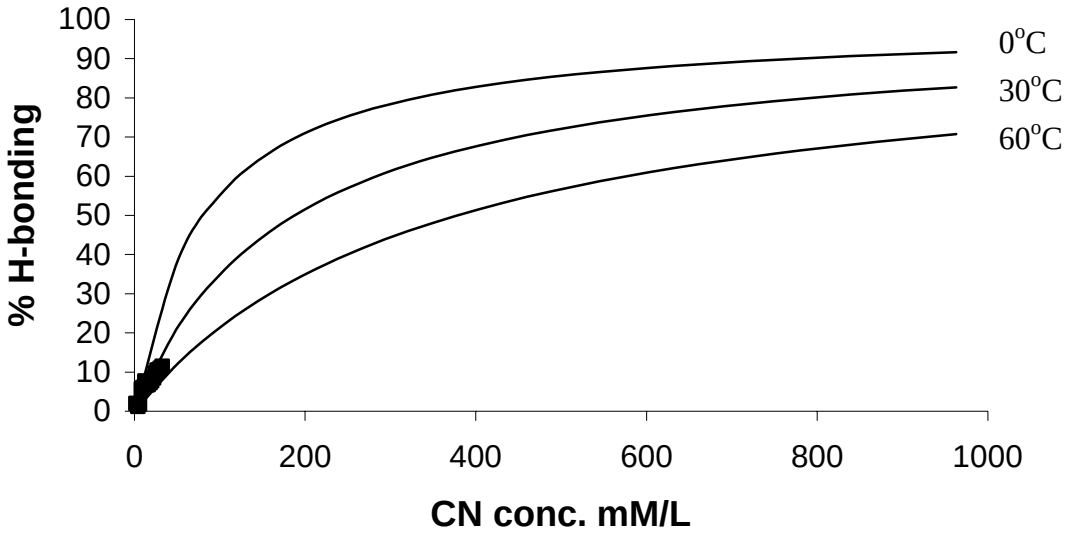

Figure 12. H-bonding between DR1 (1.0 mM) and increasing 5CB concentration. (Points are spectroscopic data and lines are result from LFHB model)

References

[1] A. J. Thote; R. B. Gupta, Ind. & Eng. Chem. Res. 42 (2003) 1129-1136.

[2] K. Matsuoka and K. Kawata, US Patent No. 6,444,280, 2002.

[3] Taihei Kawakami and Takashi Kato, Macromolecules 31 (1998) 4475-4479.

[4] S. Okada, K. Mizutani, K. Sato, H. Munakata, A. Tsuboyama, US Patent no. 6,221,444, 2001.

[5] G. C. Pimentel, and A. L. McClellan, The Hydrogen Bond, Freeman and Co., San Francisco, CA, 1960.

[6] J. M. Prausnitz and R. N. Lichlenthater and E. G. de Azevedo, Molecular Thermodynamics of Fluid Phase Equilibria, 3rd Edition, Chapter 6 Prentice-Hall, Englewood Cliffs, NJ, 1986.

[7] P. L. Huyskens, W. A. P. Luck, and Th. Zeegers-Huyskens, eds., Intermolecular Forces. An Introduction to Modern Methods and Results, Springer-Verlag, Berlin, 1991.

[8] R. L. Brinkley and R. B. Gupta, AIChE Journal 47 (2001) 948-953.

[9] S. Martinez, Methanol/Hexane Systems: I. Infrared Studies, Spectrochimica. Acta 42A (1986) 531.

[10] M. M. Coleman, P. C. Painter, Progress in PoIy. Sci. 20 (1995) 1.

[11] M. M. Coleman, C. J. Serman, D. E. Bhagwagar, and P. C. Painter, A Practical Guide to Polymer Miscibility, Pober 31 (1990) 1187.

[12] W. A. P. Luck, H. Borgholte, T. Habermehl, J. Molecular Structures 177 (1988) 523.

[13] W. A. P. Luck, Angewandte Chemie, Int. Ed. Eng. 19 (1980) 28.

[14] I. G. Economou, M. D. Donahue, AIChE J. 37 (1991) 1875.

[15] J. M. Walsh, M. D. Donahue, Fluid Phase Equiibria 52 (1989) 397.

[16] M. Ikhlaq, Chem. Eng.-London N521 (1992) 21-22.

[17] J. N. Lammers, Oil Gas J. 89 (1991) 50.

[18] E. C. Voutsas, G. C. Boulougouris,; I. G. Economou,; D. P. Tassios, Ind. Eng. Chem. Res. 39 (2000), 797-804.

[19] G. Govil and C. L. Khetrapal, Current Science (India) 34 (1965) 116-117.

[20] G. T. Crisp and Y. L. Jiang,, Tetrahedron Letters 43 (2002) 3157-3160.

[21] S. Kobayashi, Y. Miyazaki, T. Motomura, JP 100254, 2001.

[22] M. Kadowaki, H. Sato, JP 044955, 2000.

[23] M. Matsude, JP 019564, 2000.

[24] H. Xu, N. Kang, P. Xie, R. Zhang, Molecular Crystals and Liquid Crystals 373 (2002) 119-126.

[25] S. Jiang, W. Xu, B. Zhao, Y. Tian, Z. Yanqing; Y. Zhao, Materials Science and Engineering 11 (2000) 85-88.

[26] S. Masahiko and T. Fumihiko, Macromolecules 35 (2002) 7460-7472.

[27] T. Kato, H. Adachi, A. Fujishima, J. M. J. Frechet, Chemical Letters (1992) 265-268.

[28] T. Kato, J. M. J. Fréchet, Macromolecular Symposium 98 (1995) 311-326.

[29] W. S. Park, Journal of the Korean Physical Society 37 (2000) 331-334.

[30] G. H. Heilmeier and L. A. Zanoni, Applied Physical Letters, 13 (1968) 91.

[31] A. Ghanadzadeh, H. Ghanadzadeh, G. Ghasmi, Journal of Molecular Liquids 88 (2000) 299-308.

[32] J. Griffiths, K. C. Feng, Journal of Materials Chemistry 9 (1999) 2333-2338.

[33] L. Marrucci, D. Paparo, P. Maddalena, E. Massera, E. Prudnikova and E. Santamato, J. Chem. Phys. 107 (1997) 9783-9793.

[34] H. Iwanaga and K. Naito, US Patent No. 6057906, 2000.

[35] A. Kolbe, P. Kaps, M. Plass, Z. Phys. Chem. (Munich) 191 (1995) 191-95.

[36] J. E. Bertie, Z. Lan, Journal of Physical Chemistry B 101 (1997) 4111-4119.

[37] D. Jamroz, J. Stangret, J. Lindgren, J. American Chemical Society 115 (1993) 6165.

[38] E. S. Kryachko, M. T. Nguyen, J. Chemical Physics 115 (2001) 833-841.

[39] S. C. White, H. W. Thompsom, Proceedings of Royal Society A291 (1966) 460.

[40] R. K. Thomas R. K., Dissertation, Oxford, 1964.

[41] M. C. S. Lopes, H. W. Thompson, *Spectrochim. Acta* 24A (1968) 1367-1383.

[42] M. Kawaguri, T. Ohtake, N. Wakita, Jpn. Kokai Tokkyo Koho (2001) JP 2001013527.

[43] T. Kato, M. Moriyama, N. Mizoshita, Eur. Pat. Appl. (2003) EP 1338639.

[44] R. A. Heidemann, J. M. Prausnitz, Proc. Natl. Acad. Sci. U.S.A. (73) (1976) 1773-76.

[45] J. M. Walsh, M. D. Donohue, Fluid Phase Equilb. 62 (1989) 397-404.

[46] I. G. Economou, M. D. Donohue, AIChE J. 37 (1991) 1876-1894.

[47] S. H. Huang, M. Radosz, Ind. Eng. Chem. Res. 29 (1990) 2284-2294.

[48] I. G. Economou, M. D. Donohue 116 (1996) 518-29.

[49] P. L. Huyskens, J. Mol. Struct. 274 (1992) 223-246.

[50] C. Panayiotou, I. C. Sanchez, J. Chem. Phys. 95 (1991) 10090.

[51] R. B. Gupta, C. G. Panayiotou, I. C. Sanchez, K. P. Johnston, AIChE J. 38 (1992) 1243-1253.

[52] R. B. Gupta, K. P. Johnston, Fluid Phase Equilib. 99 (1994) 136-161.

[53] R. B. Gupta, J. M. Prausnitz, , Ind. Eng. Chem. Res. 36 (1996) 1226-1230.

[54] R. B. Gupta, R. L. Brinkley, AIChE J. 44 (1998) 207-213.

[55] B. A. Veytsman, J. Chem. Phys. 103 (1995) 2237-46.

[56] S. C. McGrother, R. P. Sear, G. Jackson, J. Chem. Phys. 106 (1997) 7315-7330.

[57] A. G. Vanakaras, D. J. Photinos, Mol. Cryst. Liq. Cryst. Sci. & Tech. Section A: Mol. Cryst. Liq. Cryst. 299 (1997) 65-71.

[58] B. A. Veytsman, J. Phys. Chem. 94 (1990) 8499.

[59] I. C. Sanchez, R. H. Lacombe, J. Phys. Chem. 80 (1976) 2352-2362.

CHAPTER 4

SELF-ASSOCIATION OF STRONG LEWIS ACID- BASE INTERACTIONS BETWEEN SUPERCRITICAL CO_2 AND CARBOXYLIC ACIDS

Abstract

The equilibrium constants for dimerization of three different carboxylic acids in near and supercritical CO_2 and ethane at various temperatures and densities are presented. Fourier-Transform infrared spectroscopy was used to determine the equilibrium constants by examining the C=O stretching frequencies of the monomer and dimer of the acids in solution. The equilibrium constants for formic acid, propionic acid, and trifluoroacetic acid decrease with temperature for both ethane and CO_2 solvents, and strongly depend upon CO_2 solvent density. The density dependence provides evidence for specific solvent-solute interactions between CO_2 and the carboxylic acid functional group, which is attributed to strong Lewis acid-Lewis base interactions. Since carboxylic acids contain both a Lewis acid and a Lewis base moiety, the examination of a strong acid such as trifluoroacetic acid provides insight as to whether CO_2 acts as a Lewis acid or as a Lewis base in these specific interactions. In order to verify these experimental results, *ab initio* computations were carried out to indicate

that carboxylic acids interact strongly with CO_2 as compared to a non-interacting solvent such as ethane.

Introduction

Carboxylic acids are of significant interest because of their importance in both industrial and in biological processes. Carboxylic acids are used extensively as raw materials for a wide array of products including those in the medical and foodstuff industries. Because of the importance of these acids to the human body, such as the role of formic acid in human metabolism[1], a fundamental understanding of these molecules is needed. These molecules are also used both as solvents and as additives and co-solvents under a wide range of conditions. With a thorough understanding of how these molecules interact both with themselves and with other solvents, existing processes may be optimized and new processes may be developed. Because of the emphasis on green engineering and chemistry and because of the wide range of conditions which may be employed, the use of supercritical solvents such as carbon dioxide (CO_2) in applications of carboxylic acids would be attractive. Researchers have investigated self-association of carboxylic acids in a wide variety of solvents[2-9]. Although the general trend of these studies shows that the solute-solvent interactions increase as the solvent becomes more polar, no systematic description of how the acids interact with solvents has been given. Much attention has been given to the effect of solvent density on the equilibrium

constants associated with hydrogen bonding[4,10-12]. The highly tunable density of CO_2[13] which can be used to examine these effects on such acids, along with its environmentally benign nature makes CO_2 in the near- and super-critical states an attractive solvent to study. Moreover, recent research has focused on the design of molecules soluble in CO_2[14,15], so understanding of interactions of these functional groups in carboxylic acids with CO_2 could aid in the design of new CO_2-philic compounds. Although carboxylic acids have been shown to form dimers, trimers, tetramers and even higher order oligomers, the bulk of current literature[3-9] suggest that only the monomer and the cyclic dimer of carboxylic acids exist in any appreciable quantity at low concentrations in the gas phase. This simple single dimerization allows a direct correlation between the density of a solvent and its stabilization of the monomer form of the acid. This provides a quantifiable interaction between the acid and the solvent. With that said, under limited conditions, a linear dimer has been observed for certain acids in certain solvents. Fujii et al.[3] observed a third species for acetic acid in CO_2 solutions with ethanol as a co-solvent. Additionally, Murty and Pitzer have reported that trifluoroacetic acid can exist as a linear dimer in slightly basic solvents, such as benzene[8,9]. The explanation for both of these observations is that the solvents are capable of hydrogen-bonding with the linear dimer forms of the acids, thus decreasing the energy difference between the cyclic and linear dimer forms. Here we investigate the self-association of formic acid, propionic acid, and

trifluoroacetic acid (TFA) in supercritical fluid (SCF) and near-critical CO_2 using Fourier-Transform infrared spectroscopy (FTIR). This allows the examination of the effects of carbon chain length on the dimerization constant as well as the adjustable physical properties of the SCF solvent. Because of the high solubility of perfluorinated compounds in CO_2[14], the use of TFA allows a means to study the influence of this functionality on the dimerization. The non-polar solvent ethane is also employed to provide a comparison of the effects of the solvent type on the acid dimerization of formic acid and propionic acid self-association.

Hence, the objective of the current work is to study the differences in the self-association of these carboxylic acids in an interacting solvent such as carbon dioxide as compared to that in a non-interacting solvent such as ethane. The experimental results obtained by Bell et al.[16] will be used to develop a trend in the enthalpy and entropy of hydrogen bonding of these interaction in the solvent media by the use of *ab initio* computations.

***Ab initio* Computations**

The objectives of the *ab initio* computations are to substantiate the experimental observations and to develop trends in the enthalpy of hydrogen-bond formation for formic acid, propionic acid and trifluoroacetic acid. This is done for the acids in gas phase, in CO_2 and in a non-polar solvent, ethane. Gaussian98[17,18] program was used for performing the *ab initio* computations. H-bonding energies were calculated by evaluating the energy of the H-bonded

complexes and subtracting the energies of the individual molecules from that of the complex. These energies were corrected for basis set superposition error (BSSE) using counterpoise correction method by Boys and Bernardi[19]. The procedure used for carrying out these calculations is also outlined by Wolbach and Sandler[20].

The optimized structures of dimers in gas-phase, in CO_2, and in ethane are shown in Figure 3, Figure 4, and Figure 5 respectively. Four solvent molecules were incorporated around the acid dimer to specifically study the interaction of the solvent molecules, CO_2 or the non-polar ethane with the acids. This allows computation of the enthalpy of dimer formation of formic acid, propionic acid and trifluoroacetic acid on a molecular level. Another possibility could have been to use the Self-consistent Reaction Field (SCRF)[21,22] theory with which the dielectric constant can be changed to that of the solvent. However, doing that alone incorporates only the solvent effect, but does not incorporate the specific molecular interactions between the acids and the solvents. Therefore, SCRF was not used for these computations. Table 1 shows that the hydrogen-bond formation enthalpy decreases significantly in the presence of CO_2 as compared to the gas phase energy. This implies that CO_2 specifically stabilizes the monomer relative to the cyclic dimer shifting the monomer-dimer equilibrium to the monomer side.

However, ethane, being a non-polar solvent, interacts with the acids to a lesser extent than CO_2. Hence, there is very little acid monomer stabilization in the ethane solvent. Therefore, the enthalpies of hydrogen-bond formation are very close to the gas phase values. In the cases of all the acids, there is a small decrease in the enthalpies of hydrogen-bond formation moving from gas phase to ethane solvent, while there is a relatively large decrease when the solvent is changed to CO_2.

The enthalpies of hydrogen-bond formation were observed to decrease in succession from formic acid to propionic acid to trifluoroacetic acid (cyclic) to trifluoroacetic acid (linear) in gas phase computations using HF as a basis function. However, the experimentally observed dimerization energies for trifluoroacetic acid (cyclic) are larger than those of formic acid and propionic acid. This incorrect trend is attributed to the fact that HF does not take into account the electronic correlations which play a major role in hydrogen-bonding. For this reason, calculations were repeated using MP2 basis function to incorporate the electronic effects. The trend observed using MP2 agrees well with the experimental results as seen in Table 1. The dimerization energy calculations for the carboxylic acids in CO_2 and ethane phases are currently in progress.

Establishment of the presence of trifluoroacetic acid linear dimer in CO_2

An unknown peak was observed in the FTIR spectrum of trifluoroacetic acid in CO_2 as solvent under certain conditions of density and temperature as shown in Figure 1. To establish what this peak represents, *ab initio* computations were performed to find the optimized geometry of several species. These species were the trifluoroacetic acid monomer, the cyclic trifluoroacetic acid dimer, the linear trifluoroacetic acid dimer, and a linear association of one molecule each of trifluoroacetic acid and CO_2. This was followed by frequency analyses to identify the peak location of the C=O stretch vibrations. The absolute peak locations, however, do not match the experimental results because the *ab initio* computations were performed in vacuum and do not take into account the solvent shifts. However, the differences between the peak locations of the monomer, cyclic dimer, linear dimer, and trifluoroacetic acid-CO_2 complex corresponded to our experimental differences.

Results and Discussion

Unlike the other acid systems studied which only had two distinct peaks associated with the monomer and cyclic dimer forms, TFA was observed to have three distinct peaks under certain conditions. An example of this is shown in Figure 1. This third peak only exists at the lowest temperature studied. As either the pressure, and consequently density, or temperature of the system is raised, the third spectral band essentially disappears as shown in Figure 2. This

example is given at higher density, though spectra at a higher temperature look very similar as well. *Ab initio* simulations were performed on several geometrical configurations to determine which species could be responsible for this absorbance. Because of the broadness of the peak, we expected that the species had to have an interaction much weaker than the cyclic dimer. Acid-water complexes, acid-CO_2 complexes, and the linear dimer were simulated. The peak locations for the TFA monomer and cyclic dimer were also simulated to determine the magnitude of the solvent shift. The peak location for the linear dimer matched the experimental location once the solvent shift was taken into account. Furthermore, the strength of this interaction according to these simulations is much less than the cyclic dimer interaction. This accounts for the relative breadth of the peak. Therefore the peak, near 1760 cm^{-1} is assigned to the linear dimer. It is well known that CO_2 can act as a Lewis acid[23-25]. We previously suggested that acid-base type interactions can occur with the free electrons on the carbonyl oxygen or with the hydroxyl oxygen, thus stabilizing the monomer. Studies of compounds containing carbonyl groups using *ab initio* computations[26], experimental observations[27,28], and FTIR spectroscopy[24] all supported this idea. In each case, the enhanced solubility of compounds containing carbonyl groups in carbon dioxide was attributed to the free electrons on the carbonyl oxygen interacting with the slightly acidic carbon of CO_2 in a Lewis acid - Lewis Base type interaction. However, our current studies have led

us to believe that CO_2 can act as a Lewis base and interact with the acidic proton. It is therefore possible that either one or a combination of both of these factors is responsible for the solvent-solute interactions in CO_2. Recently, Raveendran and Wallen[29] have used *ab initio* computations to study interactions of sugar acetates containing Lewis base groups with CO_2. This study suggested that a ring like structure can be formed between the sugar and a CO_2 solvent molecule with two hydrogen bonds: one between the carbonyl oxygen and the carbon of CO_2 and the other between an oxygen on the CO_2 and a proton on the methyl group of the acetate, indicating that CO_2 can act both as an electron donor and as an electron acceptor. However, the interaction with carbon dioxide acting as the Lewis acid is stronger. In our studies, the stabilization of the linear dimer of TFA is consistent with the fact that CO_2 is capable of acting as a Lewis base.

Conclusions

Both formic acid and propionic acid hydrogen-bonding studies showed that the monomer form was much more stabilized in CO_2 than in ethane relative to the dimer. As the density of the CO_2 solvent increased, the equilibrium constant decreased strongly, due to the existence of a specific interaction between the acids and the CO_2 solvent. Whereas, the equilibrium constant remained relatively constant as ethane density was increased. Both the acid monomers were stabilized by roughly the same amount relative to the acid dimers as the CO_2 density is increased. Therefore, the carbon number seems to have little

effect on the specific interactions of CO_2 with the acid functional group, suggesting no difference in steric hindrance. TFA did not exist purely as a monomer / cyclic dimer equilibrium in all conditions. Studies showed the existence of a third peak in CO_2 at a low temperature (298 K) and high densities (0.781 - 0.816 g/cm^3) which corresponded to the linear dimer of TFA. All of these results suggest that a combination of Lewis acid-Lewis base interactions between the carbon on CO_2 and the carbonyl oxygen on the acids and between an oxygen on CO_2 and the acidic proton on the acids act to stabilize the monomer. However, the interaction of the CO_2, acting as a Lewis base, with the acidic proton seems to be the dominant solvent-solute interaction. As a result, the ability of CO_2 to act both as a Lewis base (this study) and as a Lewis acid[23] and to have significant interactions should be taken into account when designing CO_2-soluble molecules.

Acknowledgements

Financial support from the National Science Foundation (CTS-0207781) and the Department of Energy – Basic Energy Sciences (DE-FG02-01ER15255) and technical assistance from Mr. Joe Aderholdt are gratefully acknowledged.

Table 1. Dimerization energies for carboxylic acids in gas phase, CO_2, and ethane using different basis sets.

	Dimerization Energies (per bond)					
Basis set:	HF/6-31+G(d,p)			MP2/6-31+G(d,p)		
	Gas Phase	with CO_2	With Ethane	Gas Phase	with CO_2	with Ethane
Formic Acid Dimer	-27.00	-20.42	-25.23	-26.83	-22.67	
Propionic Acid Dimer	-26.84	-21.40	-25.88	-27.80		
TFA cyclic dimer	-24.35	-16.05	-22.20	-29.52		
TFA linear dimer	-22.23	-14.74		-34.86		

Figures

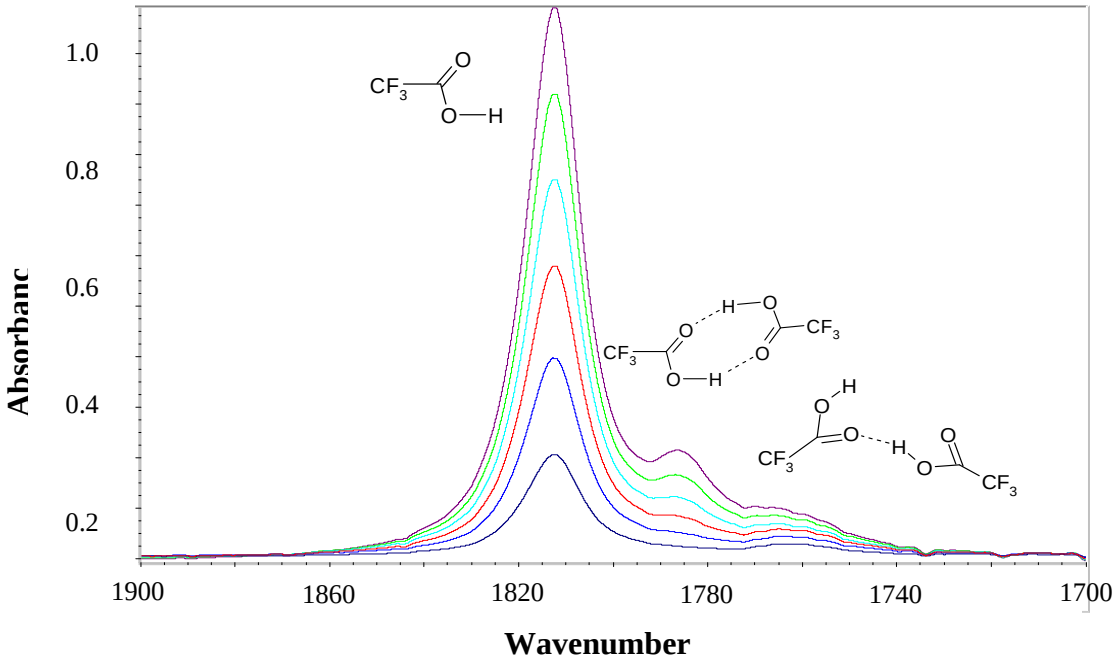

Figure 1. TFA spectra taken at 25 °C and 82.7 bar in CO_2. The three peaks shown correspond to the monomer, cyclic dimer, and linear dimer of TFA in that order as the wavenumber decreases.

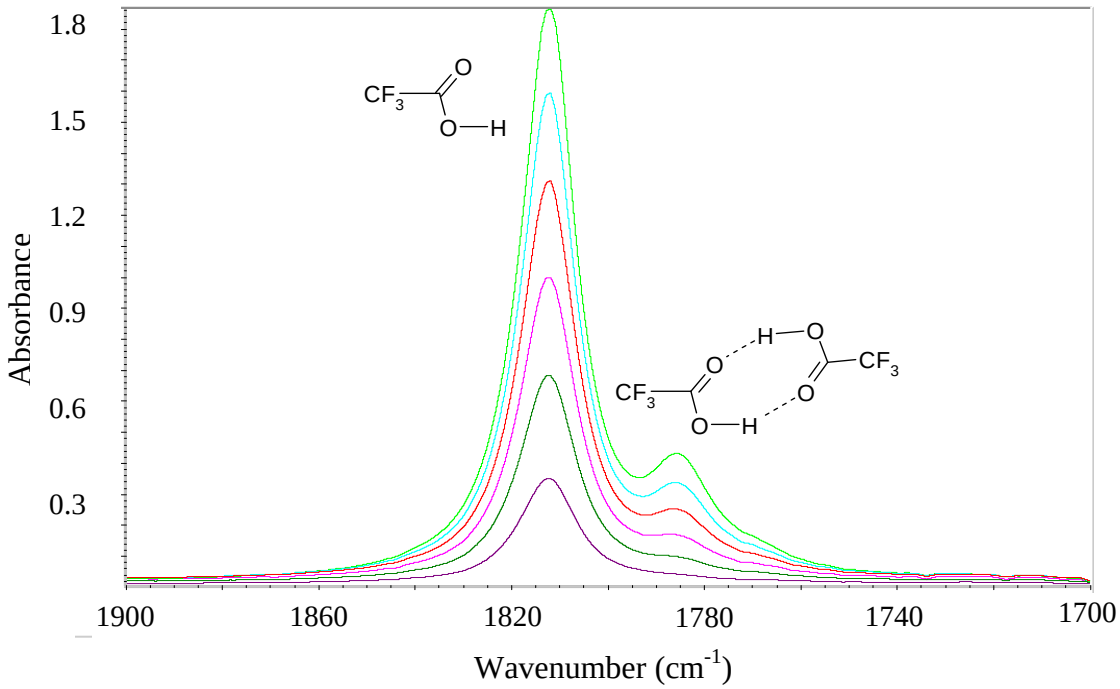

Figure 2. TFA spectra taken at 25 °C and 117 bar in CO_2. At this density (0.841 g/cm^3), only two distinct peaks, corresponding to the monomer and the cyclic dimer of TFA, are observed. The third peak, corresponding to the linear dimer of TFA, has essentially vanished.

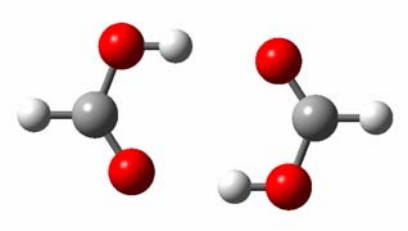

(a)

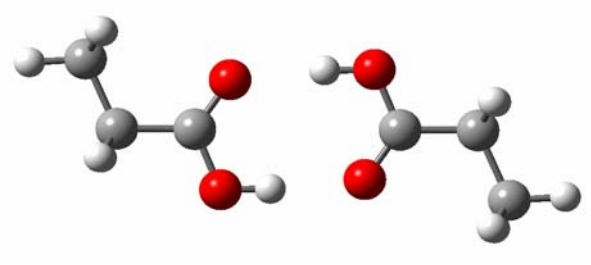

(b)

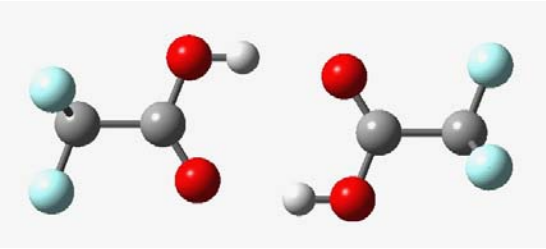

(c)

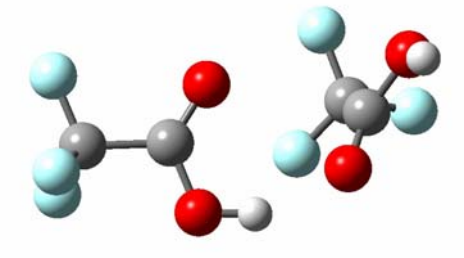

(d)

Figure 3. Acid Dimers: a) Formic Acid Dimer, b) Propionic Acid Dimer, c) Trifluoroacetic Acid Dimer (cyclic), d) Trifluoroacetic Acid Dimer (linear)

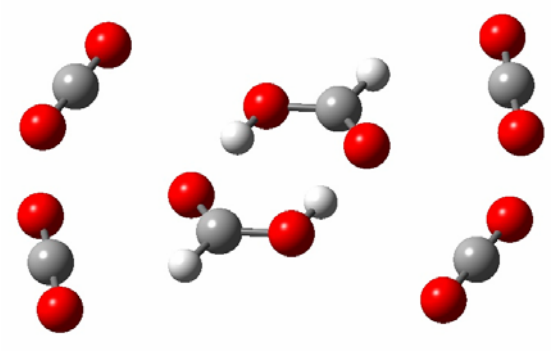

(a)

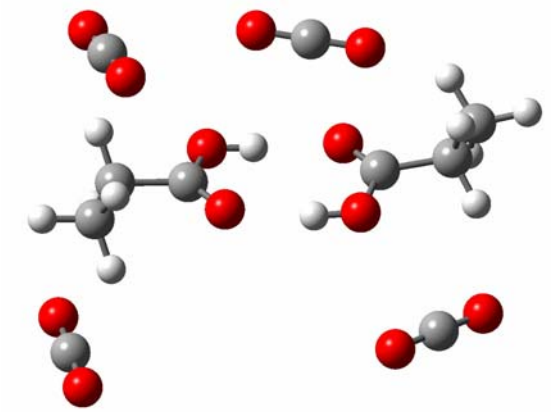

(b)

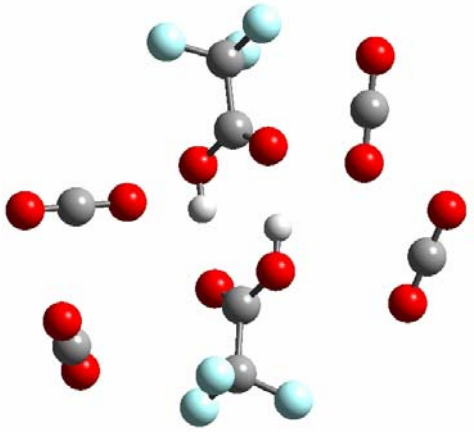

(c)

Figure 4. Optimized structures of Acid Dimers in the presence of CO_2. a) Formic Acid Dimer, b) Propionic Acid Dimer, c) Trifluoroacetic Acid Dimer (cyclic).

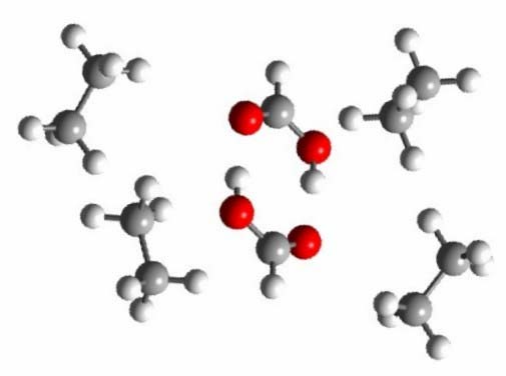

(a)

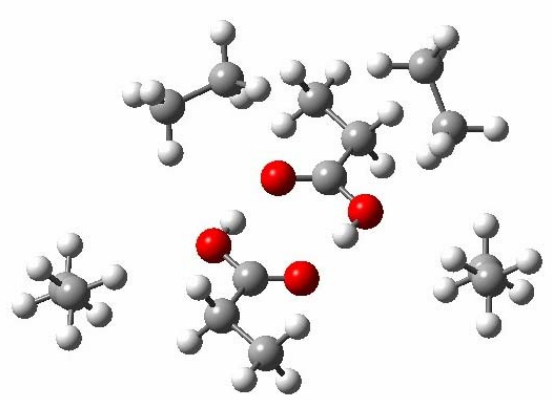

(b)

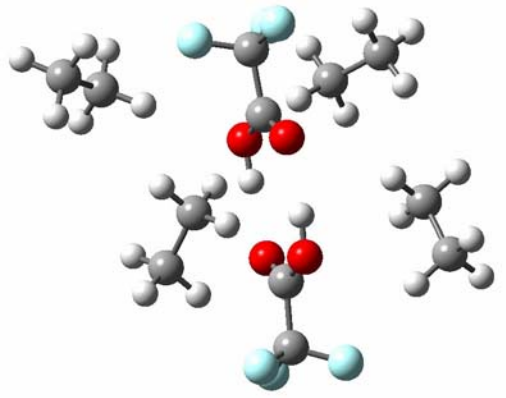

(c)

Figure 5. Optimized structures of Acid Dimers in the presence of Ethane. a) Formic Acid Dimer, b) Propionic Acid Dimer, c) Trifluoroacetic Acid Dimer

References

(1) Ramon, J. M. H.; Rios, M. A. *Chem. Phys.* **1999**, *250*, 155.

(2) Allen, G.; Caldin, E. F. *Q. Rev. Chem. Soc.* **1953**, *7*, 255.

(3) Fujii, Y.; Yamada, H.; Mizuta, M. *J. Phys. Chem.* **1988**, *92*, 6768.

(4) Park, Y.; Gupta, R. B.; Curtis, C. C.; Roberts, C. B. *J. Phys. Chem. B* **2002**, *106*, 9696.

(5) Christian, S. D.; Stevens, T. L. *J. Phys. Chem.* **1972**, *76*, 2039.

(6) Yamamoto, M.; Iwai, Y.; Nakajima, T.; Arai, Y. *J. Phys. Chem. A* **1999**, *103*, 3525.

(7) Hizagy, W. S.; Taha, A. A. *J. Phys. Chem.* **1970**, *74*, 1982.

(8) Murty, T. S. S. R. *J. Phys. Chem.* **1971**, *75*, 1330.

(9) Murty, T. S. S. R.; Pitzer, K. S. *J. Phys. Chem.* **1969**, *73*, 1426.

(10) Fulton, J. L.; Yee, G. G.; Smith, R. D. *J. Am. Chem. Soc.* **1991**, *113*, 8327.

(11) Gupta, R. B.; Combes, J. R.; Johnston, K. P. *J. Phys. Chem.* **1993**, *97*, 707.

(12) Kazarian, S. G.; Gupta, R. B.; Clarke, M. J.; Johnston, K. P.; Poliakov, M. *J. Am. Chem. Soc.* **1993**, *115*, 11099.

(13) McHugh, M. A.; Krukonis, V. J. *Supercritical Fluid Extraction: Principles and Practice*; Butterworths: Boston, 1994.

(14) Hoefling, T. A.; Beitle, R. R.; Enick, R. M.; Beckman, E. J. *Fluid Phase Equilibria* **1993**, *83*, 203.

(15) Sarbu, T.; Styranec, T. J.; Beckman, E. J. *Ind. Eng. Chem. Res.* **2000**, *39*, 4678.

(16) Bell, P. W. T., Amol J.; Park, Y.; Gupta, Ram B.; Roberts, C.B. *Industrial & Engineering Chemistry Research* **2003**, *42*, 6280.

(17) Frisch, M. J.; Trucks, G. W.; Schlegel, H. B.; Scuseria, G. E.; Robb, M. A.; Cheeseman, J. R.; Zakrzewski, V. G.; Montgomery, J. A. J.; Stratmann, R. E.; Burant, J. C.; Dapprich, S.; Millam, J. M.; Daniels, A. D.; Kudin, K. N.; Strain, M. C.; Farkas, O.; Tomasi, J.; Barone, V.; Cossi, M.; Cammi, R.; Mennucci, B.; Pomelli, C.; Adamo, C.; Clifford, S.; Ochterski, J.; Petersson, G. A.; Ayala, P. Y.; Cui, Q.; Morokuma, K.; Salvador, P.; Dannenberg, J. J.; Malick, D. K.; Rabuck, A. D.; Raghavachari, K.; Foresman, J. B.; Cioslowski, J.; Ortiz, J. V.; Baboul, A. G.; Stefanov, B. B.; Liu, G.; Liashenko, A.; Piskorz, P.; Komaromi, I.; Gomperts, R.; Martin, R. L.; Fox, D. J.; Keith, T.; Al-Laham, M. A.; Peng, C. Y.; Nanayakkara, A.; Challacombe, M.; Gill, P. M. W.; Johnson, B.; Chen, W.; Wong, M. W.; Andres, J. L.; Gonzalez, C.; Head-Gordon, M.; Replogle, E. S.; Pople, J. A. *Gaussian, Inc., Pittsburgh PA* **2001**.

(18) Foresman, J. B.; Frisch, Æ. *Exploring Chemistry with Electronic Structure Methods: 2nd Edition*; Gaussian, Inc.: PA, 1996.

(19) Boys, S. F.; Bernardi, F. *Molecular Physics* **1970**, *19*, 553.

(20) Wolbach, J. P.; Sandler, S. I. *AIChE Journal* **1997**, *43*, 1589.

(21) Frisch, Æ.; Frisch, M. J. *Gaussian98 User's Reference, Second Edition*; Gaussian Inc.: PA, 1999.

(22) Wong, M. W.; Frisch, M. J.; Wiberg, K. B. *J. Am. Chem. Soc.* **1991**, *113*, 4776.

(23) Meridith, C. J.; Johnston, K. P.; Seminario, J. M.; Kazarian, S. G.; Eckert, C. A. *J. Phys. Chem.* **1996**, *100*, 10837.

(24) Kazarian, S. G.; Vincent, M. F.; Bright, F. V.; Liotta, C. L.; Eckert, C. A. *J. Am. Chem. Soc.* **1996**, *118*, 1729.

(25) Reilly, J. T.; Bokis, C. P.; Donohue, M. D. *Int. J. Thermophys.* **1995**, *16*, 599.

(26) Nelson, M.; Borkman, R. *J. Phys. Chem. A* **1998**, *102*, 7860.

(27) Fink, R.; Hancu, D.; Valentine, R.; Beckman, E. J. *J. Phys. Chem. B* **1999**, *103*, 6444.

(28) Rindfleisch, F.; DiNoia, T.; McHugh, M. J. *J. Phys. Chem.* **1996**, *100*, 15581.

(29) Raveendran, P. W., S. *J. Am. Chem. Soc.* **2002**, *124*, 7274.

CHAPTER 5

INTRODUCTION TO SUSTAINED DRUG DELIVERY USING BIODEGRADABLE POLYMER MICROPARTICLES

Sustained drug release using biodegradable excipients has gained increasing importance over the last few decades. Various kinds of excipients include polymers derived from different origins. Table 1 gives a comprehensive list of natural and synthetic polymers that can be used as drug delivery agents. These polymers can be modified into different forms for this purpose such as films, rods, microparticles, etc. using compression molding, solvent evaporation and other such techniques.[1,2] Of these, the ones that are widely in use are in the form of microspheres. Microspheres are defined as homogenous, monolithic particles in the size range from 0.1-1000 μm and are widely used as drug carriers for controlled release.[3] Using microspheres encapsulated with drugs in them is a preferred therapeutic means of drug administration over regular delivery because of several reasons; some of them being targeted drug delivery, protection of sensitive drugs, reduction in the loss of drug and controlled drug release over a long period of time. The polymers that are mainly used in the

formation of these microspheres are polylactides, polyglycolides and their co-polymers, Poly(lactide-co-glycolide) in various ratios. Figure 1 shows the structural formulae of poly(lactic acid) and poly(glycolic acid).

These microspheres can be formed using various techniques. Some of the pharmaceutically acceptable are mainly divided into four categories[7]:

1. Emulsion-solvent evaporation technique (o/w, w/o, w/o/w)
2. Phase Separation/Coacervation technique (nonsolvent addition and solvent partitioning)
3. Interfacial polymerization
4. Spray Drying

1. Emulsion-solvent evaporation technique (o/w, w/o, w/o/w)

Various solvent evaporation techniques are outlined in

Figure 2. Oil-in-water (o/w) emulsions are more widely common as compared to water-in-oil emulsions (w/o) because of the simplicity of the process and ease of solvent removal to obtain microparticles in dried form.[4] In this process, an organic solvent (mainly dichloromethane) containing dissolved polymer and drug is emulsified in an excess of aqueous phase with the use of emulsifiers in the aqueous phase to stabilize the emulsion. Agitation is provided using some source of mixing such as impellers, magnetic stirrers, agitators etc. The concentration of the emulsifier and the extent of mixing affect the particle

size and shape. On achieving the desired droplet size, the organic phase is allowed to evaporate leading to precipitation of the dissolved polymer with the precipitated drug being encapsulated within the polymer microparticles. These solid microparticles are then recovered using filtration, centrifugation and subsequent lyophilization. The schematic of this process is depicted in Figure 3.[5]

2. Phase Separation/Coacervation Technique (nonsolvent addition and solvent partitioning)

   This method is divided into two main groups: aqueous and organic

   a) Aqueous Phase Separation: This technique is mainly used to encapsulate water-insoluble materials with an outer polymeric wall material that is soluble in water. The hydrophobic core containing the drug is dispersed in the aqueous phase containing the polymer. The drug is encapsulated by means of 'salting out' of the core material by addition of precipitating agent. This method is further classified into simple coacervation and complex coacervation.

   b) Organic Phase Separation: This technique is inverse of aqueous phase separation process where the wall material is hydrophobic and the core-material is hydrophilic in nature. The concept is to encapsulate a water-soluble material with a polymeric matrix dissolved in an organic solvent by the addition of a nonsolvent to induce phase separation. The size,

shape and quantity of the polymer separated from this method depends upon the polymer concentration, amount of nonsolvent added, and temperature conditions.

3. Interfacial polymerization

This unique film-forming technique involves polymerization of a monomer at the interface of two immiscible liquids. These types of microparticles have semi- or non- permeable membranes with an aqueous core or controlled release coating with a solid core. However, the disadvantage of this process is carrying out a reaction of the active substance with the wall material and the limitation of their solubilities.

4. Spray Drying

This technique involves spraying a pressurized solution of polymer and drug into a cryogenic chamber. The reduction in temperature and pressure results in decreased solubility of the substances leading to precipitation and formation of microparticles. This is a widely used technique in the pharmaceutical and biochemical fields. The final particle size is controlled by a number of factors such as the nozzle diameter, substance solubilities, temperatures and pressures. Another variation of this process for preparing polymer microparticles, mainly of PLA, is Rapid Expansion of Supercritical

Solvents (RESS). This process involves dissolving the polymer and drug in a supercritical fluid mixture, mainly supercritical carbon dioxide with another cosolvent such as dichloromethane, and then expanding the fluid rapidly to a state where the solubility is highly reduced. This leads to supersaturation of the solvent resulting in the formation of small and uniform microparticles.

Once these polymer microparticles containing the drug encapsulated in them are formed, the later steps are to characterize the particle size and morphology, test the percentage of drug encapsulation, study the drug release rate profiles taking into consideration polymer and drug degradation. The particle size distribution and morphology can be characterized by optical microscopy, laser light scattering, electron microscopy, videomicroscopy and such other techniques depending upon the range of particle size. Another interesting analysis technique is Differential Scanning Calorimetry (DSC). It can be not only used to determine the form and crystallinity of the polymer and drug in the microparticles but also to assess the potential interactions between the polymer and the drug molecules.

When these microparticles are used for drug delivery *in vitro*, the drug release is presume to occur in different steps. The initial upsurge in the drug concentration in the release medium is due to the burst release of the drug present on the microparticles surface. The later part of the drug release profile is developed by the diffusion of the drug from the pores and channels in the

polymer matrix. Finally, the polymer undergoes bulk degradation into lactic and glycolic acid monomers releasing the entire remaining encapsulated drug. Depending upon the polymer used, the time for complete release of the polymer could vary from a few days for PLGA polymer of various ratios, such as 50:50, 75:25, 85:15 to a few months for PLA polymer of varying molecular weights. Another issue that needs to be answered, is the decrease in the pH of the release medium from 7.4 at 37^{o}C to acidic conditions due to acid hydrolysis of PLGA polymer, resulting in the formation of lactic and glycolic acid degradation products. Studies have shown a significant drop in pH in cases where large quantities of polymer microparticles were set for release in a small quantity of release medium.[6] However, if a small quantity of polymer is suspended in a large quantity of release medium, serious effect of reduction of pH on the drug release or degradation can be neglected for particles under 200 μ.

In addition to developing a sustained release formulation for hydrophobic and hydrophilic drugs (small molecules), there is a continuous need for developing stable formulations for peptides and proteins. These formulations are lot more challenging than the ones for small molecules. That is because, in addition to the burst effect problem, proteins tend to undergo physical and chemical changes in due course of formulation, which can make the formulation completely inviable.

Chapter 5 gives an introduction to some basic concepts and methods involved in biopharmaceutics in the formulation of biodegradable polymer microparticles and their release rate study. Chapter 6 demonstrates how creating covalent bonds between monomers to form surface crosslinked polymers can bring about a desired variation in the drug release profile from biodegradable microparticles. Here, surface crosslinking is brought about by UV polymerization of different monomers on the surface of PLGA polymer microparticles, with either a hydrophobic or a hydrophilic drug encapsulated in them, in order to reduce the initial burst release of drug from the microparticles. This polymer layer on the surface creates an additional diffusional barrier by crosslinking the surface of the particle and closing the pores on the surface thereby preventing drug loss from the surface and the channels and pores on the microparticles surface. Chapter 7 talks about formation of nanoparticles of a hydrophilic drug using supercritical antisolvent technique with enhanced mass transfer (SAS-EM) where supercritical CO_2 was used as an antisolvent. These nanoparticles were then microencapsulated in PLGA microparticles using phase separation/ coacervation technique for sustained release applications. The objective of the current work was to demonstrate a uniform sustained delivery of API from PLGA microspheres by modifying the van der Waals interaction between them. Chapter 8 gives an overview of different technique that could be used to obtain better encapsulation efficiencies of other therapeutic compounds

in polymer microparticles. Another concept under the title of Solvent Evaporation Rate Study (SERS) talks about controlled evaporation of solvent from the oil-in-water emulsion in a typical solvent evaporation technique to improve the morphology and reduce porosity of the polymer microparticles as a part of the future recommendations.

Commercial Products

There are various commercial products in the market based on microencapsulation technology for long term sustained drug release, a list of which is summarized in Table 2.

Tables

Table 1. Biodegradable Polymers used in Drug Delivery Systems[7]

	Animal Proteins	Animal Polysaccharides	Plant Polysaccharides
Natural Polymers	Albumin Collagen Gelatin Fibrinogen	Chitin Chitosan Hyaluronic Acid	Starch Dextrin Dextran Alginic Acid
Synthetic Polymers	Poly(lactic acid) Poly(glycolic acid) Poly(lactic/glycolic acid)	Poly(β-hydroxy butyric acid Poly(ε-caprolactone Polyanhydrides	Poly(ortho esters) Polyalkyl cyanoacrylate

Table 2. List of Commercial Products based on Sustained Delivery Application.

Brand Name	API	Treatment	Manufacturer
Lupron Depot®	Leuprolide Acetate	Prostate Cancer, Endometriosis	TAP Pharmaceuticals
Nutropin Depot®	Human Growth Hormone	growth hormone deficiency	Genentech
Zoladex	Goserelin Acetate	Prostate Cancer	Zeneca
Prolease®, Medisorb®	Multiple drugs	Multiple diseases	Alkermes
Alzamer®	Proteins and small molecules	Multiple diseases	Alza Corp.

Figures

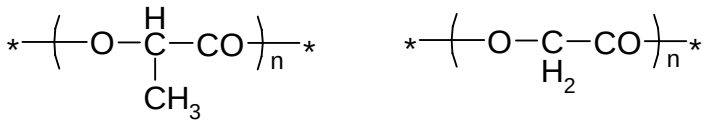

Poly(lactic acid) Poly(glycolic acid)

Figure 1. Structural formulae of poly(lactic acid) and poly(glycolic acid)

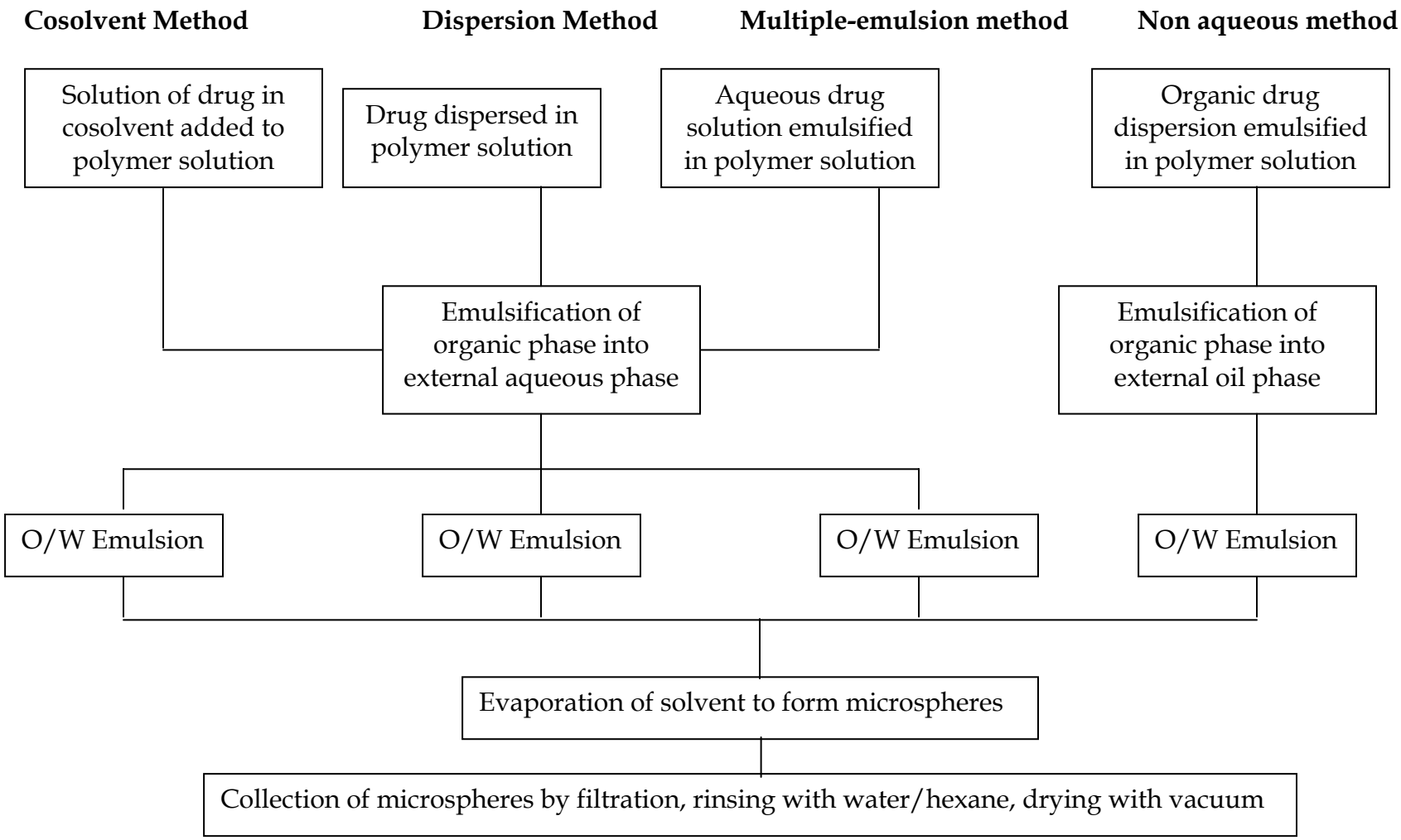

Figure 2. Schematic representation of various solvent evaporation methods

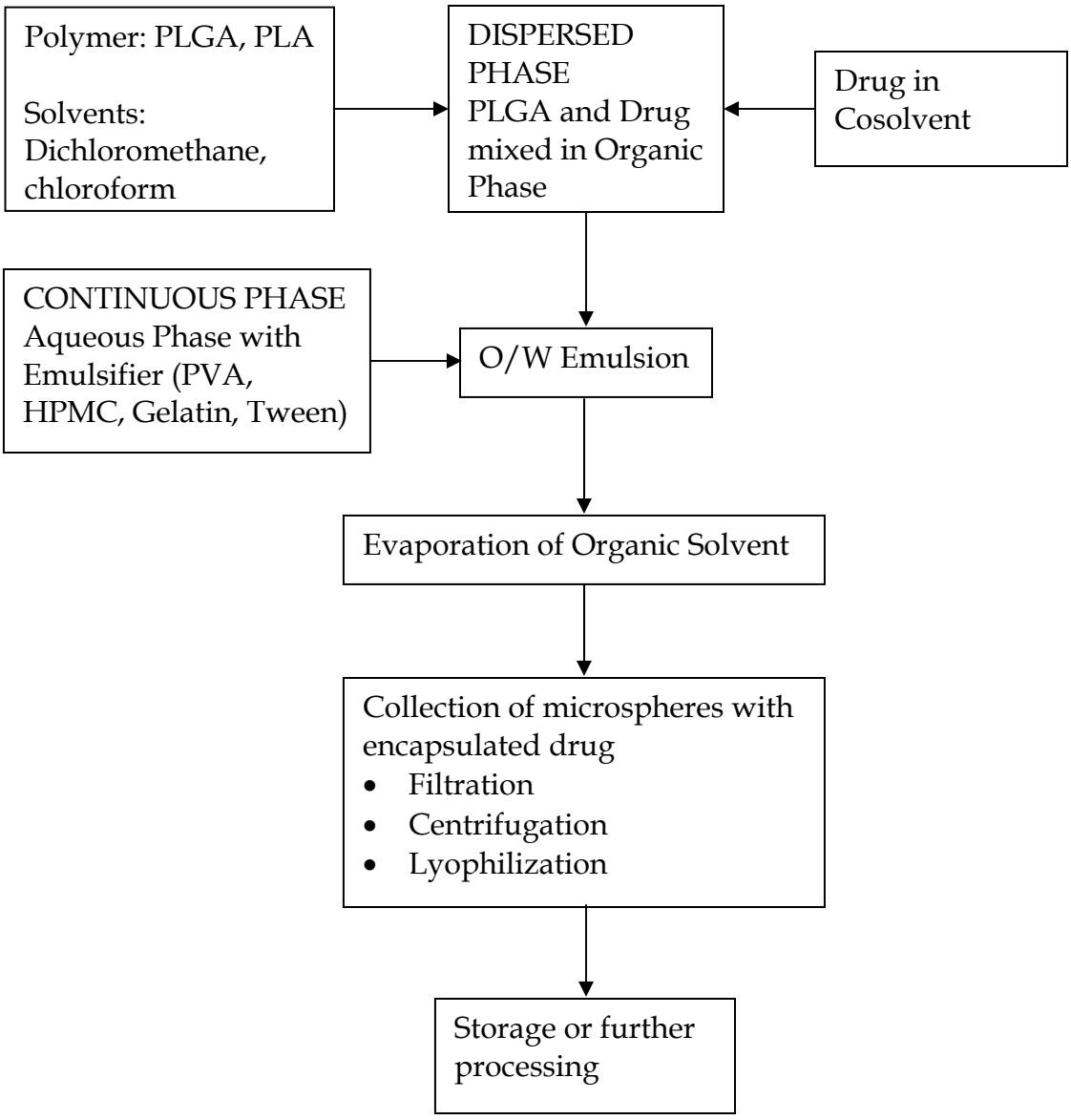

Figure 3. Schematic representation of O/W emulsion-solvent evaporation technique for the formation of PLGA microspheres.

References

[1] Holland S. J., Tighe B. J., Gould P. L. "Polymers for biodegradable medical devices. 1. The potential of polyesters as controlled macromolecules release systems" J. Controlled Release 4 (1986) 155-180.

[2] Rafler G., and Jobmann M. "Controlled release systems for biodegradable polymers" Pharm. Ind. 56 (1994) 565-570.

[3] Wise D. L. "Handbook of Pharmaceutical Controlled Release Technology, Marcel Dekker, Inc., NY, 16 (2000) 329-338.

[4] Sprockel O. L., and Prapaitrakul W. "A comparison of microencapsulation by various emulsion techniques" Int. J. Pharm. 58 (1990) 123-127.

[5] Jalil R., and Nixon J. R., "Biodegradable of poly(lactic acid) and poly(lactide-co-glycolide) microcapsules: problems associated with preparative techniques and release properties" J. Microencapsulation 7 (1990) 297-325.

[6] Witschi, C.; Doelker, E. "Influence of the microencapsulation method and peptide loading on poly(lactic acid) and poly(lactic-co-glycolic acid) degradation during in vitro testing." Journal of Controlled Release 51 (1998) 327-341.

[7] Okada H., and Toguchi H. "Biodegradable microspheres in drug delivery" Crit. Rev. Ther. Drug Carrier Systems 12 (1995) 1-99.

CHAPTER 6

REDUCTION IN THE INITIAL BURST RELEASE OF DRUGS FROM PLGA MICROPARTICLES BY SURFACE CROSSLINKING

Abstract

Sustained release approaches have evolved eventually in the application of the delivery of drugs encapsulated in polymers. However, the most persistent problem that remains is the initial burst release of the drug which can exceed the toxic limits. Dexamethasone, a hydrophobic drug, was encapsulated in PLGA microparticles using solvent evaporation method. The drug release profile of these microparticles was studies and the initial burst was reduced by crosslinking of microparticle surface using ethylene glycol dimethacrylate and tri(ethylene glycol) dimethacrylate. Due to surface crosslinking, an additional diffusional resistance was created which prevented easy dissolution of the drug into the release medium and reduced initial burst release by almost 67%. Moreover, the time required for reaching a steady state release was also observed to be delayed, prolonging the sustained drug delivery. This concept was further tested with a hydrophilic drug, the sodium salt of dexamethasone phosphate, encapsulated in PLGA polymer microparticles and was observed to reduce the burst release as well.

For synthesizing the polymer microparticles containing dexamethasone, an o/w microemulsion and solvent evaporation technique was used; whereas, for those containing dexamethasone phosphate, w/o/o/o phase coacervation technique was used. The surface crosslinking was performed by ultraviolet radiation.

Introduction

In sustained drug release applications, the drug is usually given at one time in a bulk quantity to a specific target in the body and is expected to be delivered over a period of typically several months. The drug is encapsulated in a biodegradable polymer and is initially released by diffusion through the pores in the microparticles and later on by the erosion of the polymer within the particle. However, a serious problem is initial burst effect. Burst effect in sustained release formulations is termed as a large initial quantity of drug released from the encapsulated drug capsule before the release rate reaches a stable profile[1]. This phenomenon could be useful in some cases like cancer treatment, wound treatment, etc.[2] However, the burst release is not desirable in sustained drug delivery applications, because the dosage of the drug encapsulated is large extended to be reduced over long period of time. In some cases, even a small percentage of the drug released would increase its local concentration to an extent near or above that at which the drug becomes a toxin

in vivo[3]. As a result, the defense mechanism of the body would try to resist the increase in the toxicity level by forming additional layers of tissues on the polymer surface, thereby disrupting the entire release profile and mechanism.[4,5] Any drug released during the burst stage may also be metabolized and excreted without even being effectively utilized. Even if the drug is not toxic, this amount of drug released is essentially wasted, which is undesirable inside the body as well as for the cost of the pharmaceuticals.[6] Hence, there is a need to reduce the burst effect.

Several researchers have observed burst release without giving advanced explanations. Others have tried to explore the mechanisms of burst and prevent it by several methods such as surface coating of the polymer,[7,8,9] changing the surfactant,[10] changing the molecular weight of the polymer,[11] and including the burst effect in models to simulate the release process.[12,13,14]

Burst release has been attributed to various physical, chemical and processing parameters, but for the most part, no substantial studies have been examined the underlying mechanisms of burst release in monolithic polymeric systems[1]. There are several possible causes for burst release. One is the desorption or release of the drugs that have been absorbed or trapped on the surface of the device.[15,16,17] Another is non-uniform drug loading. Migration or redistribution of drug, facilitated by convection during evaporation, can lead to higher surface concentrations as the polymer is dried.[18,19] Lastly, the porous

structure of some polymer networks can also lead to an initial burst as drug diffusion is less hindered in water-filled macropores formed during solvent evaporation.[20] Pores are usually formed on the polymer particle surface by the use of salts and volatile compounds that evaporate during the formation and solidification of the particles.

Reduction in burst release of drugs is vital in the pharmaceutical industry because it is unpredictable and hence undesirable in majority of the cases. Even if it is desirable in some cases, the amount of burst release of drugs cannot be well controlled[21]. Earlier attempts to reduce burst release include surface extraction[22] to reduce the burst release of proxyphylline drug from PVA hydrogels, surface coating[23] of lidocaine encapsulated in PLLA (poly-l-lactide), and chitosan of varying molecular weights and viscosity to form double-walled polymer microspheres. A novel microencapsulation technique was developed[21] with high efficiency of encapsulation and low burst effect by microencapsulating pentamidine/polyvinyl alcohol (PVA) hydrogel for crosslinking in poly(lactide-co-glycolide) (PLGA) using a solvent evaporation technique. They observed reduction in the burst effect and drug loss, and controlled *in vitro* release of the drug pentamidine for 80 days. A similar study was conducted[13] by encapsulating dexamethasone in PLGA nanoparticles based on a single oil-in-water (o/w) emulsion and further crosslinking these nanoparticles in PVA hydrogels. The *in vitro* drug release tests showed that the crosslinking of PVA

hydrogel, which acts as a diffusional barrier for the drug release, is the controlling parameter in the release of dexamethasone. Another attempt[12] was to synthesize macroporous poly(sucrose acrylate) hydrogel containing high-density spherical microgels embedded inside low-density macrogel phase for the controlled release of macromolecules through the hydrogel matrix. The release of protein from the low-density macrogel results in the initial burst, while the release from the high-density microgels gives rise to the sustained release of protein.

A different methodology to crosslink the particles is to use UV as a source of polymerization. Highly crosslinked hydrogel spheres were fabricated[24] using UV photopolymerization of poly(ethylene glycol) diacrylate (PEG-DA) and pentaerythritol triacrylate (PETA) with 2,2-dimethoxy-2-phenyl-acetophenone (DMPA) as the photoinitiator. A co-monomer that can create non-covalent interactions between the hydrogel and the encapsulated drug was added,[25] which can significantly affect the drug release rates. Using ATR/FTIR, a reduction in the swelling rates of the hydrogels and controlled drug release rates with a reduction in initial burst for increasing concentrations of co-monomer additions was observed. Chitosan, being easily biodegradable and relatively non-toxic to the body and skin, is a potential drug delivering agent. Azidated chitosan was photo-crosslinked to azidated epichlorohydrin using UV light and was used as a drug carrier for a model drug, such as theophylline. The process

of UV crosslinking was analyzed by ATR/FTIR to observe functional group changes upon crosslinking and the drug carrier was demonstrated to show controlled release of the drug with a reduction in the initial burst release.[26]

Dexamethasone (Figure 1) is a synthetic adrenocortical steroid possessing basic glucocorticoid activity. It is very sparingly soluble in water (0.1 mg/ml)[27]. It is among the most active members of its class, being about 25-30 times as potent as hydrocortisone. Moreover, dexamethasone is readily absorbed from the gastrointestinal tract. It can be used as a glucocorticosteroid in various applications including apoptosis,[28] anti-inflammatory,[29] protective agent against the neurotoxic actions of cisplatin,[30] for the treatment of chronic eustachian tube dysfunction,[31] for the prevention of post operative nausea and vomiting.[32] Dexamethasone 21-phosphate disodium salt (Figure 1) is a crystalline water soluble salt of the same drug. It is highly soluble in water.

In order to encapsulate hydrophobic drugs, an oil-in-water (o/w) solvent evaporation method has been utilized to synthesize polymer microparticles of biodegradable polymers such as PLGA or PLA with the drug encapsulated in them.[33] However, this method is not very successful for water soluble drugs because the drug gets partitioned out into the external aqueous phase leading to decreased drug loading.[34] As a result, water-oil-water (w/o/w) double emulsion techniques have been attempted to encapsulate water-soluble drugs.[35,36] However, there have been problems with the emulsion stabilities and the drug

getting distributed from the inner aqueous phase to the external aqueous phase during the formation of the double emulsion.[37] Therefore, there have been attempts to use oil-in-oil (o/o)[38], solid-in-oil-in-oil (s/o/o)[39] and s/o/o/o[40,41] emulsion techniques for encapsulation of water soluble drugs. In this work, o/w solvent evaporation technique was employed for the encapsulation of the hydrophobic dexamethasone and w/o/o/o phase coacervation technique[41,42] for the encapsulation of the hydrophilic dexamethasone phosphate. Also, the effect of the presence of NaCl salt in the aqueous phase of o/w emulsion on the extent of drug encapsulation was studied.

Recently, dexamethasone was encapsulated in PLGA microparticles and burst release was observed.[43] The objective of this work is to reduce the burst release of dexamethasone by surface preferential crosslinking polymerization of another monomer on the PLGA microparticles, thereby providing an additional diffusional resistance for the release of surface drug.[24] Also, the effect of multiple layers of crosslinked polymer on the reduction in the burst release and control of release profile were also studied. This work was further extended to reduction of burst release of highly hydrophilic salt of the same drug; to demonstrate that this technique is also applicable for highly water soluble drugs.

Materials

Poly(lactide-co-glycolide) (PLGA 50:50; inherent viscosity = 0.39 dL/g in HFIP @ 30^{o}C) was obtained from Birmingham Polymers. Polyvinyl alcohol (PVA; avg. mol. wt. = 30,000–70,000), dexamethasone, sodium salt of dexamethasone-21-phosphate, and rhodamine-B were obtained from Sigma Chemicals. Dichloromethane (99.9% ACS HPLC grade), silicon oil (dimethicone, 350 cSt), ethylene glycol dimethacrylate (EGDMA, 98%), Tri(ethylene glycol) dimethacrylate, (Tri(EG)DMA, 95%), 2,2-dimethoxy-2-phenyl acetophenone (DMPA, 99%) were purchased from Sigma Aldrich, and methanol (HPLC grade), acetonitrile (HPLC grade), phosphate buffer saline (PBS, Labchem Inc., pH=7.4), hexane (HPLC grade), and distilled deionized (DIUF) water were obtained from Fisher Scientific. All the materials were used as received.

Apparatus and Procedure

1. Microsphere Preparation

PLGA microspheres loaded with dexamethasone were prepared by oil-in-water (o/w) emulsion technique.[43] The oil (organic) phase consisted of 20 mg dexamethasone and 100 mg PLGA dissolved in the mixture of 4.5 ml dichloromethane and 0.5 ml methanol. The aqueous phase was constituted of 1 wt % PVA in 100 ml distilled water. To study the effect of addition of salt to the aqueous phase, NaCl salt was added to the aqueous phase to form a 1 N NaCl

solution. PVA acts as a water based surfactant and NaCl makes the aqueous phase more polar, thereby reducing the solubility of hydrophobic drug in the aqueous phase. Separate experiments were conducted in presence and absence of NaCl salt in the aqueous medium to study the effect of the salt on the encapsulation efficiency. A microemulsion of organic phase containing the drug and the polymer was formed in the aqueous phase by means of stirring at 1000 rpm. On mechanical stirring, the organic phase is broken down into smaller droplets in the aqueous phase and stabilized by the surfactant. The organic solvent from of the droplets starts evaporating, causing the drug and the polymer to precipitate in the form of microspheres. The drug gets encapsulated in the polymer microspheres during the hardening process. The resulting emulsion was stirred overnight on a magnetic stirrer at a relatively low rpm to allow complete evaporation of dichloromethane and hardening of polymer microspheres. After sufficient evaporation, the resulting solution was then centrifuged at 3400 rpm (Fisher Scientific) to sediment the particles down. The microspheres were then washed twice with DIUF water to remove excess surfactant, salt (in the case of experiments where salt was used in the aqueous phase), and wash-off any drug adhered to the polymer surface. The concentrated suspension was then lyophilized using Labconco® lyophilizer for complete removal of solvent and stored for further processing.

PLGA microspheres loaded with dexamethasone phosphate were prepared by w/o/o/o phase co-acervation technique.[42] 50 mg of dexamethasone phosphate was dissolved in 0.25 ml of water and added to 5 ml of dichloromethane to form a water-in-oil suspension by using ultrasonic vibration at 120 W for 1 min. Five ml of 350 cSt silicon oil was then added to this metastable suspension resulting in the phase coacervation of the organic phase. This caused PLGA to precipitate in the form of microspheres. This solution is then added to 75 ml of hexane to extract out the dichloromethane and silicon oil. Successive washings with pure hexane and then drying under heavy vacuum using Labconco® lyophilizer resulted in the formation of PLGA microparticles with dexamethasone phosphate encapsulated in them.

2. Surface Crosslinking

A portion of these microparticles obtained from the above processes were exposed to a mixture of UV crosslinker and photoinitiator respectively for UV polymerization of the crosslinking monomer over the surface of the microparticles. The crosslinking process was carried out using two different crosslinking monomers, EGDMA and Tri(EG)DMA. Both the crosslinkers were allowed to equilibriate overnight with inhibitor remover beads to remove hydroquinone inhibitors before use. The photoinitiator used is 2,2-dimethoxy-2-phenyl-acetophenone (DMPA). The apparatus for applying crosslinker and photoinitiator onto the microparticles surface is shown in Figure 2. Here, CO_2

taken in a syringe pump and pressurized to 1000 psig and 5°C. This liquid CO_2 was passed through a solution injection device in which a 0.09 gm of EGDMA 0.01 gm of DMPA is taken. CO_2 carries the EGDMA-DMPA solution in liquid form and is sprayed using a 75 μ nozzle onto microparticles. As a result, this mist forms a coating of the crosslinker and photoinitiator over the microparticle surface. After making sure that the particles are well coated, they were exposed to UV light at 254 nm (UV-A) at 5 mW/cm^2 using a Spectrolinker XL-1500 UV crosslinker (Spectronics Corporation) for 1 hour in 3 intervals of 20 minutes each. This process was carried out in intervals to prevent over-heating of the microparticles due to prolonged UV exposure. The microparticles were mixed well during the process of UV exposure to make sure that all the EGDMA absorbed on the microparticles is polymerized to poly(ethylene glycol dimethacrylate) (PEGDMA). When using Tri(EG)DMA, a similar procedure was used.

To study the effect of multiple layers of surface crosslinking, increasing layers of EGDMA as well as Tri(EG)DMA were coated and polymerized on PLGA microparticles in individual experiments. For this purpose, 2 sets of 200 mg of microparticles were each sprayed with EGDMA and Tri(EG)DMA and exposed to UV for 1 hour in 3 intervals of 20 minutes each. Fifty mg of these microparticles were separated for release rate study and the rest was again sprayed with another layer of EGDMA and Tri(EG)DMA respectively. This

procedure was repeated twice to obtain 50 mg of microparticles coated and crosslinked with 1 layer, 2 layers, and 3 layers of polymerized EGDMA and Tri(EG)DMA respectively.

3. Particle size analysis

The microparticles were analyzed for their sizes and surface morphology using a scanning electron microscope (SEM: Zeiss, model DSM 940). The microparticles were initially spread on a carbon tape glued to an aluminum stub and coated with Au/Pd using a Sputter Coater® (Pelco, model Sc-7) under a vacuum of 0.8 mbar. The microparticles were coated 4 times for a 30 sec interval instead of 2 coats of 60 sec intervals to avoid melting of the polymer because of over-heating. The microparticles were then observed under SEM and micrographs were recorded. Multiple images of different areas of the SEM stub were recorded for microparticles size analysis.

4. Confocal laser scanning fluorescence microscopy

In order to observe the presence of coating over the microparticle surface, a saturated solution of rhodamine-B dye was prepared in the mixture of EGDMA and DMPA and sprayed over the PLGA microparticles as described above. These microparticles, after surface crosslinking using UV, were observed under confocal laser scanning microscope (CLSM: BioRad® MRC 1024 using LaserSharp 2000 software). Ar/Kr laser was used to excite rhodamine-B dye.

Triple labeling was used to observe red, green and FaRed (blue) emission of the dye. Z-series optical cross-sections of the microparticles were obtained to observe the distribution of the dye around the microparticle surface at different cross-sections of the microparticle.

5. Extent of encapsulation measurement

In order to determine the content of dexamethasone actually encapsulated in the polymer matrix, a known quantity of the microparticles were mixed in acetonitrile. The resulting solution was analyzed for the dexamethasone content using HPLC technique as described below. To determine the same for dexamethasone phosphate, a different technique was utilized. The polymer is soluble in dichloromethane, whereas the drug in soluble in water. Using this concept, 11 mg of PLGA microparticles containing dexamethasone phosphate were dissolved in 1 ml of dichloromethane and this was then equilibriated with 10 ml of distilled water. This aqueous phase, assuming that the drug was totally partitioned in the aqueous phase, was then tested for dexamethasone phosphate content using HPLC analysis method for dexamethasone phosphate.

6. *In-vitro* release rate study

The crosslinked and non crosslinked polymer particles were then used to study the release rate of drugs from the polymer. For this purpose, they were suspended in 100 ml of 0.05 M phosphate buffer saline (PBS, pH=7.4) at 37^{o}C in

an incubator, and stirred at 50 rpm. Samples, after being filtered from a 5 μm filter, were taken periodically and analyzed for UV absorbance of dexamethasone in the PBS buffer using Waters HPLC (Model 600, Waters Corp.). The HPLC was equipped with a 7725i six-port injection valve (Rheodyne), model 600 HPLC pump, model 2410 refractometer and model 2487 Dual λ UV spectrometer with the wavelengths set to 242 nm and 207 nm. A Spectronic Genesys2® UV spectrophotometer was used to initially detect the wavelength at which dexamethasone absorbs the maximum of UV light and was found to be 242 nm. The second wavelength of 207 nm was used because EGDMA was shown to absorb UV light at this wavelength. So, a verification of no additional peak at 207 nm would verify the fact that EGDMA was totally polymerized during the crosslinking process. The mobile phase used for HPLC analysis of dexamethasone was 0.05 M PBS itself and acetonitrile in the ratio of 60:40 flowing at 1 ml/min through a 3.9 mm x 150 mm Novapak C-18 column.[44] The drug was observed to elute in about 2.2 minutes. In the case of dexamethasone phosphate, the mobile phase had to be changed to an acidic medium to maintain the sodium salt of dexamethasone phosphate in undissociated form. Hence, the mobile phase was modified to 0.05 M PBS : ACN : 75% acetic acid (AA) in the ratio of 70:28:2.

Results and Discussion

During the particle formation process, when organic phase is added to the aqueous media, methanol is the first to diffuse into the aqueous phase and carries dichloromethane alongwith it. However, dichloromethane, having a limited solubility in water, starts to evaporate out. PLGA and dexamethasone (solubility in water: 0.1 mg/ml)[27] being poorly soluble in water, precipitate and form microspheres. They are held apart and not allowed to agglomerate due to the presence of continuous mixing of the bulk phase and PVA present in the aqueous phase which acts as a surfactant.

In the case of dexamethasone phosphate, the drug has a higher affinity towards the aqueous phase and prefers to be in the aqueous phase. On sonication, the aqueous phase is broken down into small droplets forming a metastable water-in-oil suspension in the dichloromethane phase. On addition of silicon oil, with sufficient mixing, phase coacervation takes place leading to precipitation of the PLGA polymer in the form of microspheres. This gives a w/o/o suspension of the aqueous phase entrapped in dichloromethane which is further entrapped in the silicon oil. This silicon oil is extracted by the hexane phase, which on the application of vacuum, is evaporated to give dry microparticles of PLGA polymer with dexamethasone phosphate encapsulated in them.

1. Particle size and morphology

Microparticles loaded with dexamethasone were observed under the Scanning Electron Microscope (SEM) for particle size analysis. These microparticles were observed to be spherical with sizes ranging from 30-40 μm (Figure 3) for those loaded with dexamethasone using solvent evaporation method, and about 100-120 μm (Figure 4) for those loaded with dexamethasone phosphate using phase coacervation method. The surface morphology was observed to be slightly irregular for particles which were not crosslinked. Upon surface crosslinking of the particles, the surface became relatively smoother implying that EGDMA or Tri(EG)DMA formed a thin crosslinked layer on the particle surface (Figure 3). Moreover, the particle diameter did not change substantially suggesting that the surface layer was very thin. A direct evidence to reduction in the number of pores due to surface crosslinking of the microparticles surface can be seen in Figure 5. Reduction in number of pores is a direct relation to reduction in burst release of the drug from the microparticles.

2. Confocal fluorescence microscopy

The confocal laser scanning microscopy (CLSM)[45,46,47] provided direct evidence to the above observation. Images taken at different cross-sectional levels of the microparticles showed the presence of fluorescent dye only on the surface of the microparticles with occasional penetration to some extent in larger particles (Figure 6).

3. Percentage encapsulation

The microparticles were analyzed for the percentage of the drug encapsulated in the polymer matrix and were observed to have 26% of the drug encapsulated in the polymer. The drug has a solubility of 0.1 mg/ml in water.[27] As a result, 10 mg out of a total of 20 mg of the drug is lost in 100 ml of water. Out of the remaining 10 mg, some of the drug stays on the polymer surface which is washed away in the washing process, during the centrifuging and in the process of lyophilization of microparticles. As a result, only around 5 mg drug gets encapsulated leading to an effective encapsulation of 26%.

However, the percentage of drug encapsulated in the cases, where the aqueous phase constituted of 1 N NaCl solution, was observed to be as high as 96%. NaCl, being an ionic compound, makes the aqueous phase highly polar thereby reducing the solubility of the drug in the aqueous phase. This helps in better encapsulation of the drug in the non-polar polymer matrix and minimal drug loss.

4. *In-vitro* release rate study of the drugs from PLGA microspheres

During the formation of these microspheres, dexamethasone gets partially encapsulated within the microspheres and partially adsorbed on the microspheres. If the drug is dispersed homogenously within the microspheres, a constant release rate of the drug is expected. If it is encapsulated in the form of small clusters within the polymer matrix, the release rate is expected to reach a

maximum in a short period of time because of channeling within the microspheres.[48]

The results of *in-vitro* release of dexamethasone and dexamethasone phosphate are shown in Figure 8 and Figure 9, respectively. The release profile from the conventional microparticles was characterized by an initial burst release followed by a continuous release. However, the initial burst was observed to be lowered by about 3-fold in the case of surface crosslinked polymer. This can be attributed to the presence of an additional diffusional resistance to the release of the drug from the polymer surface. The surface crosslinking polymerization of EGDMA to P(EGDMA) reduces the number of pores as well as creates an additional barrier to the release of the drug. The possible phenomenon is sketched in Figure 7. The release of dexamethasone is of a diffusional type as seen in Figure 8. Moreover, the time required to reach the steady state release was also extended as a result of surface crosslinking from 15 hours for conventional microparticles to about 24 hours for surface crosslinked microparticles.

To ensure that the reduction in burst release was due to polymerization of an additional monomer, either EGDMA or Tri(EG)DMA, and not just due to spraying of the monomer over the PLGA microparticles, three different release rate studies were conducted in comparison. One set consisted of the original microparticles, another with the microparticles coated with the monomer but not

polymerized, and the third set consisted of the coated and UV crosslinked EGDMA. All the three sets were analyzed for their release rates profiles on a comparative study.

In another experiment where three sets of release rate studies were conducted simultaneously, the release profiles evidently showed that the release profiles for the microparticles that were only coated either with the EGDMA or Tri(EG)DMA monomer and not polymerized was not very different from that for the original microparticles. Whereas the release profile of the microparticles that were coated with the monomer and polymerized showed a clear reduction in burst release from 61% of the drug released from original particles down to about 7% of the drug for surface crosslinked microparticles. Moreover, the time to reach the the steady state release was also extended from 10 hours in case of the original microparticles to 120 hours in case of the surface crosslinked microparticles. These observations are clear from the release profiles shown in Figure 10.

In another set of experiments where seven different sets were analyzed simultaneously to study the effect of multiple layers of surface crosslinked EGDMA and Tri(EG)DMA, the release profiles in case of both the monomers showed further reduction in burst release with every additional layer of the surface crosslinked polymer. Moreover, the release profile from the microparticles coated and crosslinked with three layers shows almost no burst

release with a gradual and uniform increase in the drug release with time until it reaches a steady state value. The time required to reach the steady state release was observed to be extended. These observations are evident from the release rate profiles shown in Figure 11.

The factors that govern the type of release rate from a drug-encapsulated polymer microsphere system are M_w of the polymer,[11,49,50] size of the microspheres,[51] drug loading,[52] drug distribution in the polymer matrix, etc. The factors affecting the drug distribution within the polymer matrix which in turn would determine type of release rate are the polymer to drug ratio and the steps involved in the process of hardening of the polymer microspheres. In this study, the polymer to drug ratio used was 5:1 and the particles were dried using lyophilization process. For such ratios, with lyophilization, there is greater likelihood that the drug would get encapsulated in small pockets within the polymer matrix and would release in bulk quantities due to channeling effects. A monodispersed encapsulation with gradual drug release over a longer period of time could be expected with higher polymer to drug ratios.

Conclusion

Dexamethasone encapsulated PLGA microparticles were produced in the size range of 30-40 μm using the solvent evaporation technique, Dexamethasone phosphate loaded PLGA microparticles were produced in the size range of 100-120 □m using phase coacervation method. The surface crosslinking of these

microparticles creates a diffusional barrier which can significantly reduce the initial burst release of dexamethasone and dexamethasone phosphate from the microparticles and, at the same time, extend the time for steady state release as well. Multiple layers of these barriers can further help in reducing the burst release and prolonging the steady state drug release rate.

Acknowledgement

Authors would like to thank Dr. W. R. Ravis, Department Head of Pharmacal Sciences, Auburn University for his technical advice and Dr. M. E. Miller, Biological Sciences, Auburn University for the use of SEM and CLSM.

Figures

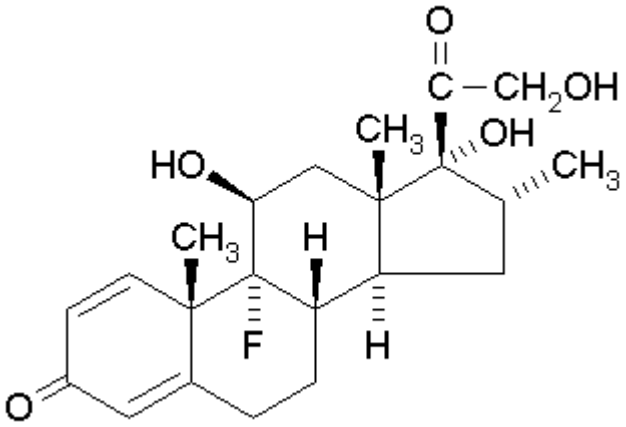

Dexamethasone

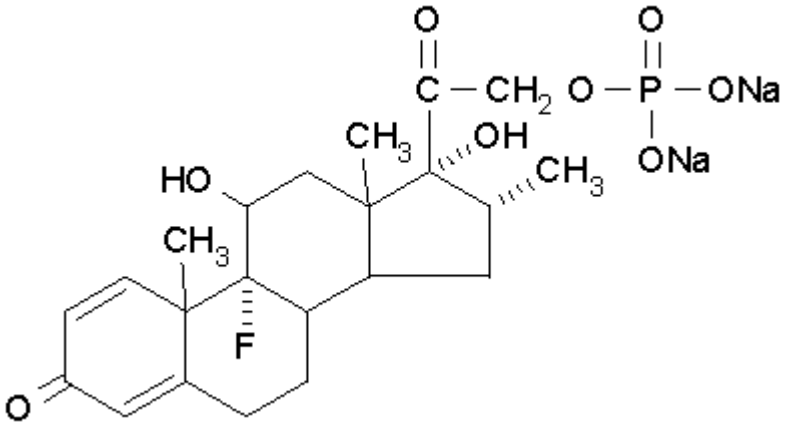

Dexamethasone phosphate

Figure 1. Chemical structure of dexamethasone and dexamethasone phosphate.

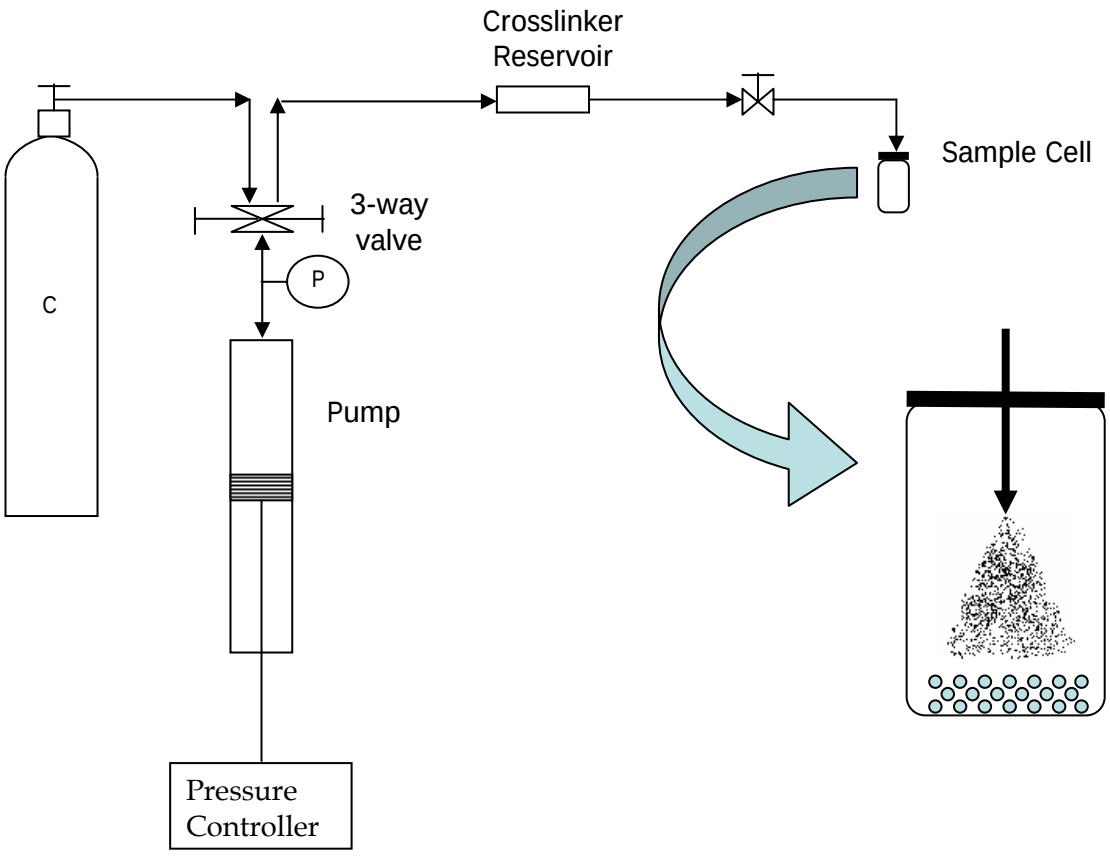

Figure 2. Apparatus for crosslinker and photoinitiator spraying on PLGA microparticles.

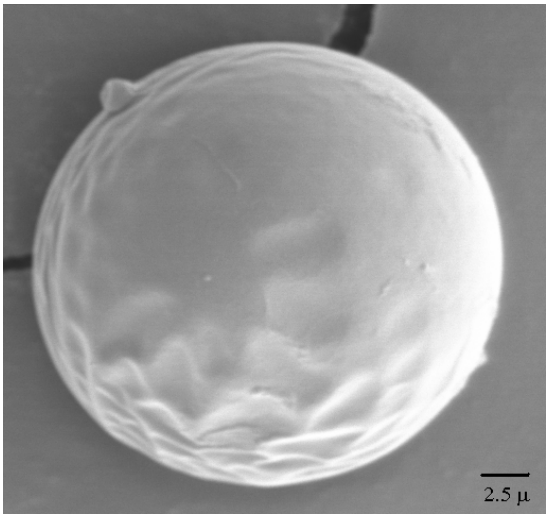

Non crosslinked PLGA particle, x3000, diameter = 26 μm

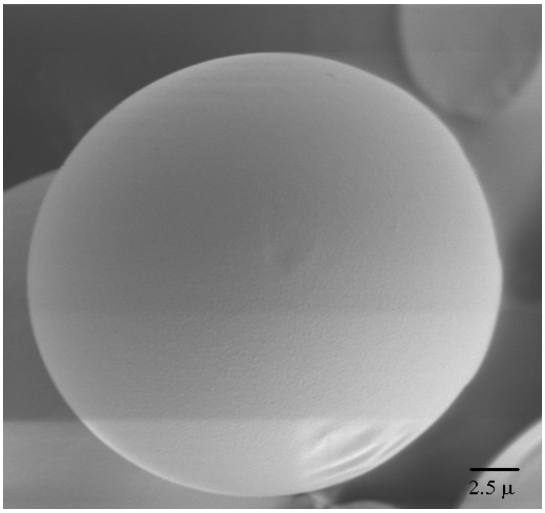

Surface crosslinked PLGA particle, x3000, diameter = 26 μm

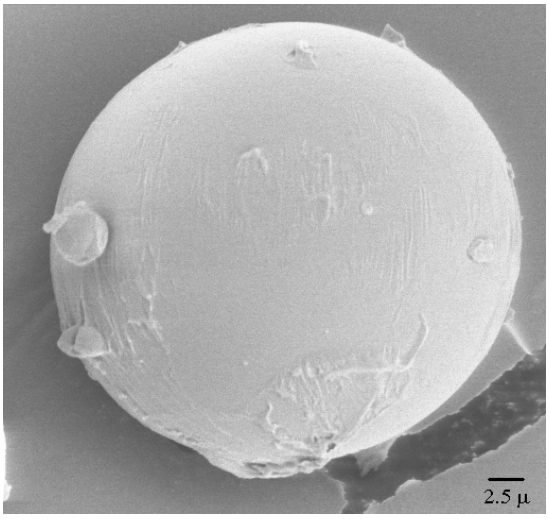

Non crosslinked PLGA particle, x2000, diameter = 40 μm

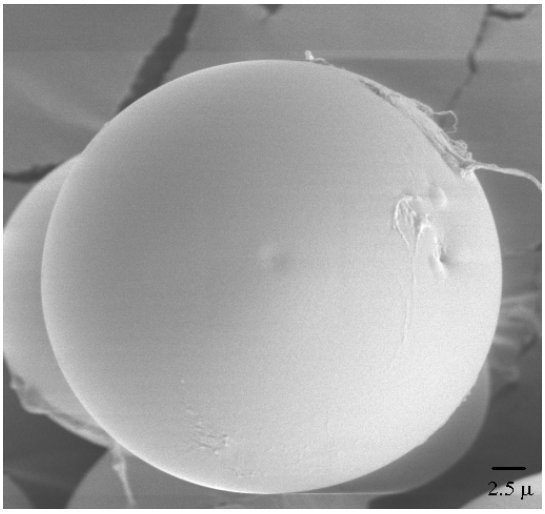

Surface Crosslinked PLGA particle, x2000, diameter = 40 μm

Figure 3. SEM micrographs of dexamethasone encapsulated PLGA non crosslinked and surface crosslinked polymer particles made from solvent evaporation technique.

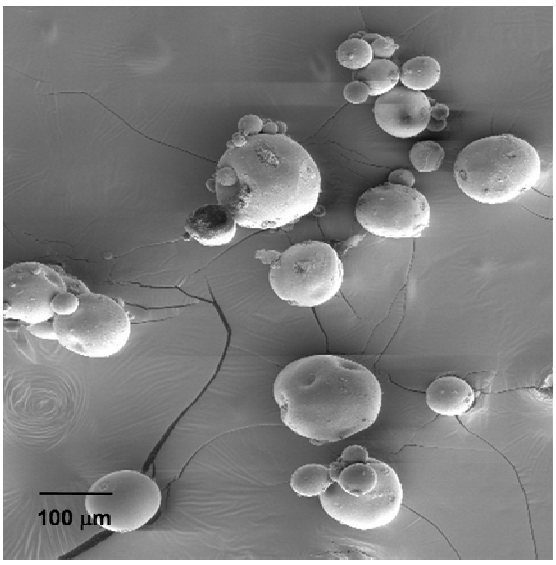

Original PLGA microparticle, x100, diameters ~ 80-120 μm

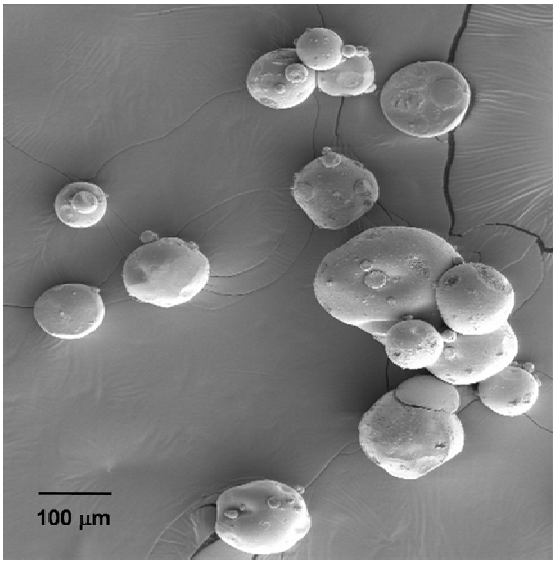

Surface Crosslinked PLGA microparticle, x100, diameters ~ 80-120 μm

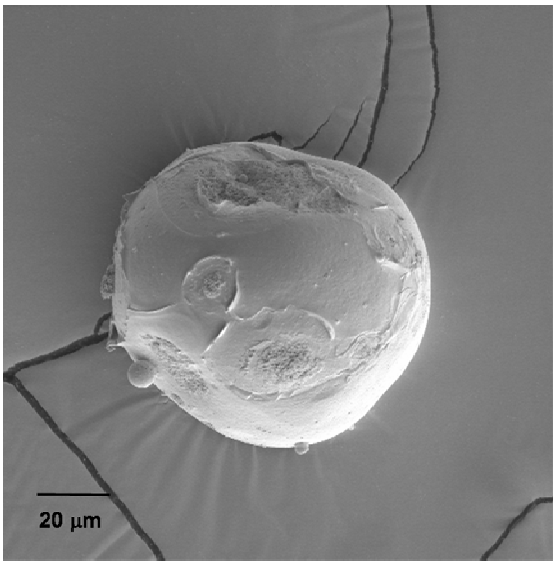

Original PLGA microparticle, x500, diameter = 105 μm

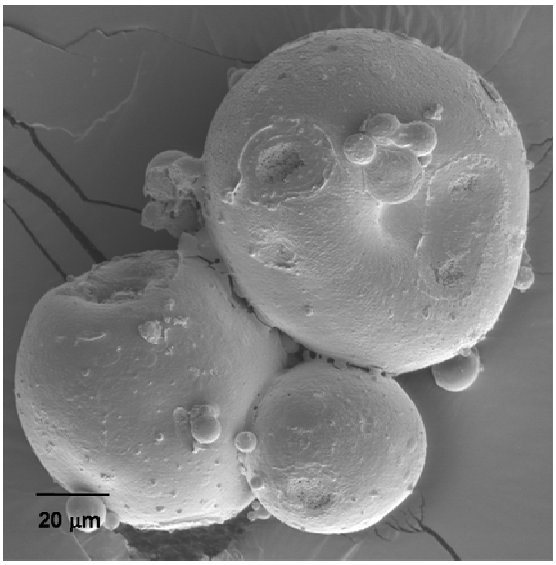

Surface PLGA microparticle, x500, diameters = 90-100 μ

Figure 4. SEM micrographs of dexamethasone encapsulated PLGA original and surface crosslinked microparticles made from phase coacervation technique.

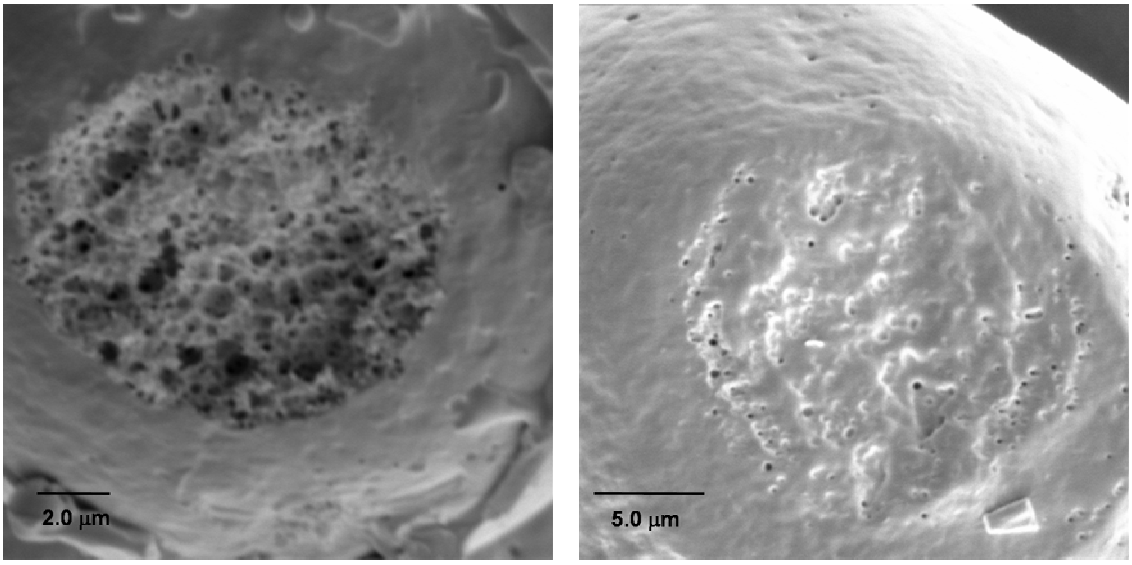

Original PLGA microparticle, x5000, crater of 20 μm with pore size < 1 μm	Crosslinked PLGA microparticle, x3000, crater of 20 μm with pore size < 1 μm

Figure 5. Magnified images of microparticle surface to provide an evidence to reduction in porosity on the surface due to surface crosslinking of EGDMA on PLGA microparticles.

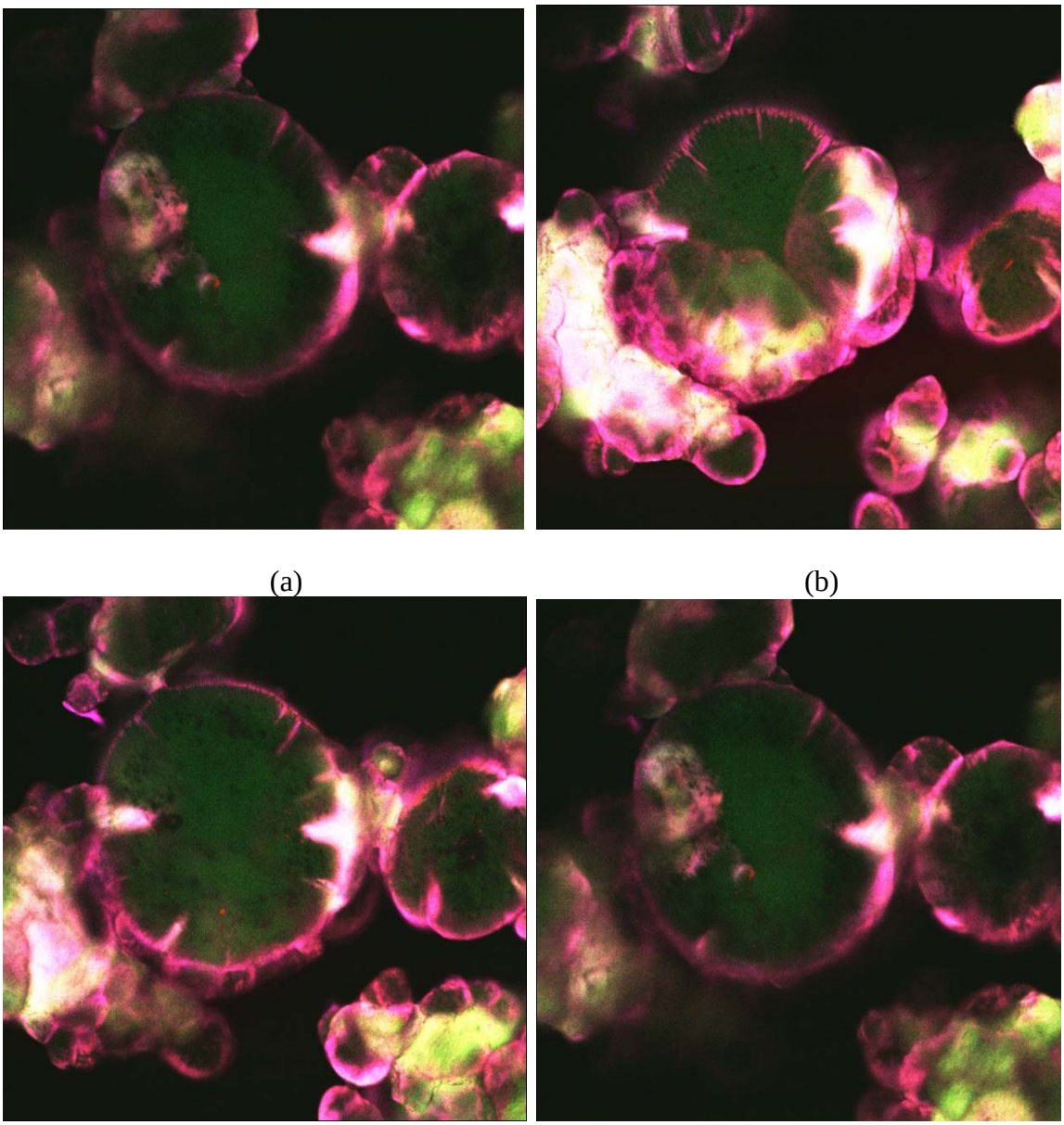

(a) (b)

(c) (d)

Figure 6. Cross-sectional images of PLGA microparticles coated with P(EGDMA) and Rhodamine-B using confocal laser scanning microscope images. (Triple labelling)

(a) Top Level, (b) Top Center Level, (c) Bottom Center Level, (d) Bottomost Level

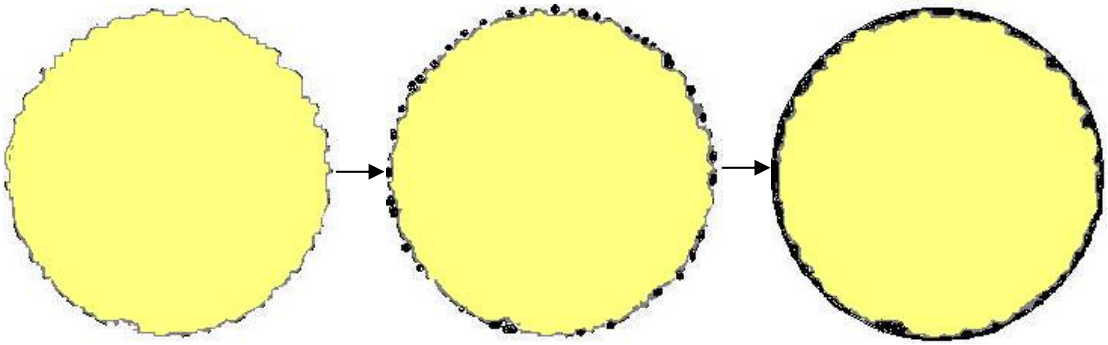

Drug Microparticle (size range: 40-50 μm)

Drug Microparticle (size range: 40-50 μm) with EGDMA

Drug Microparticle with surface crosslinking.

Figure 7. Schematic representation of the surface crosslinking process.

(a)

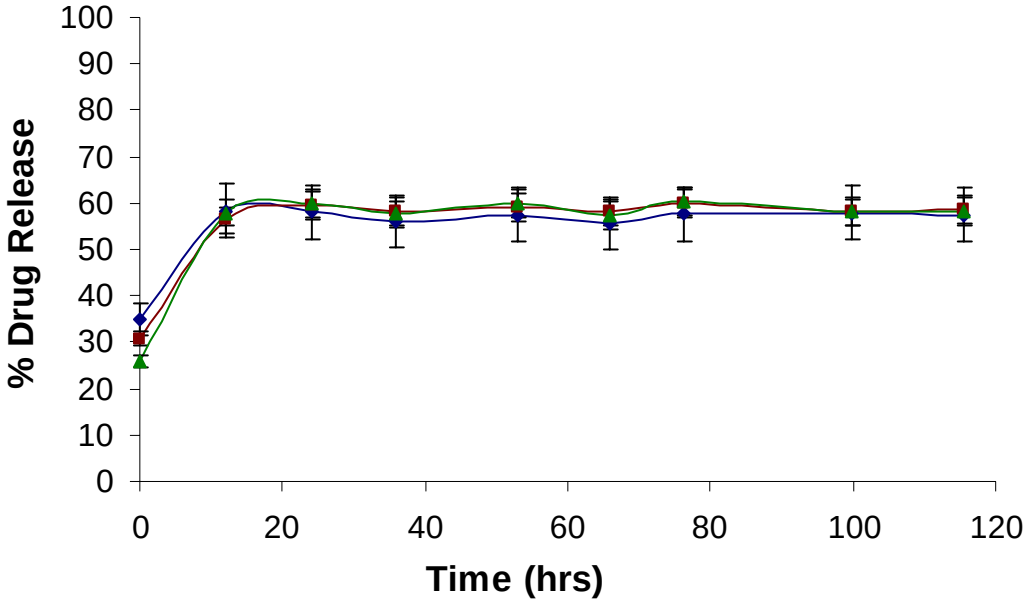

(b)

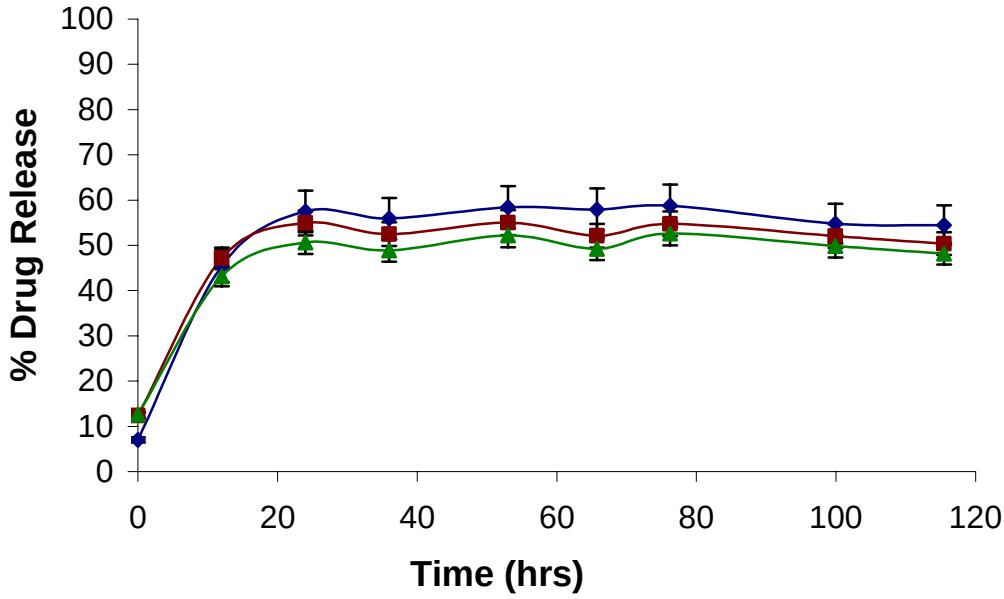

Figure 8. Drug release profile from (a) original and (b) surface crosslinked polymer microparticles loaded with dexamethasone formed by the solvent evaporation technique. Experiements were performed in triplets.

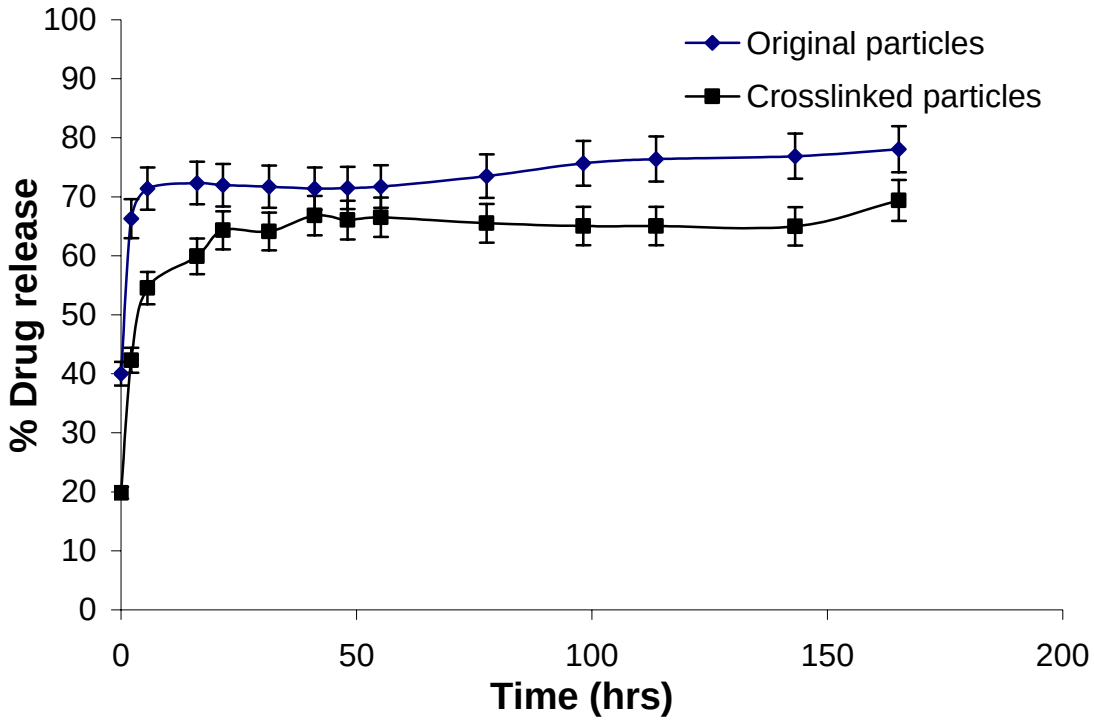

Figure 9. Drug release profile from original and surface crosslinked polymer microparticles loaded with dexamethasone phosphate formed by the phase coacervation technique.

(a)

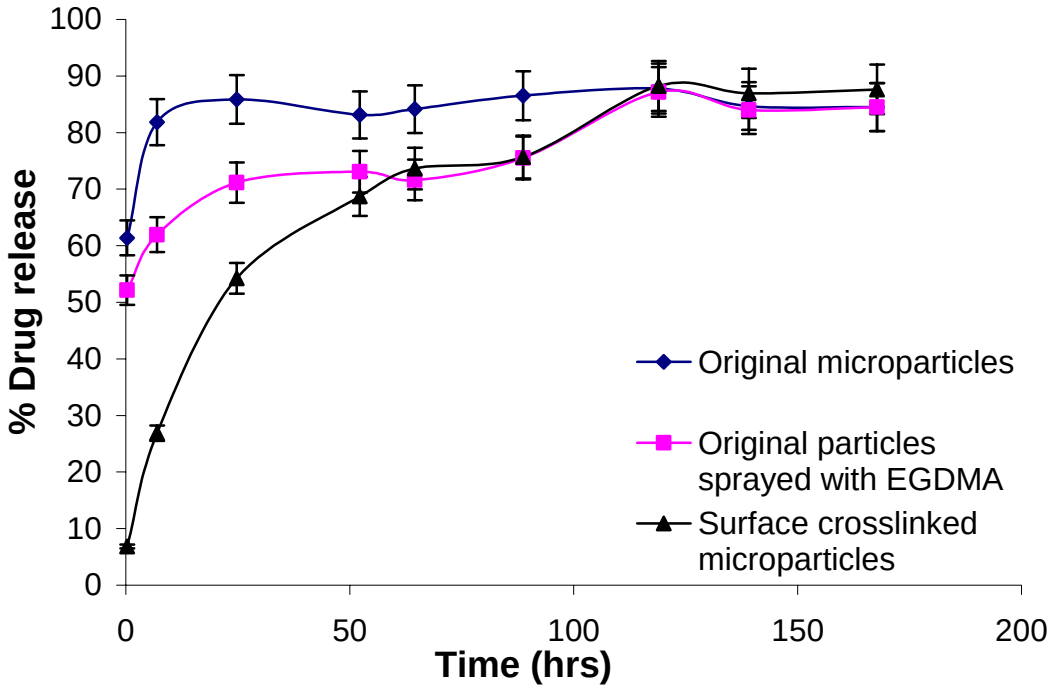

(b)

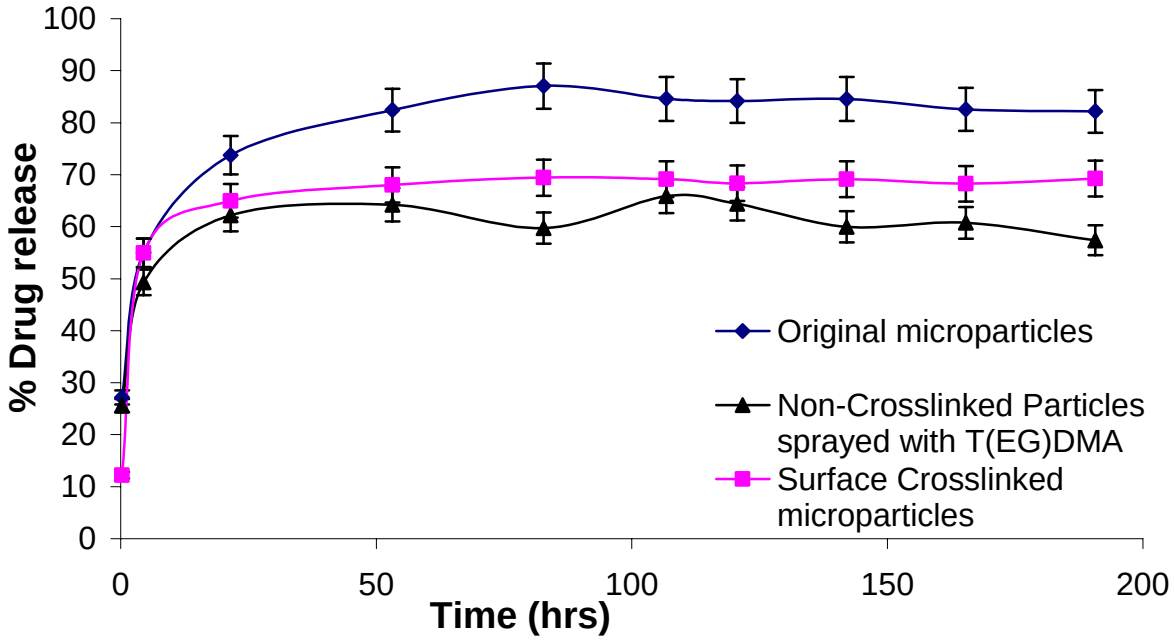

Figure 10. Dexamethasone release profile from original, only coated but not crosslinked, and surface crosslinked microparticles using (a) EGDMA, and (b) Tri(EG)DMA.

(a)

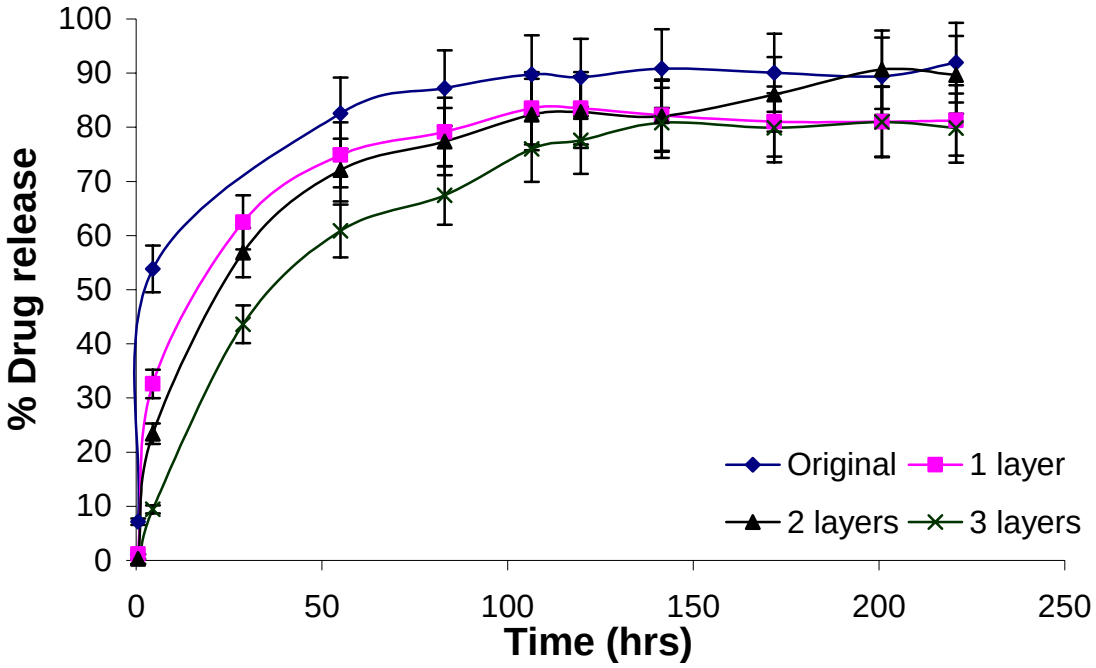

(b)

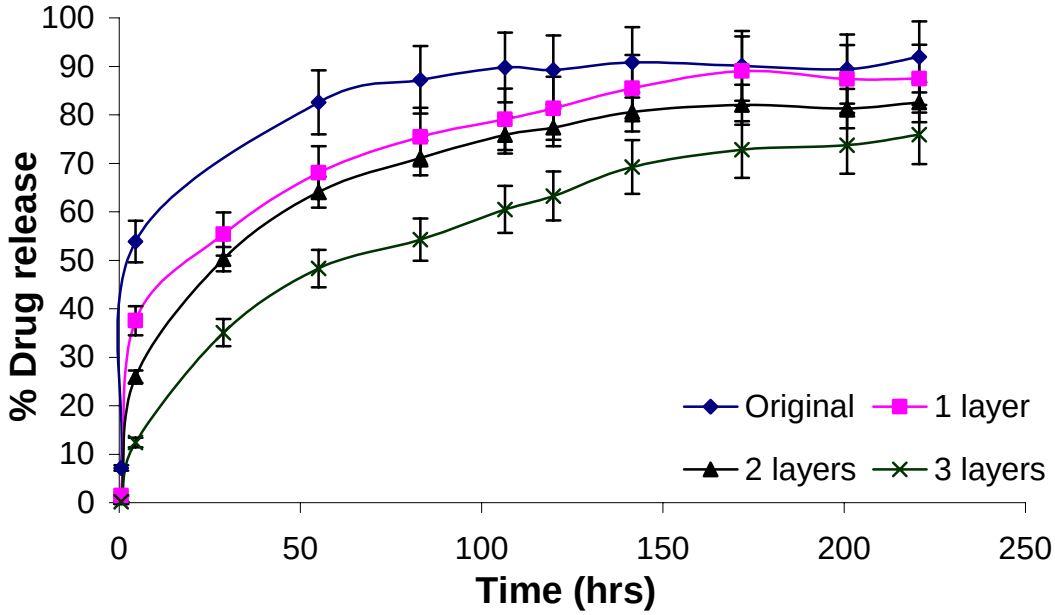

Figure 11. Dexamethasone release profiles from surface crosslinked microparticles with 1 layer, 2 layers, and 3 layers of (a) EGDMA and (b) Tri(EG)DMA compared to that from the original microparticles.

References

[1] X. Huang, C. S. Brazel, *J. Controlled Release* 73 (2001) 121-136.

[2] J.A. Setterstrom, T.R. Tice, W.E. Meyers, J.W. Vincent, *Second World Congress on Biomaterials 10th Annual Meeting of the Society for Biomaterials,* Washington, DC, (1984) 4.

[3] M. L. Shively, B. A. Coonts, W. D. Renner, J. L. Southard, A. T. Bennet, *J. Control. Release* 33 (1995) 237–243.

[4] B. D. Ratner, A. S. Hoffman, F. J. Shoen, J. E. Lemons, editors. *Biomaterials science: an introduction to materials in medicine.* New York: Academic Press, 1996.

[5] S. L. Robbins, R. Cotran, V. Kumar, editors. *Basic pathology.* Philadelphia, PA: Saunders, 1992.

[6] B. Jeong, Y. H. Bae, S. W. Kim, *J. Control. Release* 63 (2000) 155–163.

[7] D. S. T. Hsieh, W. D. Rhine, R. Langer, *J Pharm Sci* 72 (1983) 17–22.

[8] M. T. Peracchia, R. Gref, Y. Minamitake, A. Domb, N. Lotan, R. Langer, *J Control Rel* 46 1997 223–31.

[9] H. M. Redhead, S. S. Davis, L. Illum, *J Control Rel* 70 (2001) 353–63.

[10] T. G. Park, S. Cohen, R. Langer, *Macromolecules* 25 (1992) 116-22.

[11] C. X. Song, V. Labhasetwar, H. Murphy, X. Qu, W. R. Humphrey, R. J. Shebuski and R. J. Levy, *J. Control Release* 43 (1997) 197-212.

[12] N. S. Patil, J. S. Dordick, D. G. Rethwisch, *Biomaterials*, 17 (1996) 2343-2350.

[13] M. G. Cascone, P. M. Pot, L. Lazzeri, Z. Zhu, *J. Mat. Sci.: Mat. in Medicine*, 13 (2002) 265-269.

[14] B. Narasimham, R. Langer, *Polym. Mater. Sci. Eng. Proc.* 76 (1997) 558–559.

[15] T. W. Chung, Y. Y. Huang, Y. Z. Liu, *Int. J. Pharm.* 212 (2001) 161-169.

[16] A. G. A. Coombes, M. K. Yeh, E. C. Lavelle, S. S. Davis, *J. Control. Release* 52 (1998) 311-320.

[17] H. Rafati, A. G. A. Coombes, A. Adler, J. Holland, S. S. Davis, *J. Control. Release* 43 (1997) 89-102.

[18] S. K. Mallapragada, N. A. Peppas, P. Colombo, *J. Biomed. Mater. Res.* 36 (1997) 125-130.

[19] Y. Y. Huang, T. W. Chung, T.W. Tzeng, *Int. J. Pharm.* 182 (1999) 93-100.

[20] M. van de Weert, R. van't Hof, J. van der Weerd, R. M. A. Heeren, G. Posthuma, W. E. Hennink, D. J. A. Crommelin, *J. Control. Release* 68 (2000) 31-40.

[21] T. K. Mandal, L. A. Bostanian, R. A. Graves, S.R. Chapman, *Pharmaceutical Research* 19 2002 1713-1719.

[22] X. Huang, B. L. Chestang, C. S. Brazel, *Int. J. Pharmaceutics*, 248 (2002) 183-192.

[23] S. H. Chiou, W. T. Wu, Y. Y. Huang, T. W. Chung T. W., *J. Microencapsulation*, 18 (2001) 613-625.

[24] M. B. Mellott, K. Searcy, M. V. Pishko, *Biomaterials* 22 (2001) 929-941.

[25] N. B. Graham, M. E. McNeill, *Biomaterials* 5 (1984) 27-37.

[26] S. R. Jameela, S. Lakshmi, N. R. James, A. Jayakrishnan, *J. Appl. Poly. Sci.*, 86 (2002) 1873–1877.

[27] Merck Index, 12th Edition, Merck & Co., Inc. Whitehouse Station, NJ (1996).

[28] C. W. Distelhorst, *Nature* 9 (2002) 6-19.

[29] M. T. Brahmapurikar, P. J. Moghe, M. Mateenuddin, N. L. Sadre, *Indian. J. Pharmacy.* 12 (1980) 243-246.

[30] R. H. Scott, A. J. Woods, M. J. Lacey, D. Fernando, J. H. Crawford, P. L. R. Andrews, *Naunyn-Schmiedeberg's Arch Pharmacol* 352 (1995) 247-255

[31] H. Silverstein, J. P. Light, L. E. Jackson, S. I. Rosenberg, J. H. Thompson, *ENT Journal*, 82 (2003) 28-32.

[32] J. J. Wang, S. T. Ho, S. C. Lee, Y. C. Liu, C. M. Ho, *Anesth Analg* 91 (2000) 1404-07.

[33] Bodmeier, R., McGinity, J.W., *J. Microencapsul.* 4-4 (1987) 279–288.

[34] Bodmeier, R., McGinity, J.W., *Pharm. Res.* 4 -6 (1987) 465–471.

[35] Heya, T., Okada, H., Tanigawara, Y., Ogawa, Y., Toguchi, H., *Int. J. Pharm.* 69 (1991) 69–75.

[36] Yamakawa, I., Tsushima, Y., Machida, R., Watanabe, S., *J. Pharm. Sci.* 81 (1992) 899–903.

[37] Ficheux, M.-F.; Bonakdar, L.; Leal-Calderon, F.; Bibette, J. *Langmuir* 14 (1998) 2702-2706.

[38] Jalil, R., Nixon, J.R., *J. Microencapsul.* 6 (1989) 473–484.

[39] Iwata, M., McGinity, J.W., *Pharm. Res.* 10 (1993) 1219–1227.

[40] M. Iwata, T. Tanaka, Y. Nakamura, J.W. Int. J. Pharm. 160 (1998) 145–156.

[41] M. Iwata, Y. Nakamura, J.W. McGinity, *J. microencapsulation*, 16 (1999) 49-58.

[42] Rickey, Michael E.; Ramstack, J. Michael; Kumar, Rajesh, United States Patent Application 20030118660 (2003).

[43] T. Hickey, D. Kreutzer, D. J. Burgess, F. Moussy, *Biomaterials* 23 (2002) 1649–1656.

[44] D. Lamiable, R. Vistelle, H. Millart, V. Sulmont, R. Fay, J. Caron, H. Choisy, *J. Chromatography* 378 (1986) 486–91.

[45] C. Berkland, K. Kim, D. W. Pack, *J. Cont. Rel.* 73 (2001) 59-74.

[46] C. Berkland, M. King , A. Cox, K. Kim, D. W. Pack, *J. Cont. Rel.* 82 (2002) 137–147.

[47] C. Berkland, K. Kim, D. W. Pack, Pharm. Res., 20 (2003) 1055-62.

[48] A. Streubel, J. Siepmann, R. Bodmeier, *Eur. J. Pharm. Sci.* 18 (2003) 37–45.

[49] R. E. Eliaz, J. Kost, *J Biomed Mater Res* 50 (2000) 388–96.

[50] H. Murakami, M. Kobayashi, H. Takeuchi, Y. Kawashima, *J Cont. Rel* 67 (2000) 29–36.

[51] J. M. Anderson, M. S. Shive, *Advanced Drug Delivery Reviews* 28 (1997) 5–24.

[52] Mandal T. K., *DrugDev. Ind. Pharm.* 24 (1998) 623-629.

CHAPTER 7

NANOPARTICLE FORMATION OF A HYDROPHILIC DRUG USING SUPERCRITICAL CO_2 AND MICROENCAPSULATION FOR SUSTAINED RELEASE

Abstract

Purpose: To produce nanoparticles of a hydrophilic drug using supercritical CO_2, encapsulate the obtained nanoparticles into polymer microparticles using an anhydrous method and study their sustained *in-vitro* drug release.

Methods: Hydrophilic drug, dexamethasone phosphate, is dissolved in methanol and injected in supercritical CO_2 with ultrasonic field for enhanced molecular mixing (SAS-EM technique). Supercritical CO_2 rapidly extracts methanol leading to instantaneous precipitation of drug nanoparticles. The nanoparticles are then encapsulated in poly(lactide-co-glycolide) polymer using anhydrous s/o/o/o technique. This results in the well-dispersed encapsulation of drug nanoparticles in polymer microspheres. *In-vitro* drug release from these microparticles is studied.

Results: Using supercritical CO_2 as an antisolvent, nanoparticles of dexamethasone phosphate were obtained in the range of 150-200 nm. Upon encapsulation in PLGA, composite microspheres of size ~70 μm were obtained. The i*n-vitro* drug release of these nanoparticles/microparticles composite shows sustained release of dexamethasone phosphate over a period of 700 hours with almost no initial burst release.

Conclusions: Nanoparticles of dexamethasone phosphate can be produced using SAS-EM technique. When microencapsulated, these particles can provide sustained drug release without initial burst release. Since the complete process is anhydrous, it can be easily extended to produce sustained release formulation of other hydrophilic drugs.

Keywords: sustained/controlled drug release, dexamethasone phosphate, PLGA, SAS-EM, s/o/o/o, supercritical, nanoparticle.

Introduction

Formulations for sustained release of active pharmaceutical ingredients (API) using biodegradable polymer microencapsulation have been developed for delivery via oral,[1,2] transdermal,[3,4] subcutaneous depot[5] and other routes. A wide variety of microencapsulation procedures have been developed such as oil-in-

water (o/w) solvent evaporation,[6] water-oil-water (w/o/w) double emulsion,[7] hydrous water-oil-oil[8] water-oil-oil-oil (w/o/o/o),[9] solid-oil-water (s/o/w),[10] anhydrous solid-oil-oil-oil (s/o/o/o)[16] and some novel phase separation techniques.[9,11] However, various problems with drug encapsulation, drug release, protein instabilities, aggregation and denaturation still persist.[12] Some advances have been made in resolving these problems and stabilizing these API.[13] However, the problem with hydrophilic drugs still persists in that the drug particles are not very small as compared to the encapsulating polymer microparticles or is encapsulated in the form of small clusters within the polymer matrix, resulting in high initial release.

Hence, the objective of this work is to produce sustained release formulations made of biodegradable PLGA microparticles, with fine nanoparticles of a hydrophilic drug, dexamethsone phosphate encapsulated in them. Formulation is achieved in two steps. The first step is reducing the particle size of the drug particles by the use of supercritical antisolvent technique with enhanced mass transfer (SAS-EM®).[14] The second step is the use of s/o/o/o phase separation/coacervation technique[15] for microencapsulation of drug nanoparticles. Both these steps are completely anhydrous and hence are easily extendible to formulations of hydrophilic drugs including rigid proteins.[16,17]

Dexamethasone is a synthetic adrenocortico-steroid possessing basic glucocorticoid activity. A crystalline, water-soluble salt of the same drug, disodium salt of dexamethasone phosphate, is utilized here. It is highly soluble in water and has been used in various drug delivery applications including ocular inserts,[18] ocular injections[19] and polymer-lipid controlled release devices.[20]

Two different issues have been addressed in this work. One of the problems with sustained drug delivery devices is early release of most of the hydrophilic drug within few days with a substantial loss of drug during the few initial hours, termed as 'initial burst release'. This problem can be approached by reducing the particle size. Earlier attempts to reduce particle sizes involve spray-freeze drying of suspensions containing the API,[21,22] where particles size around 1-2 μm with some around sub-micron range were obtained. In this work, this problem was resolved by reducing the particle size of the API by SAS-EM technique such that the relative size of the drug is very small as compared to the size of the polymer microparticles allowing the drug to be well dispersed in the polymer matrix. The other problem was a poor percentage encapsulation of the drug in the polymer microparticles resulting in a heavy loss of the API during the formulation process itself. Out of the available microencapsulation techniques, the anhydrous s/o/o/o technique gives maximum encapsulation efficiencies for hydrophilic drugs and proteins.[10] Moreover, this technique does

not require use of any surfactants, which greatly lowers the chances of protein becoming unstable,[23] aggregrated,[24] or denatured[25].

Materials

Poly(lactide-co-glycolide) (PLGA 50:50; inherent viscosity = 0.39 dL/g in HFIP @ 30^{o}C) was obtained from Birmingham Polymers. Sodium salt of dexamethasone-21-phosphate was obtained from Sigma Chemicals. Dichloromethane (99.9% ACS grade), silicon oil (dimethicone, 350 cSt) were purchased from Sigma Aldrich, and methanol (HPLC grade), phosphate buffer saline (PBS, Labchem Inc., pH=7.4), and hexane (HPLC grade) were obtained from Fisher Scientific. All the materials were used as received.

Apparatus and Procedure

1. Formation of Drug Nanoparticles

SAS-EM process for forming drug nanoparticles is explained in depth by Gupta and Chattopadhyay.[26] A schematic of the SAS-EM apparatus is shown in Figure 1. The main component of the apparatus is a high-pressure precipitation cell (R) with an approximate total volume of 110 cm^{3}. A titanium horn (H, Sonics and Materials, Inc.) having a tip of 1.25 cm in diameter is attached to the

precipitation cell to provide the ultrasonic field generated by a 600 W (max. power), 20 kHz ultrasonic processor (U, Sonics and Materials, Inc). The volume of the precipitation cell with horn in place is approximately 80 cm^3. The ultrasonic processor is designed to deliver ultrasound at constant amplitude. The experiment was carried out at constant temperature and constant pressure of the supercritical CO_2 medium. Critical temperature and pressure of CO_2 is 31^oC and 1071 psi. Hence, to maintain supercritical conditions, the experiments were carried out at 40^oC and 1500 psi. The constant pressure was maintained by using an ISCO syringe pump (Model 500D), which continuously delivers supercritical CO_2 at constant pressure, and constant temperature by heating coil, temperature sensor and RTD controller device. Supercritical CO_2 was fed inside the precipitation cell through the inlet port located at the bottom of the vessel and purged from the exit located at the top of the vessel through an inline membrane filter to prevent the loss of any drug particles. The precipitation cell was allowed to reach steady temperature and pressure conditions. After adjusting the ultrasonic intensity to the desired value, 10 mg/ml dexamethasone phosphate solution in methanol was injected into the precipitation cell at a rate of 2 ml/min using a pump (Lab Alliance, Series 1500, dual head piston pump with pulse dampener). During the injection process, a minor purge of 1 ml/min was continuously left running to allow methanol extracted by CO_2 to be purged out

of the system. The solution was injected through a 1/16th in. PEEK tubing of internal diameter 100 μm that acts as a nozzle. The nozzle is horizontal to the horn and touches the center of the horn so that the liquid jet experiences maximum ultrasonic intensity. These ultrasonic vibrations break the liquid jet into very fine droplets, their diameter being controlled by the ultrasonic intensity, which in turn is controlled by changing the amplitude of the ultrasonic vibration. 90 W was used to drive the ultrasonic horn.[14]

After injecting the solution, the ultrasound is turned off and the system is allowed to purge with fresh CO_2 almost 5 times the volume of the precipitation cell to completely remove methanol from the cell. The cell is then depressurized and drug nanoparticles are collected.

2. Microencapsulation of drug nanoparticles

Drug nanoparticles obtained from SAS-EM were encapsulated in PLGA microspheres by using the non-aqueous s/o/o/o[27,28] solid dispersion technique. 400 mg PLGA was first dissolved in 5 ml dicloromethane. 20 mg dexamethasone phosphate nanoparticles were then finely dispersed into 5 ml PLGA/ dichloromethane by sonication. A fine suspension of drug nanoparticles with no sedimentation was obtained. Under continuous mixing using a Corning® magnetic stirrer at around 1000 rpm, five ml of 350 cSt silicon oil was added to this suspension resulting in the coacervation of the organic phase. This caused

PLGA to precipitate in the form of microspheres encapsulating drug nanoparticles. This suspension was added to 75 ml hexane, pre-cooled to 5^{o}C, to extract out the dichloromethane and silicon oil. The microparticles were collected by vacuum filtration through a Whatman no. 1 filter paper. The microparticles were washed with cold hexane, to remove residual dichloromethane, and silicon oil. These microparticles were then air dried under mild vacuum to remove residual hexane.

Similar procedure was repeated for the encapsulation of dexamethasone phosphate particles as provided by the supplier without any further particle modification (termed as "unprocessed drug particles" henceforth) for comparative analysis.

3. Particle size analysis

The unprocessed drug particles, drug nanoparticles obtained from the SAS-EM process as well as the encapsulated drug/polymer microparticles obtained from the s/o/o/o technique were analyzed for their sizes and surface morphology using a scanning electron microscope (SEM: Zeiss, model DSM 940). The particles were initially spread on a carbon tape glued to an aluminum stub and coated with Au using a Sputter Coater® (Pelco, model Sc-7 and Electron Microscopy Systems, model EMS 550) under a vacuum of 0.2 mbar. The sputter coating process involves applying vacuum of 0.1 mbar to the microparticles in a

closed chamber. The particles are then coated with a Au vapor in presence of a small purge of Argon gas at 0.2 mbar. The Au layer is coated to make the particle surface conductive to electrons in the SEM. The particles were coated 4 times for a 30 sec interval instead of a single coat of 2 minutes to avoid melting of the polymer because of excessive heating. The sputter coater adds Au layer of ~10 nm thick in 2 minutes. Hence, the amount of Au coated in 2 minutes is insubstantial as compared to the size of the microparticles (about 50-100 μm) so as not to alter the microparticles morphology or surface texture on a micron level. The microparticles were then observed under SEM and micrographs were recorded. Multiple images of different areas of the SEM stub were recorded for microparticles size analysis.

4. Extent of encapsulation measurement

To determine the percentage of drug nanoparticles that were not encapsulated into the polymer (termed as surface drug), 5 mg of the microparticles were suspended in 2 ml of PBS buffer. This aqueous buffer was then filtered through a 5 μm Alltech® syringe filter and tested for the drug content using HPLC (Model 600, Waters Corp.) for dexamethasone phosphate. The HPLC is equipped with a 7725i Rheodyne® six-port injection valve, model 600 HPLC pump controller with dual head pump, model 2410 refractometer and model 2487 Dual λ UV spectrometer. To determine the total amount of

dexamethasone phosphate encapsulated, a different technique was utilized. The polymer is soluble in dichloromethane, whereas the drug is soluble in PBS buffer. Using this concept, 5 mg of PLGA microparticles containing dexamethasone phosphate were dissolved in 1 ml of dichloromethane and this was then equilibrated overnight with 2 ml of PBS buffer. The aqueous phase was then tested for dexamethasone phosphate content using HPLC for dexamethasone phosphate. This method of analysis was validated by mixing known amounts of polymer, and drug in known quantities of PBS buffer and dichloromethane.[29] In HPLC, the mobile phase was kept acidic to maintain the sodium salt of dexamethasone phosphate in un-dissociated form. Hence, the mobile phase was modified to 0.05 M PBS buffer : acetonitrile : acetic acid in the ratio of 70:28:2 flowing at 1 ml/min through a 3.9 mm x 150 mm Novapak C-18 column. The UV wavelength for dexamethasone phosphate in HPLC detector was set to 244 nm.

5. In-vitro release rate study

The microparticles were taken to study the release rate of the drug from the polymer over a period of time. For this purpose, two simultaneous experiments were carried out. About 50 mg of PLGA microparticles, containing drug nanoparticles encapsulated in them, were suspended in 100 ml of 0.05 M phosphate buffer saline (PBS, pH=7.4) at 37^{o}C in an incubator, and stirred at 50

rpm. Simultaneously, 50 mg of PLGA microparticles, containing unprocessed drug particles encapsulated in them, were also suspended in 100 ml PBS at similar conditions. For in-vitro release study, PBS at pH=7.4 at 37^{o}C resembles to the environment that the drug would experience when it is in contact with the blood inside human body. 50 rpm is USP standard to simulate the hydrodynamic behavior inside body.[30] These particles are meant for subcutaneous applications. Hence, eventhough the PLGA microparticles will not experience the buffer conditions, the drug content that is assimilated in the blood will experience buffer conditions. Samples, after being filtered using a 5 μm filter, were taken approximately once or twice a day and analyzed for dexamethasone phosphate using HPLC as described above.

Results and Discussion

The process of supercritical antisolvent precipitation with enhanced mass transfer is well explained earlier.[31] In this technique, the drug is dissolved in a solvent, which is miscible with supercritical CO_2. When the solution is injected in supercritical CO_2 in the form of a fine spray, CO_2 acts as an antisolvent and removes the organic solvent from the fine droplets resulting in the formation of drug microparticles. In order to achieve a further reduction in the particle size, ultrasonic vibrations are used to enhance mass transfer between supercritical

CO_2 and the organic medium. This helps in the formation of even smaller droplets and instantaneous removal of the solvent resulting in the formation of drug nanoparticles.

The process of phase separation/ coacervation has been well established.[32] In this case, the ratio of drug to polymer was maintained to 1 : 20 in order to achieve a good dispersion of the drug in the polymer matrix. The polymer was about 6 wt. % of the polymer solvent i.e. dichloromethane. The percentage of silicon oil to dichloromethane was maintained around 42 : 58. Considering these percentages, the percentages of PLGA : dichloromethane : silicon oil was around 3.4 : 55.8 : 40.8. These percentages lie within the "stability window" for perfect microencapsulation of drug particles into the polymer microparticles.[33,34] Moreover, the rate of addition of silicon oil was maintained close to 5 ml/min for better coacervation efficiency.[35]

1. Particle size and morphology

The unprocessed dexamethasone phosphate particles as provided by the supplier were ~50-100 μm irregular shaped crystalline particles (Figure 2a). By the SAS-EM technique, dexamethasone phosphate particles were converted into nanoparticles of 150-200 nm size (Figure 2b).

The microencapsulation of dexamethasone phosphate nanoparticles into the PLGA microparticles mostly yielded composite particle ranging from 70-80

μm with a few smaller particles in 10-15 μm range (Figure 3a-b). Since the size ratio of drug nanoparticle to polymer microparticle is about 1:400, the drug nanoparticles can be imagined to be well dispersed within the polymer microparticle matrix. Whereas, the encapsulation of unprocessed drug particles resulted in some smaller particles in the range of 40-50 μm and some extremely large particles of about 100-120 μm (Figure 3c-d). This implies that only part of the drug particles got encapsulated and part of the PLGA particles did not have any drug particles encapsulated in them. These particles are definitely not the ones that can exhibit sustained drug release.

2. Percentage encapsulation

For microencapsulation of drug nanoparticles, drug-to-polymer ratio was taken as 1:20. For the case where the unprocessed drug particles as provided by the supplier were used, out of the total quantity of drug taken, about 16% of the drug was left unencapsulated during the process of s/o/o/o phase separation. Out of the remaining 84%, 5% of the total drug was not encapsulated inside the microspheres and was present on the surface. Hence, the net drug encapsulated was only 80%. This shows that only smaller drug particles were encapsulated leaving behind the larger ones. The microencapsulation procedure involves sonication before the addition of silicon oil (coacervate), which helps in creating a better suspension and increased encapsulation of existing large drug particles. However, for the case where drug nanoparticles were used for encapsulation, the

surface drug was only about 1.5%. The net percentage of drug nanoparticles encapsulated was about 90% with very little loss of drug.

3. In-vitro release rate study of the microencapsulated drug

In-vitro drug release of dexamethasone phosphate nanoparticles encapsulated in PLGA microparticles was compared to that from the unprocessed drug particles as provided by the supplier also encapsulated in PLGA microspheres. The in-vitro drug release of the unprocessed drug particles (but microencapsulated) showed an initial burst release of about 5% at time zero and all the drug was released within 24 hours (Figure 4a). This is not advisable for sustained drug release. Whereas, the in-vitro drug release of the nanoparticles (also microencapsulated) obtained using SAS-EM showed a continuous release for 700 hours (Figure 4b). The release profile showed almost zero burst release with ~15% release in the first 60 hours followed by a stationary state upto 200 hours during which only 22% of the encapsulated drug was released. This was followed with continuous increase in the drug release rate upto 500 hours during which 75% of the drug was released followed by continued release of the drug over time. From the sustained drug release profile, it can be clearly inferred that the drug was well dispersed in the polymer matrix allowing gradual release of the drug with polymer degradation as opposed to initial burst release observed in the case[29] where w/o/o/o phase separation technique was used for the encapsulation of dexamethasone phosphate.

Conclusion

Nanoparticles of dexamethasone phosphate can be produced using SAS-EM® technique. When microencapsulated, these nanoparticles provide a high encapsulation efficiencies and sustained drug release without initial burst release. Since the complete process is anhydrous, it can be easily extended to produce sustained release formulation of other hydrophilic drugs.

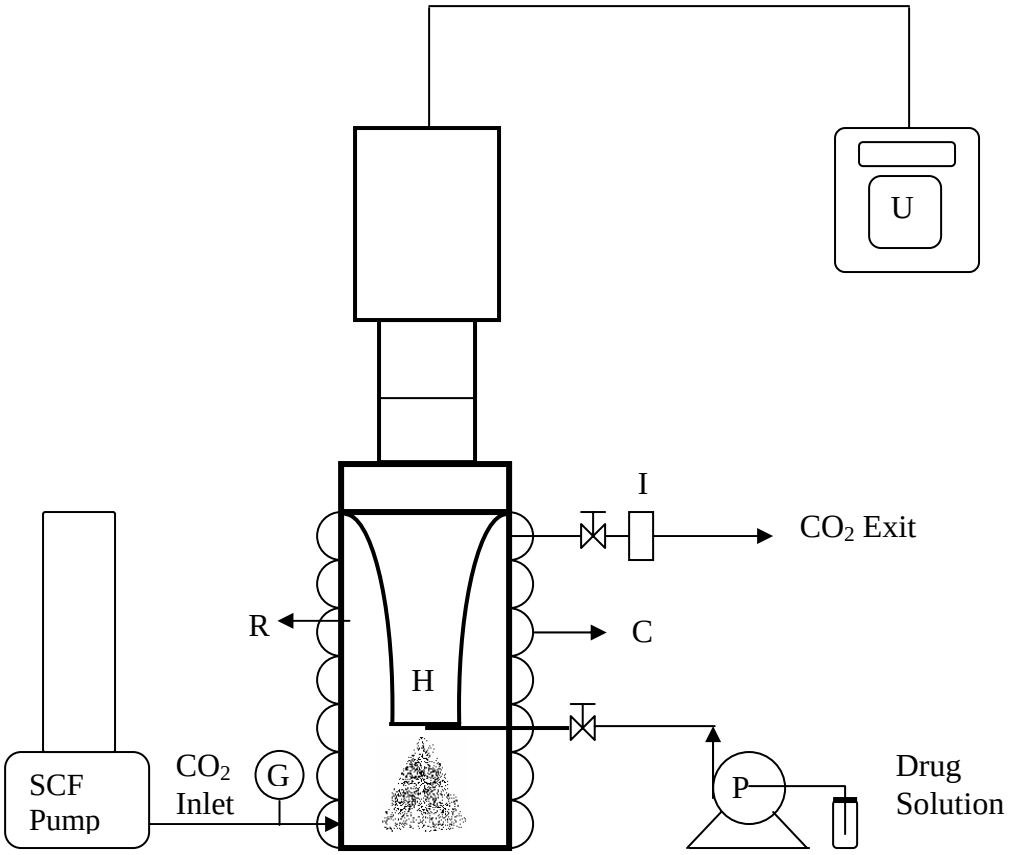

R: Precipitation Cell
SCF Pump: ISCO Syringe Pump for supercritical CO_2
I: Inline Filter
U: Ultrasonic Processor
P: High Pressure Dual Head Liquid Pump with Pulse Dampener
G: Pressure Guage
C: Heating Coil with Temperature Sensor and RTD Controller

Figure 1. Schematic of SAS-EM apparatus.

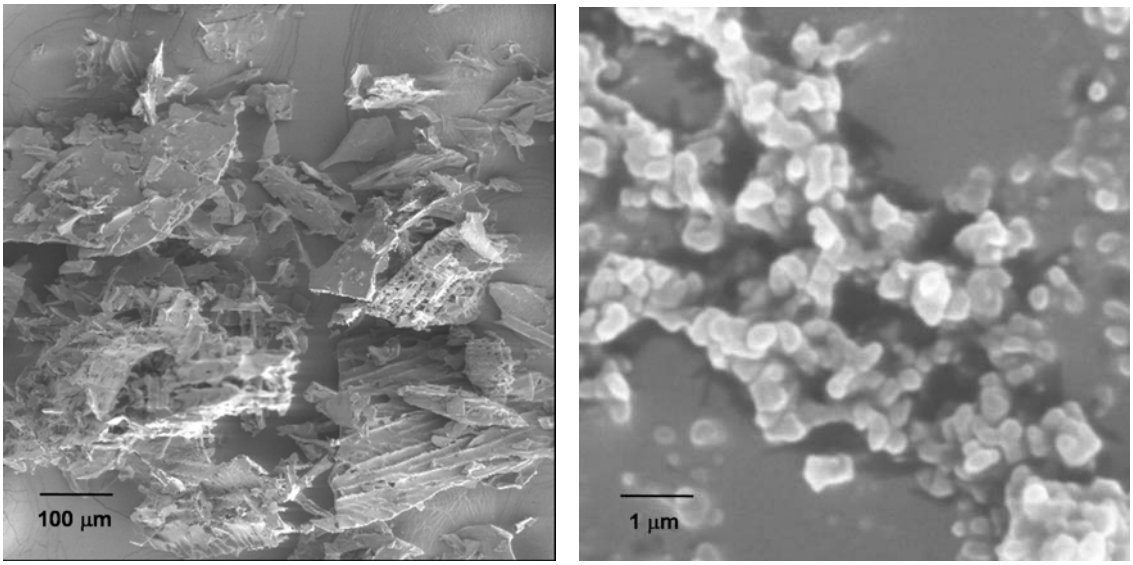

(a) (b)

Figure 2. SEM micrographs of (a) dexamethasone phosphate microparticles as provided by the supplier and (b) dexamethasone phosphate nanoparticles obtained by SAS-EM.

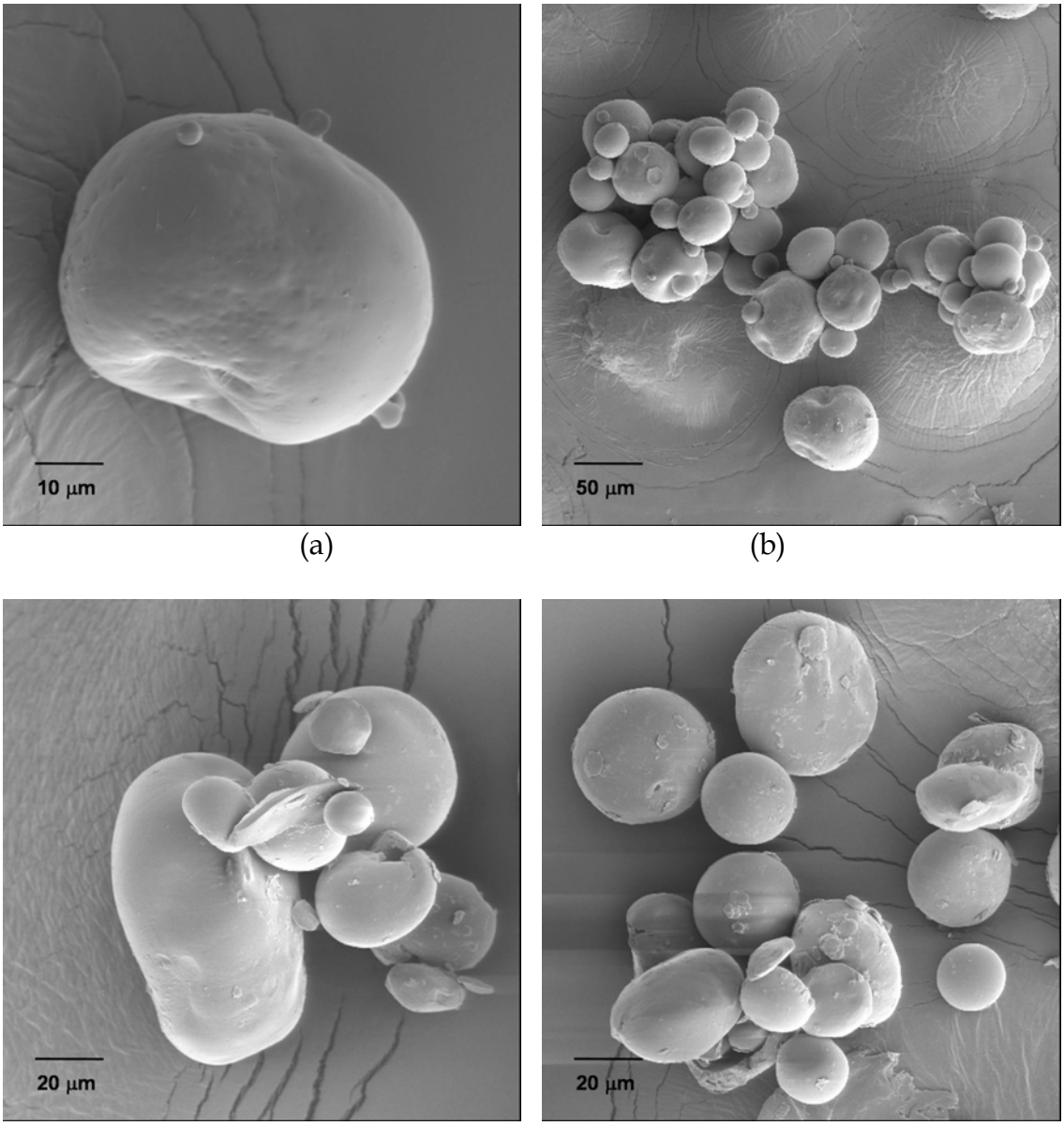

(a) (b)

(c) (d)

Figure 3. SEM micrographs of drug/polymer microparticles containing (a-b) drug nanoparticles and (c-d) unprocessed drug particles. Each microparticle contains 10 wt.% dexamethasone phosphate nanoparticles, and 90 wt.% PLGA.

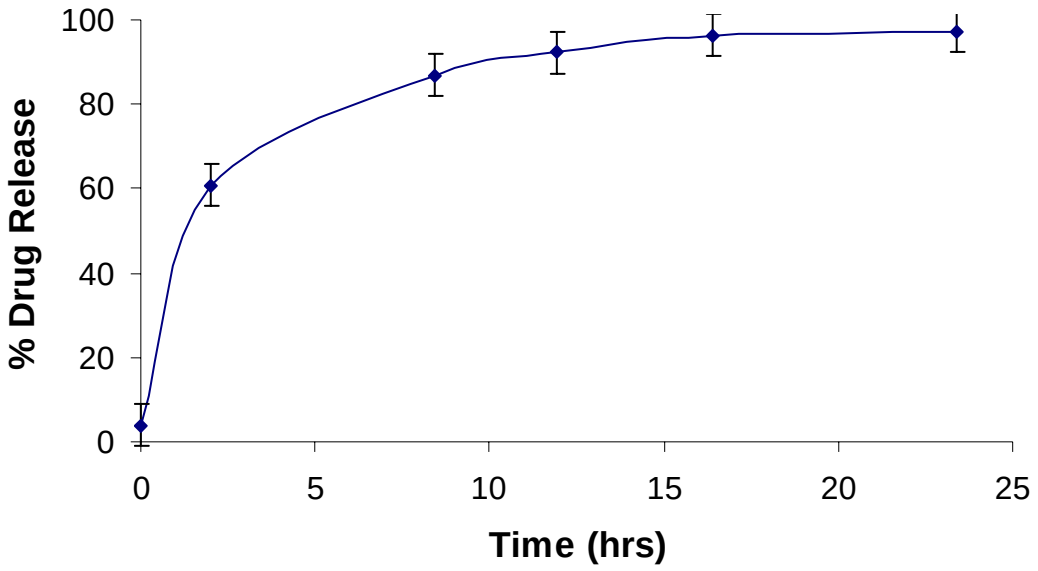

Figure 4a. *In-vitro* release profile of dexamethasone phosphate from PLGA microencapsulated drug microparticles as provided by the supplier (Figure 2a).

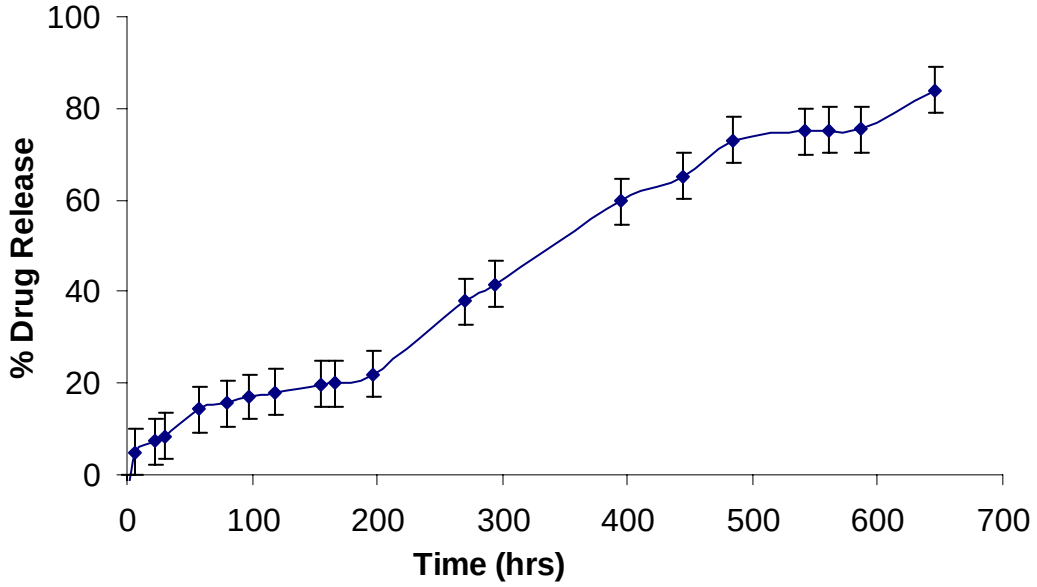

Figure 4b. *In-vitro* release profile of dexamethasone phosphate from PLGA microencapsulated drug nanoparticles obtained from SAS-EM (Figure 2b). (n=1)

References

[1] Ul-Ain, Q.; Sharma, S.; Khuller, G. K. *Antimicrobial Agents and Chemotherapy* 47 (2003) 3005-3007.

[2] Shalaby, W. S. W.; Jackson, R.; Blevins, W. E.; Park, K. *Polymer Preprints* (American Chemical Society, Division of Polymer Chemistry) 33 (1992) 470-471.

[3] Karande, P.; Jain, A.; Mitragotri, S. *Nature Biotech.* 22 (2004) 192-197.

[4] Cormier, M. J. N.; Trautman, J. C.; Kim, H. L.; Samiee, A. P.; Neukermans, A. P.; Edwards, B. P.; Lim, W. L.; Poutiatine, A. I. PCT Int. Appl. (2001).

[5] Johnson, O. L.; Herbert, P. *Drugs and Pharm. Sci.* 126 (2003) 671-677.

[6] Bodmeier, R.; McGinity, J.W. *J. Microencapsulation* 4 (1987) 279–288.

[7] Herrmann, J.; Bodmeier, R. *Eur. J. Pharm. Biopharm.* 45 (1998) 75-82.

[8] Viswanathan, N. B.; Thomas, P. A.; Pandit, J. K.; Kulkarni, M. G.; Mashelkar, R. A. *J. Cont. Rel.* 58 (1999) 9-20.

[9] McGee, J. P.; Davis, S. S.; O'Hagan, D. T. *J. Cont. Rel.* 34 (1995) 77-86.

[10] Iwata, M.; Tanaka, T.; Nakamura, Y.; McGinity, J. W. *Int. J. Pharm.* 160 (1998) 145-156.

[11] Mandal, T. K. Drug Dev. Ind. Pharm. 24 (1998) 623-629.

[12] Jiang, W.; Schwendeman, S. P. *Biotech. and Bioengg.* 70 (2000) 507-517.

[13] Schwendeman, S. P. *Crit. Rev. Therapeutic Drug Carrier Systems* 19 (2002) 73-98.

[14] Chattopadhyay, P.; Gupta, R. B. *Ind. Eng. Chem. Res.* 40 (2001) 3530-3539.

[15] Carrasquillo, K. G.; Stanley, A. M.; Aponte-Carro, J. C.; De, J. P.; Costantino, H. R.; Bosques, C. J.; Griebenow, K. *J. Cont. Rel.* 76 (2001) 199-208.

[16] Iwata, M.; Nakamura, Y.; McGinity, J. W. *J. Microencapsulation* 16 (1999) 49-58.

[17] Johnson, O. L.; Jaworowicz, W.; Cleland, J. L.; Bailey, L.; Charnis, M.; Duenas, E.; Wu, C.; Shepard, D.; Magil, S.; Last, T.; Jones, A. J. S.; Putney, S. D. *Pharm. Res.* 14 (1997) 730-735.

[18] Ellis, E. J.; Ellis, J. Y. *PCT Int. Appl.* (2003) WO 2003013477.

[19] Baeyens, V.; Kaltsatos, V.; Boisrame, B.; Varesio, E.; Veuthey, J.-L.; Fathi, M.; Balant, L. P.; Gex-Fabry, M.; Gurny, R. *J. Cont. Rel.* 52 (1998) 215-220.

[20] Sankaram, M. *PCT Int. Appl.* (2000) WO 2000003660.

[21] Costantino, H. R.; Johnson, O. L.; Zale, S. E. *J. Pharm. Sci.* 93 (2004) 2624-2634.

[22] Costantino, H. R.; Firouzabadian, L.; Wu, C.; Carrasquillo, K. G.; Griebenow, K.; Zale, S. E.; Tracy, M. A. *J. Pharm. Sci.* 91 (2002) 388-395.

[23] Sah, H. *J. Pharm. Sci.* 88 (1999) 1320-1325.

[24] Sah, H. *PDA J. Pharm. Sci. Tech.* 53 (1999) 3-10.

[25] van de Weert, M.; Hennink, W. E.; Jiskoot, W. *Pharm. Res.* 17 (2000) 1159–1167.

[26] Gupta, R. B.; Chattopadhyay, P. *U.S. Patent 6,620,351* (2003).

[27] Iwata, M.; Tanaka, T.; Nakamura, Y.; McGinity, J. W. *Int. J. Pharm.* 160 (1998) 145–156.

[28] Iwata, M.; Nakamura, Y.; McGinity, J. W. *J. Microencapsulation*, 16 (1999) 49-58.

[29] Thote, A. J., Chappell, J. T. Jr., Kumar R., Gupta R. B. *Drug Dev. Ind. Pharm.* 1 (2005) 43-57.

[30] Bempong, D. K.; Adkins, R. E. Jr.; Lindauer, R. F.; White, P. A.; Mirza, T. Pharmacopeial Forum, 25 (1999).

[31] Chattopadhyay, P.; Gupta, R. B. *AIChE J.* 48 (2002) 235-244.

[32] Ruiz J. M.; Tissier, B.; Benoit J. P. *Int. J. Pharm.* 49 (1989) 69-77.

[33] Stassen, S.; Nihant, N.; Martin, V.; Grandfils, C.; Jerome, R.; Teyssie, Ph. *Polymer* 35 (1994) 777-785.

[34] Nihant, N.; Stassen, S.; Grandfils, C.; Jerome, R.; Teyssie, P. *Poly. Int.* 32 (1993) 171-176.

[35] Nihant, N.; Grandfils, C.; Jerome, R.; Teyssie, P. *J. Cont. Rel.* 35 (1995) 117-125.

CHAPTER 8

FUTURE RECOMMENDATIONS

1. The concept of microencapsulation of API nanoparticles in polymer microparticles for sustained release has been proved for hydrophilic drugs and extended to formulation of a protein; i.e. lysozyme. An intermediate between the two are small chain and long chain peptides of therapeutic importance, such as Melanocyte Stimulating Hormone Inhibiting Factor 1 (MIF1) and Insulin respectively. Developing a sustained release formulation for these API would a significant contribution to the sustained release formulation of therapeutic amino acids and proteins.
2. An intended study is the monitoring of the rate of organic solvent evaporation in an o/w emulsion for a better improvement in the quality of obtained polymer microparticles used for sustained drug delivery.

   In a conventional solvent evaporation process for the production of PLGA microparticles containing hydrophobic API, the rate of evaporation is not controlled. This results in highly porous polymer particle through which most of the drug is immediately released, causing a burst effect.

   Hence, the idea is to control the rate of evaporation of the organic solvent by controlling the flow rate of an inert carrier gas, say nitrogen, through an

enclosed solvent evaporation apparatus. This process involves monitoring the rate of solvent evaporation, which is further controlled by the nitrogen using gas phase FTIR analysis of the organic solvent vapors, which in this case would be dichloromethane.

The figure below is from a literature where the mechanism of solvent evaporation during the microencapsulation processes was studied and its solvent evaporation rate was predicted. Based on this concept, the idea of controlled evaporation can be further developed. Figure 1 represents the schematic of the Solvent Evaporation Rate Study (SERS). Figure 2 shows the morphological difference between the microparticles obtained from the controlled solvent evaporation process to the particles obtained from the conventional process, where both the particles were exposed to the aqueous environment for the same amount of time. The particles obtained the controlled evaporation are lot more uniform as compared to the ones from the conventional process and have less number of pores on the surface as well. More research into controlling the parameters of controlled evaporation and development of a solvent release profile is required to make this process sound convincing. Once the particle size and morphological characteristics are optimized, the drug release rate from these particles should be compared for the reduction of initial burst release and the extent of sustained release that can be obtained from these microparticles.

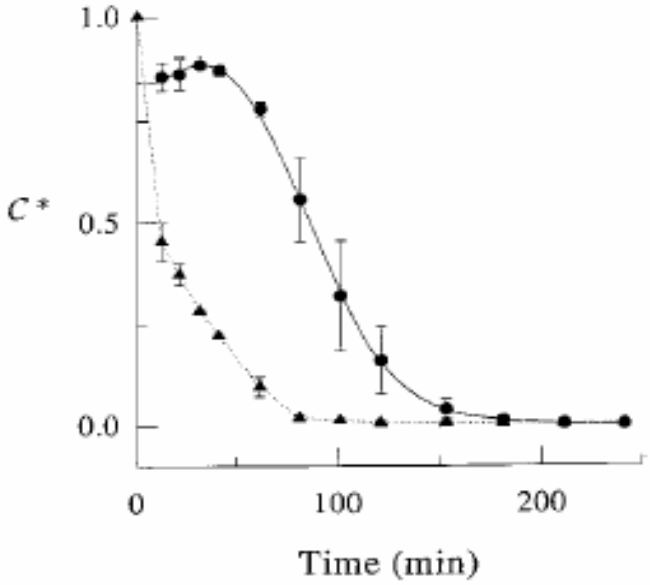

Figure 7—The concentration decline of MC during microencapsulation of triamcinolone acetonide by the solvent evaporation method. The concentration in dispersed (▲) and continuous phases (●) were normalized by the initial MC concentration in the polymer C_{DP}^0 (i.e., $C^* = C_{DP}/C_{DP}^0$) and by the solubility of MC in 0.3% PVA aqueous solution (i.e., $C^* = C/C_s$), respectively. The plotted data are mean ± SD ($n = 2$). (—) is a sixth-order polynomial fit, $q_6(t)$, and (·····) connects data points.

1

- Juan Wang and Steven P. Schwendeman, "Mechanisms of Solvent Evaporation Encapsulation Processes: Prediction of Solvent Evaporation Rate", Journal of Pharmaceutical Sciences, 88(10), 1999, 1090-99.

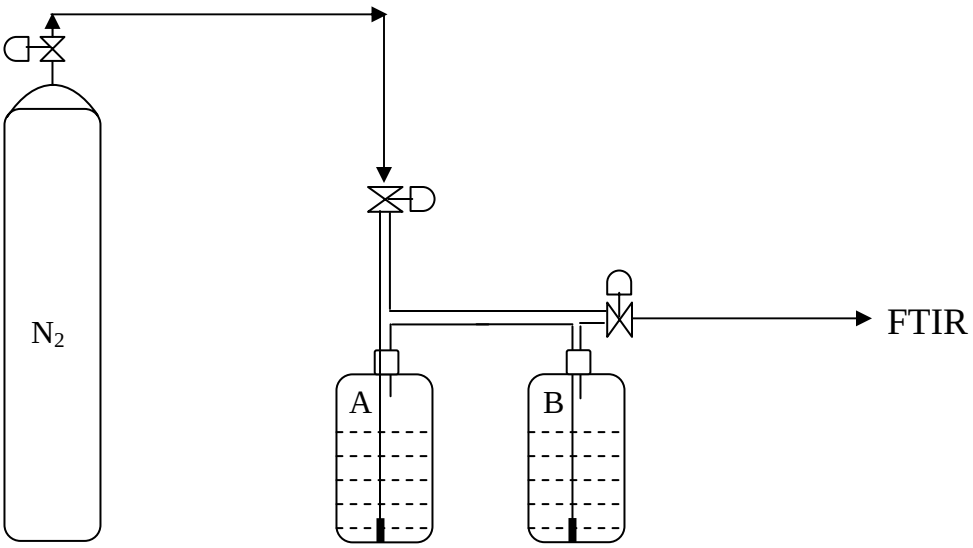

N_2: Nitrogen Supply

A: Water to wet Nitrogen

B: Oil-in-water emulsion for solvent evaporation

Figure 1. Schematic of Solvent Evaporation Rate Study (SERS)

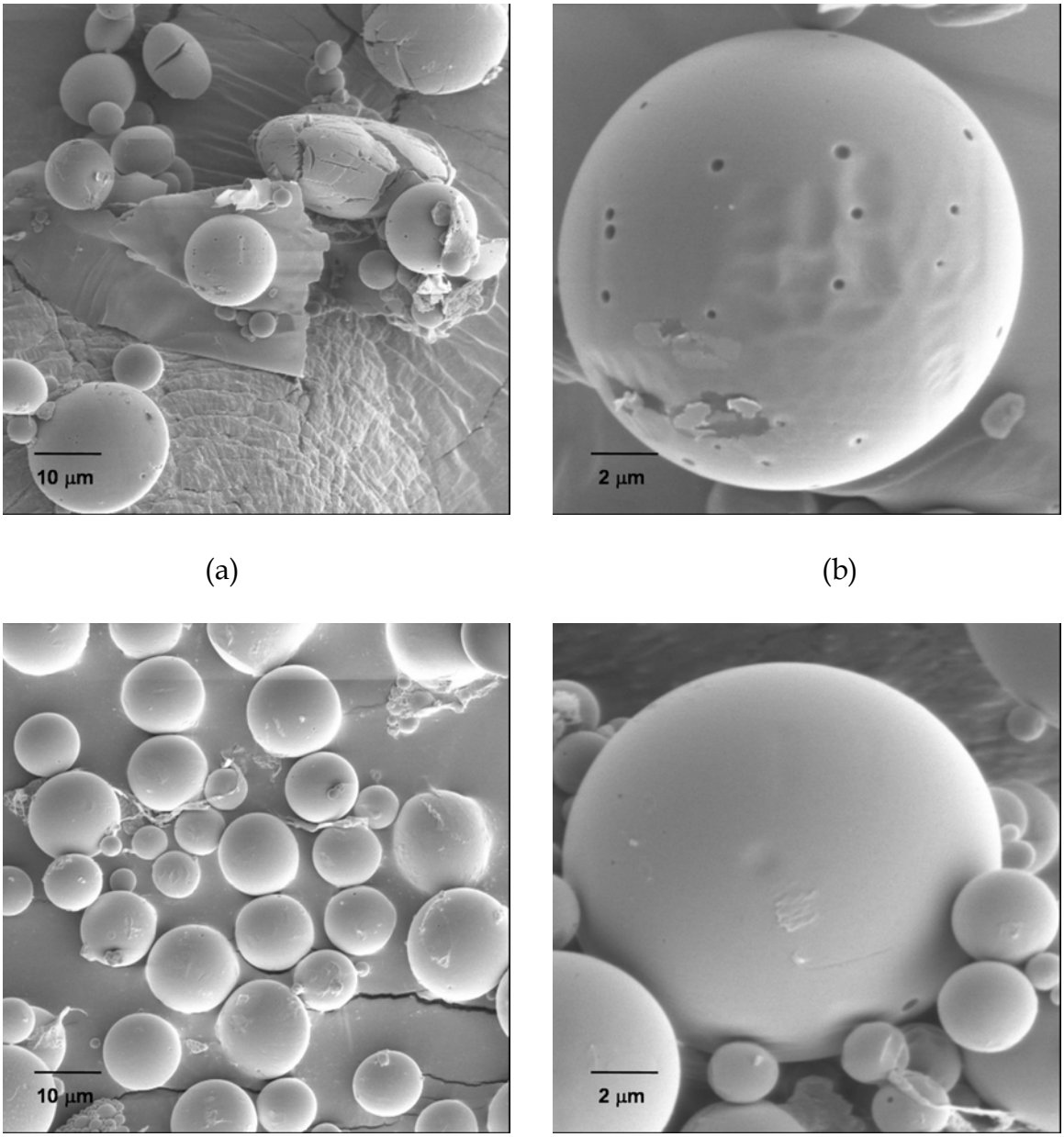

Figure 2. Comparison between PLGA microparticles obtained from (a-b) Natural Solvent Evaporation and (c-d) Controlled Solvent Evaporation (Nitrogen flow rate 2-3 ml/min). Both the particles were exposed to the aqueous environment for the same amout of time.

PUBLICATIONS

This dissertation is a collection of the following papers published in peer-reviewed journals:

Journal Papers

1. Thote, Amol J.; Gupta, Ram B., "Formation of Nanoparticles of a Hydrophilic Drug using Supercritical CO2 and Microencapsulation for Sustained Drug Release", Nanomedicine 1(1) (2005) 85-90.

2. Thote, Amol J.; Chappell, John T. Jr.; Kumar, Rajesh; Gupta, Ram B., "Reduction in the Initial-Burst Release by Surface Crosslinking of PLGA Microparticles containing Hydrophilic or Hydrophobic Drugs", Drug Development and Industrial Pharmacy 1 (2005) 43-57.

3. Bell, Philip W.; Thote, Amol J.; Park, Y.; Gupta, Ram B.; Roberts, C.B., "Strong Lewis-acid Lewis-base Interactions between Supercritical Carbon Dioxide and Carboxylic Acids: Effect of Self Association", Industrial & Engineering Chemistry Research 42 (2003) 6280-6289.

4. Thote, Amol J.; Gupta, Ram B. "Hydrogen-bonding of a Dichroic Dye with a Liquid Crystal for Application to LCDs", Fluid Phase Equilibria 220 (2004) 47-55.

5. Thote, Amol J.; Gupta, Ram B. "Hydrogen-bonding Effects in Liquid Crystals for Application to LCDs", Industrial & Engineering Chemistry Research 42 (2003) 1129-1136.

Conference Presentations

1. Thote, Amol J.; Gupta, Ram B., "Formation of Nanoparticles of a Hydrophilic Drug using Supercritical Carbon Dioxide and its Microencapsulation for Sustained Drug Release" ISSF, Orlando, FL, May 2005.
2. Thote, Amol J.; Gupta, Ram B., "Formation of Nanoparticles of a Hydrophilic Drug using Supercritical Carbon Dioxide and its Microencapsulation for Sustained Drug Release" Nanotech2005, Anaheim, CA.
3. Thote, Amol J.; Chappell, John T. Jr.; Gupta, Ram B.; "Formation of Dexamethasone/PLGA Microparticles: Controls of Size and Initial Burst Release", Nanoparticles 2004, Orlando, FL, March 2004.
4. Thote, Amol J.; Gupta, Ram B., "Formation of Dexamethasone/PLGA Microparticles: Controls of Size and Initial Burst Release", AIChE Annual Meeting, San Francisco, California, Nov. 2003.
5. Bell, Philip W.; Thote, Amol J.; Park, Y.; Gupta, Ram B.; Roberts, C.B., "Lewis Acid and Lewis Base Interactions between CO_2 and Carboxylic Acids using High Pressure FTIR and NMR Spectroscopy", AIChE Annual Meeting, San Francisco, California, Nov. 2003.

6. Bell, Philip W.; Thote, Amol J.; Park, Y.; Gupta, Ram B.; Roberts, C.B., "Supercritical Fluid Solvent Effects on Carboxylic Acid Dimer Formation", ISSF, Versailles, France, 2003.
7. Bell, Philip W.; Thote, Amol J.; Park, Y.; Gupta, Ram B.; Roberts C. B.; "Supercritical Fluid Solvent Effects on Carboxylic Acid Dimer Formation", AIChE Annual Meeting, Indianapolis, Indiana, Nov. 2002.
8. Thote, Amol J.; Ram B. Gupta, "Hydrogen Bonding Effects Liquid Crystals and Dichroic Dyes", AIChE Annual Meeting, Reno, Nevada, Nov. 2001.